UNIVERSITY OF SOUTHAMPTON

Phase Sensitive Parametric Amplifiers and Their Applications

by

Joseph Kagga Kakande

A thesis submitted in partial fulfillment for the degree of Doctor of Philosophy

in the

Faculty of Physical and Applied Sciences

Optoelectronics Research Centre

March 2012

UNIVERSITY OF SOUTHAMPTON

ABSTRACT

FACULTY OF PHYSICAL AND APPLIED SCIENCES
OPTOELECTRONICS RESEARCH CENTRE

Doctor of Philosophy

by Joseph Kagga Kakande

Phase sensitive amplification (PSA) is a remarkably powerful tool if implemented correctly - it allows amplification with a noise figure lower than quantum mechanics normally dictates, and also allows the development of systems that coherently process the phase of their optical inputs. PSA at infrared wavelengths can be achieved using second or third order optical nonlinearities - indeed the first demonstrations of PSA utilised degenerate three photon mixing in bulk crystals, allowing the observation of effects such as quantum quadrature squeezing. This PhD research project was aimed at translating the fascinating science of PSAs into applications, based on Kerr nonlinearity in optical fibres, capable of being deployed in modern core optical networks runnning at 40 Gbit/s and higher. This objective was an integral part of the European Union FP7 project PHASORS.

Studies, both theoretical and experimental, were carried out on wideband non-degenerate PSAs. The inline cascaded fiber optic parametric amplifier (FOPA), in which a first phase insensitive FOPA is used to generate phase locked signal-idler pairs, followed by a second FOPA in which PSA takes place, was used to experimentally demonstrate PSA gain characteristics in linear and saturated modes of operation, with PSA obtained over 20 nm in the telecom C-band. Focus was then re-directed towards applying a dual pump PSA to DPSK regeneration. The amplitude and phase limiting characteristics of these devices were experimentally studied, in particular revealing that amplitude saturation arises due to an interplay between input phase and nonlinear phase matching along the nonlinear fibre. This feature was used to identify a regime of operation for DPSK regeneration combining simultaneous phase and amplitude regeneration.

A practical DPSK regenerator based on a degenerate dual pump phase sensitive FOPA was built. The device advanced the state of the art by incorporating a pump synthesis stage that allowed black-box operation. Detailed measurements using noise sources with varying frequency distributions in both amplitude and in phase, are presented, and the ability of the system to improve the phase and amplitude characteristics of signals at its input was verified. Also presented are results showing the regenerator installed in the middle of an 800 km dark fiber link. Finally, a novel scheme was proposed and demonstrated that utilised parametric mixing to perform arbitrary phase quantization. This relied on the coherent addition of an M-level PSK signal with a conjugated (M-1)th phase harmonic, scaled by a coefficient m, to achieve M-level phase quantization. The concept was successfully demonstrated with QPSK data signals at 56 Gbaud, as well as used to quantize lower bandwidth test signals from 2 to 6 phase levels.

Contents

List of Figures

Declaration of Authorship

I, Joseph Kagga Kakande

declare that the thesis entitled

Phase Sensitive Parametric Amplifiers and Their Applications

and the work presented in it are my own, and have been generated by me as the result of my own original research.

I confirm that:

- this work was done wholly or mainly while in candidature for a research degree at this University;
- where any part of this thesis has previously been submitted for a degree or any other qualification at this University or any other institution, this has been clearly stated;
- where I have consulted the published work of others, this is always clearly attributed;
- where I have quoted from the work of others, the source is always given. With the exception of such quotations, this thesis is entirely my own work;
- I have acknowledged all main sources of help;
- where the thesis is based on work done by myself jointly with others, I have made clear exactly what was done by others and what I have contributed myself;
- parts of this work have been published as: [See *List of Publications*]

Joseph Kagga Kakande

March 2012

Nomenclature

1P	Single Pump
2P	Dual Pump
ASE	Amplified Spontaneous Emission
CW	Continuous Wave
DFA	Doped Fibre Amplifier
DFB	Distributed Feedback
DFG	Difference Frequency Generation
DGD	Differential Group Delay
DLI	Delay Line Interferometer
DPSK	Differential Phase Shift Keying
DQPSK	Differential Quadrature Phase Shift Keying
DCF	Dispersion Compensating Fibre
DS	Dispersion Slope
DSF	Dispersion Shifted Fibre
EDFA	Erbium-Doped Fibre Amplifier
EOM	Electro-optic Modulation
FEC	Forward Error Correction
FOPA	Fibre Optic Parametric Amplifier
FWHM	Full Width at Half Maximum
FWM	Four Wave Mixing
GVD	Group Velocity Parameter
HNLF	Highly Nonlinear Fibre
IL	Injection Locked
KTP	Potassium titanyl phosphate
MZM	Mach-Zender Modulator
NDFWM	Non-degenerate Four Wave Mixing
NF	Noise Figure
NLSE	Nonlinear Schrödinger Equation
NOLM	Nonlinear Optical Loop Mirror
NPN	Nonlinear Phase Noise
NRZ	Non Return-to-Zero
OBPF	Optical Band Pass Filter

OIL	Optical Injection Locking
OOK	On-Off Keying
OSA	Optical Spectrum Analyser
OSNR	Optical Signal to Noise Ratio
OSO	Optical Sampling Oscilloscope
PC	Polarization Controller
PHASORS	Phase Sensitive Amplifier Systems and Optical Regenerators and their Applications
PI	Phase Insensitive
PIA	Phase Insensitive Amplifier
PI-FOPA	Phase Insensitive Fibre Optic Parametric Amplifier
PM	Polarization Maintaining
PMD	Polarization Mode Dispersion
PM-QPSK	Polarization Multiplexed Quadrature Phase Shift Keying
PPLN	Periodically Poled Lithium Niobate
PS	Phase Sensitive
PSA	Phase Sensitive Amplification or Phase Sensitive Amplifier
PSD	Power Spectral Density
PS-FOPA	Phase Sensitive Fibre Optic Parametric Amplifier
PSK	Phase Shift Keying
QPSK	Quadrature Phase Shift Keying
RF	Radio Frequency
SBS	Stimulated Brillouin Scattering
SHG	Second Harmonic Generation
SMF	Single Mode Fibre
SNR	Signal to Noise Ratio
SPM	Self Phase Modulation
SSFM	Split Step Fourier Method
WDM	Wavelength Division Multiplexing
XPM	Cross Phase Modulation
ZDW	Zero Dispersion Wavelength

Acknowledgements

Francesca Parmigiani and Radan Slavík, who I learnt from, and worked with, all the way through this research project. Periklis Petropoulos and Dave Richardson who perfectly managed the balance between providing direction and intellectual freedom. And to all four of you, for being friends and making every day of my PhD studies such a pleasure, I will always be grateful.

Chapter 1

Introduction

1.1 Motivation

The development of the erbium-doped fibre amplifier (EDFA) revolutionized communications, enabling mass access to data transfer over inter-continental distances. By adopting wavelength division multiplexing (WDM), coupled with higher on-off-keying (OOK), data signaling rates of 800 Gbit/s down a single fibre were commercially mainstream for long haul and high capacity backbone communications by the late nineties, and the lay perception of the optical fibre was as a channel of effectively limitless bandwidth. However, demand for bandwidth has started to outstrip supply due to the emergence of bandwidth intensive services, such as high definition video streaming. To meet the expected rise in capacity requirements over the coming decades, a combination of higher signaling rates, coupled with higher spectral efficiency, have become a key research goal.

The ability to signal not only in amplitude but also in phase has long been exploited in radio telecommunications to boost spectral efficiency. In fibre communications, formats such as differential phase shift keying (DPSK) and differential quadrature phase shifted keying (DQPSK) are known to offer significant benefits over amplitude only formats such as on-off keying (OOK). DPSK in particular offers considerable advantages in terms of resilience to transmission impairments such as dispersion and nonlinearity, as well as an inherent 3 dB improvement in receiver sensitivity over OOK if balanced detection is utilised [1]. Polarization multiplexed QPSK (PM-QPSK) has recently become the standard for longhaul 100 Gbit/s optical transmission.

Traditionally, end-to-end optical fibre links have been characterised by their *Capacity*Distance* product, in units of bit/s·km, measured at a fixed received signal quality. This should in principle allow for a system metric that accounts for all engineerable

system parameters, from transmitter hardware, signal coding, optical fibre and amplifier specifications, detection technology, and receiver-side signal detection and post-processing. In most current commercial systems, the *Capacity*Distance* product is limited by two main factors; the widely deployed doped fibre amplifiers (DFAs) have a finite amplification bandwidth,while noise pickup during transmission degrades signal quality as the distance increases.

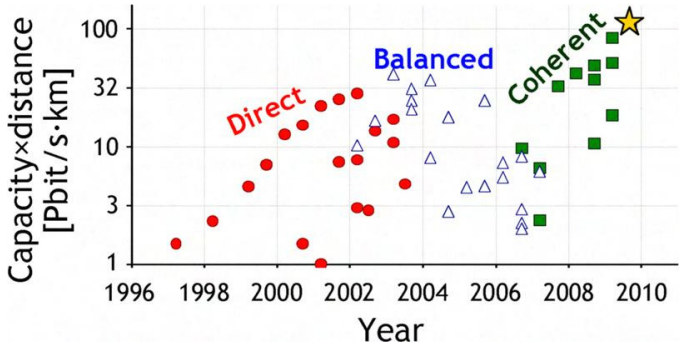

FIGURE 1.1: Evolution over time of the *Capacity*Distance* product for three different detection schemes, taken from [2].

As shown in Fig. 1.1, the performance of fibre optic links has increased significantly since the maturity of the EDFA in the mid-nineties. Increase in the number of WDM channels, as well as scaling the per-channel data rates to 40 Gbit/s whilst using direct detection increased the capacity by improving both spectral efficiency in bits/s/Hz, as well as the overall transmission bandwidth. The deployment of balanced detection and sophisticated error correction improved receiver sensitivity, therefore augmenting further the maximum transmission distance (reach). Finally, the resurgence in the use of coherent detection allowed for an increase in spectral efficiency by the adoption of higher order modulation formats, such as coherent quadrature phase shift keying (QPSK) [2], as well as the reach due to the ability to digitally compensate, in real-time, for both linear and nonlinear transmission impairments [3].

The $Capacity * Distance$ product, whilst a measure of the state of the art, is a parameter that does not incorporate all the variables of interest from a system perspective. Current commercial realisations of fibre transmission systems have to be extremely efficient with regard to cost, as measured in financial capital, as well as in energy requirements. The term cost will be used hereforth to cover both capital and energy, and will be interchangeably applied to both.

Fibre optical parametric amplifiers (FOPAs), which can be both phase sensitive (PS) and phase insensitive (PI), possess a wide range of properties that potentially allow them to improve the performance of fibre optic communication links, as measured using the $Capacity * Distance/Cost$ metric. These properties are discussed below.

Capacity

Despite the common perception outside of the optics community that the optical fibre as a transmission medium offers limitless bandwidth, only several narrow spectral windows are utilised for long-haul transmission due to the loss characterictics of silica, as well as the operating regions of DFAs. Optical amplifiers operating in the near infrared can be manufactured by doping optical fibres with rare earth elements, such as erbium, ytterbium and thulium. EDFAs are the dominant technology in use in current fibre optic communication systems. Since their development [4], they have revolutionised optical communications due to their ability to amplify multiple signals in the C-band (1530-1565 nm), which is the spectral region of minimum loss in silica optical fibres. They are polarization and phase insensitive, offer low noise figure (NF) limited by the 3 dB quantum limit [5], as well as high gains of up to about 60 dB [6]. DFAs have also been shown operating in the L-band (1565-1625 nm) by increasing the erbium concentration [7], and in the S-band (1460-1530 nm) by doping with thulium [8].

DFAs are often utilised in conjunction with Raman amplification to improve performance in long span links. Raman gain [9] can be obtained either in lumped devices, or implemented in a distributed fashion along the transmission fibre. Raman amplifiers offer wider operating bandwidths than DFAs, with a figure of 160 nm achieved by using a tellurite based fibre [10]. As PI devices, their NF is quantum limited to 3 dB. Incorporating distributed Raman amplification reduces the need for high signal peak powers, subsequently lessening the impact of nonlinearities in the link. As such most high capacity 'hero' experiments incorporate distributed Raman amplification [2, 3].

FOPAs can be used to increase capacity in a single device as they can have gain bandwidths significantly greater than those achievable with DFAs. Laboratory demonstrations have shown that it is possible to scale the gain up to the 70 dB level [11], and by careful design achieve gain bandwidth in excess of 300 nm [12]. In addition to large bandwidths, the central wavelength of FOPAs can be tuned by adjusting the pump(s) wavelengths and powers [13], allowing gain in spectral windows not accessible with DFAs. These FOPA properties could be used to increase the channel count of WDM systems significantly beyond that possible with DFAs, increasing capacity accordingly.

Distance

The reach of fibre links is limited by noise, seeded either linearly due to quantum noise resulting from loss and quantum limited amplification, as well as nonlinearly due to interactions between the propagating signal and other optical waves in the same fibre [14]. Optical amplification can be used to compensate for loss. Typically, DFAs are required every 60 - 120 km, compensating for around 12 - 24 dB worth of losses. As discussed in Section 3.2.1.2, it is possible to minimise noise pickup in links by using low

NF lumped amplifiers and pre-compensating for the loss by amplifying before the lossy element.

Phase sensitive amplification (PSA) as a process has long been known to offer the possibility of amplification of optical signals with NF below the 3 dB quantum noise limit experienced by all other classical amplifiers, including DFAs. In fibre, phase sensitive fibre optic parametric amplifiers (PS-FOPAs) are operated by having the signal and idler fields present at the input to the FOPA. If used to replace DFAs in multi-span links, PS-FOPAs can provide a 3 dB overall NF improvement, which could be used to double the transmission distance [15]. While the theory is four decades old, the associated requirements of narrow linewidth and high power pumps that are phase locked to the signals (and idlers) being amplified limited research efforts in this field for a long time. In the early nineties however, following the development of the EDFA and the implementation of the first long distance optical fibre transmission networks, interest in the PSA was reignited as a means to extend the reach of the said networks, by reducing the noise accumulated during repeated amplification [16]. PSA was demonstrated shortly afterwards in a parametric amplifier based on second order nonlinearity in a Potassium titanyl phosphate (KTP) crystal, with a noise figure under 3 dB measured [17]. FOPA equivalents using highly nonlinear fibre (HNLF) were subsequently studied and demonstrated [18, 19]. FOPA gain can also be distributed along the transmission span [20, 21], matching, and even exceeding, the noise benefits of using distributed Raman amplification.

While optical amplification can be used to offset the detrimental impact of loss, the presence of optical nonlinearity means that beyond a certain peak power level, amplification degrades, rather than enhances the received signal quality. An alternative solution to noise pickup is to periodically regenerate the signal, restoring it back to its original quality. The first commercial regenerators utilised a process referred to as Optical-Electrical-Optical (OEO) conversion. This involves the noisy optical signal (i) being detected using a photoreceiver thereby converting it into an analog electrical signal, (ii) re-digitising the analog signal thereby removing the noise, and (iii) re-modulating this digital stream onto a new non-degraded optical carrier. Digital error correction can also be used on the electrical signal, enhancing the performance of the system significantly.

FOPAs can also be used to perform all-optical signal regeneration. In PI mode, they can be used to limit the intensity of signals via a gain saturation mechanism [22]. This has been used to regenerate the intensity of DPSK signals [23], reducing the nonlinear pickup of noise in transmission spans following the regenerator, with demonstrations showing reach enhancement [24]. The extinction ratio of OOK signals can also be increased using a higher-order four wave mixing (FWM) effect in FOPAs, allowing for another optical regeneration mechanism [25].

In PS mode, two pump symmetric (degenerate) FOPAs can directly eliminate phase noise from DPSK signals due to their π-periodic step phase characterictics. When saturated, they can also use the same amplitude limiting function described earlier to eliminate amplitude noise [26]. This combination of effects can be used to perform simultaneous phase and amplitude regeneration of DPSK signals [26, 27]. This phase regeneration capability could be used to extend the reach of DPSK-bearing fibre links. This configuration however is limited to two-level PSK signals, and not the higher order modulation formats such as QPSK that are superceding DPSK.

Cost

For a very long time, all-optical signal processing has been considered to be able to replicate, but at significantly higher speeds, certain functions that could otherwise only be performed using electronics. All-optical switching was demonstrated as early as 1983 [28] using nonlinear interactions in a $LiNbO_3$ waveguide. By 1990, it was anticipated that Kerr based switches with their associated functionality such as regeneration, sampling and multiplexing, would be required to overcome the limits of electronic devices, in novel *all-optical* networks [29].

The rapid growth of the internet has led to estimates that by 2025 the internet will consume 7% of the 2010 global electricity supply [30]. Such predictions have meant that the power efficiency of systems involved in optical networks has become an issue of utmost importance. For a long time, research literature on all-optical signal processing has stated that all-optical techniques are more power efficient, and consequently *greener* than electrical (OEO) alternatives, an assertion repeated in the introductory paragraph of the majority of papers today on this subject.

In reality, advances in the field of semiconductor electronics have meant that OEO based switches are currently more efficient than their all-optical counterparts, once the power consumption of both the switch and ancillary devices (such as optical pump amplifiers for many Kerr-based devices) is taken into account. Because of the intrinsically low switching energy of modern CMOS transistors, estimates suggest that OEO techniques currently outperform (albeit marginally) their all-optical counterparts when it comes to simple binary operations, as shown in Fig. 1.2 [30].

PS-FOPAs can potentially lead to power reductions in a number of ways. In long optical links with large repeater spacings, the net power consumption of the link (including transmitter, receiver and repeaters) is dominated by the consumption of the amplifiers [31]. In this regime, if DFAs could be replaced by PS-FOPAs of identical power consumption but with 3 dB less noise figure, the repeater spacing could be doubled, leading to significant reductions in energy use, as well as cost due to the typical overheads per repeater (maintenance, installation, warehousing etc).

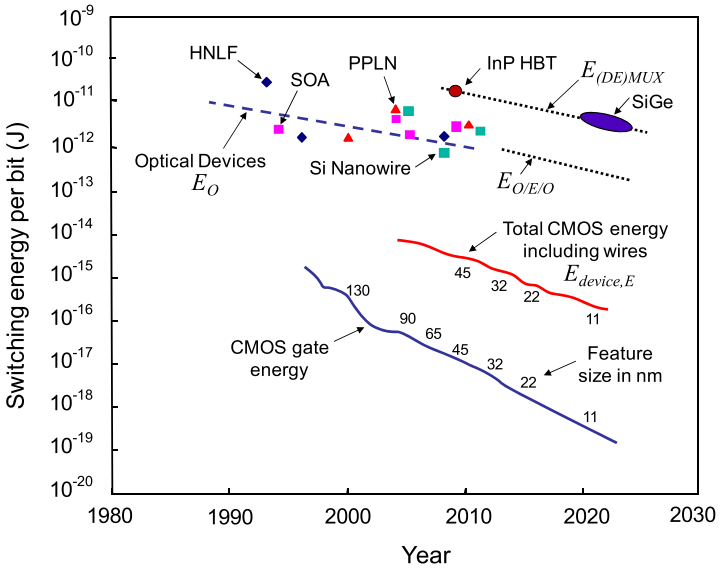

FIGURE 1.2: Device energies per bit against time at 100 GHz, taken from [30].

In addition, while it is clear that OEO switches acting on single bit/symbol inputs perform well enough in energetic terms to render optical equivalents redundant, the situation could be reversed with the advent of complex modulation formats. A fully coherent regenerator for a single polarization QPSK signal would require a local oscillator, dual channel high speed analog-to-digital converter, a high speed digital chip, and a QPSK transmitter. For a hypothetical 50 Gbit/s QPSK coherent (DSP based) regenerator, the 25 optical Gsymbols/s received would be transformed to two 150 Gbit/s serial electrical streams due to the requirement of at least 6 bit/symbol resolution in the ADCs for optimal performance [32]. As a result, an electrical regenerator would need to process at least 12 times as many symbols as an equivalent all-optical device that directly regenerated each received symbol. This internal symbol-multiplication, inherent to coherent OEO regenerators, may make it possible for all-optical regenerators to become competitive, as it overcomes the per-bit switching disadvantage relative to OEO approaches shown in Fig. 1.2. Crucially, moving to even higher order modulation formats, such as 8-PSK, would make all-optical processing even more competitive.

Research Aims

With all this in mind, PS-FOPAs could lead to significant cost reductions in future optical networks carrying high spectral efficiency phase encoded signals, due to a two-fold effect; a reduction in the number of amplifiers per span, as well as a more energetically efficient means of signal regeneration. It is only of recent that PS-FOPAs have become technologically feasible, due to advances in high power narrow linewidth lasers, optical phase locking techniques, availability of fibres with high nonlinearity and low dispersion,

as well as increased stimulated Brillouin scattering (SBS) thresholds. In July 2008, the University of Southampton and six other international collaborators started work on a European Union FP7 funded project titled "Phase Sensitive Amplifier Systems and Optical Regenerators and their Applications", often referred to by the acronym PHASORS. The PHASORS project targeted the development and applications of fibre based PSA technology in 40 Gbit/s broadband core networks. The objectives of PHASORS included:

- Development of a reliable technology base for the realisation of practical PSAs
- Investigation of both interferometric and non-interferometric fibre based approaches for PSA.
- Demonstration of a non-interferometric based PSA system.
- Demonstration of a PSA with a record noise figure of less than 1 dB.
- Demonstration of the benefits of the low noise properties of PSA for transmission applications.
- Demonstration of the use of PSAs for the regeneration of phase encoded signals.

The University of Southampton was involved in several tasks within the project, including the design and fabrication of highly nonlinear microstructured fibers suitable for PSA, characterisation of narrow linewidth laser and phase locking systems, and the development of practical regenerators for phase encoded signals. The project partners all contributed in different ways to these work packages. OFS Denmark designed and fabricated silica based highly nonlinear fibers, including the high SBS threshold samples used in the regeneration work later in this thesis. Eblana Photonics manufactured narrow linewidth semiconductor lasers which proved suitable for injection locking, enabling black box PSA operation. The University of Athens assisted with theoretical support, including numerically simulating the regenerator designs. University College Cork carried out research in optical phase locked loops and optical injection locking, and knowledge was exchanged with Southampton on these key sub-systems. The University of Chalmers was engaged in building wideband PSAs for low noise amplification, and joint work was carried out between Chalmers and Southampton early on in experimentally studying PSA behaviour. EXFO Sweden, whose expertise is in the field of ultra-high speed all-optical sampling, provided their high speed complex sampling scope allowing for some advanced evaluation of the regenerator prototypes. Last but not least, OneFive Gmbh carried out research into narrow linewidth lasers based on external cavity technology, although these were not used in the experiments detailed in this thesis.

This PhD research project was aimed at novel system demonstrations of PSAs within PHASORS, with particular emphasis on using them for all-optical DPSK regeneration,

as well as finding ways to extend their functionality to coping with higher order modulation formats such as QPSK. This meant that a lot of the experimental work here presented utilised devices fabricated by the project partners. In addition, some of the experiments were carried out in collaboration either with the external project partners, or with University of Southampton researchers working on PHASORS, particularly Dr. Francesca Parmigiani and Dr. Radan Slavik. Whenever experiments were performed jointly under such circumstances, it is explicitly stated in this thesis.

1.2 Outline

Chapter 2 provides a basis for the theoretical aspects of the work in this thesis. Key effects during signal propagation in optical fibres are presented, including dispersion and nonlinear refraction. Fibre optical parametric amplification is introduced, as well as the phase matching technique that allows efficient parametric amplification by careful selection of the pump(s) wavelengths relative to the fibre zero dispersion wavelength. This is followed by a mention of some of the detrimental inelastic scattering mechanisms to be minimised in FOPA design, particularly stimulated Brillouin scattering. The Nonlinear Schrödinger Equation is shown and its solution by use of the Split Step Fourier Method described. This was used to perform numerical simulations of the parametric devices used for amplification and regeneration, as described in later chapters. Finally, the process of injection locking of semiconductor lasers is introduced; it plays a key role in the phase sensitive regeneration demonstrations in this thesis.

In Chapter 3, phase sensitive amplification is introduced as a technique to obtain amplification with a NF below the 3 dB quantum limit of classical amplifiers. A basic introduction to the theory is presented, including the formulae revealing that replacing classical quantum limited (PI) amplifiers with PSAs in a multi-span link should yield a net 3 dB link margin improvement. The inline cascaded FOPA, in which a first phase insensitive FOPA is used to generate phase locked signal-idler pairs, followed by a second FOPA in which PSA takes place, is used to experimentally demonstrate single pump PS-FOPA gain characteristics in linear and saturated modes of operation. An improved PSA configuration is then shown, it allows a comparison of single and dual pump PS-FOPAs, and includes several modifications aimed at improving PSA performance relative to the first demonstration. PS amplification over 20 nm is shown with gain variations under 1 dB. Finally, FOPAs in PI and PS mode are used to amplify a wideband optical comb. A PI-FOPA was used to flatten a triangular -10 dB/THz input comb spectrum, and high gains of 33 dB were obtained at the FOPA gain peak. In PS mode, a clear 4 dB NF improvement was shown, as compared to the PI-FOPA.

Chapter 4 studies issues regarding the application of the degenerate 2P PS-FOPA for DPSK signal regeneration. The analytical gain functions of the PS-FOPA, as presented

in Chapter 3, are simplified to show how in the linear high gain regime the device transfer function can be approximated by adding to the input signal its phase conjugate. Results of numerical modelling using the parameters of several in-house HNLFs show that good phase regenerative performance could be delivered in a PS-FOPA if PS swings over 15 dB are achieved. These conclusions are then verified in an experiment based on a degenerate 2P PS-FOPA in a 2 m bismuth oxide fibre, showing that close to an order of magnitude reduction in small signal phase fluctuations at the PS-FOPA input could be practically obtained. PI and PS saturation in a FOPA are experimentally contrasted, and the dynamics of saturation in a PS-FOPA are practically studied. The experiment reveals that saturation in a PS-FOPA is more complex than in a PI device due to an interplay between input phase and nonlinear phase matching along the FOPA fibre, which modifies the amplitude transfer characteristics quite markedly, particularly at high input signal levels. This feature is used to identify a regime of operation for DPSK regeneration combining simultaneous phase and amplitude regeneration.

Chapter 5 discusses the implementation of a DPSK regenerator based on a degenerate dual pump FOPA. The device advanced the state of the art by incorporating a pump synthesis stage that allowed black-box operation. This involved the mixing of the incoming DPSK signal with a local pump, generating a modulation stripped idler that was then enhanced using injection locking, providing the second required pump. Detailed measurements using sinusoidal phase and amplitude noise are shown confirming the regenerative effects up to 40 Gbit/s. The regenerator was then modified to make it less susceptible to thermal and acoustic perturbations and assessed with an input DPSK signal impaired by artificial broadband non-deterministic noise, and later by real noise generated by transmission through an 800 km installed link. Modest BER enhancement was obtained due to the particular noise statistics in the experiments. The analog error correction ability of the regenerator is discussed, before concluding with an assessment of the impact of uncompensated signal dispersion.

In Chapter 6, the need for multilevel phase quantization is discussed. A novel scheme is introduced, relying on the coherent addition of an M-level PSK signal with a conjugated (M-1)th phase harmonic, scaled by a coefficient m, to achieve M-level phase quantization. A simple analytical theory can be used to predict the optimal value of m, located using a numerical misfit factor minimization process. The concept is successfully demonstrated with QPSK signals, relying on a two stage parametric process - in the first stage a third order phase harmonic is generated, and in the second this is mixed with the original signal. A further simplification to the system is to combine the two processes in a single fibre, by mixing a QPSK signal with two pumps in an HNLF. Constellation measurements taken up to 56 Gbaud (112 Gbit/s) show up to a four-fold reduction in the phase error variance. The device is capable of reducing noise in both phase and amplitude via a saturation mechanism, similar to the DPSK regenerator. The generalised concept

is further demonstrated up to 6-PSK. Finally, the conclusions from all this work are addressed in Chapter 7.

Chapter 2

Background

2.1 Introduction

This chapter starts off by briefly covering some of the classical theory of wave propagation in dielectric media within the context of signal propagation in optical fibres. Linear dispersion and nonlinear refraction are described, followed by the process of parametric amplification, which is the basis for most of the experimental work described in this thesis. The method of optimising parametric amplification by phase matching is presented. This is followed by a mention of some of the inelastic scattering mechanisms in fibre of relevance to parametric amplifier design, particularly SBS. Methods of suppressing SBS are described, including several experimental realisations. The Nonlinear Schrödinger Equation is introduced and its solution by use of the Split Step Fourier Method described. This was used to perform numerical simulations of the parametric devices used for amplification and regeneration, as described in later chapters. Finally, the process of injection locking of semiconductor lasers is briefly introduced due to its incorporation in the PSK regeneration demonstrations in several chapters of this thesis.

2.2 Wave Propagation Effects

2.2.1 Chromatic Dispersion

Chromatic dispersion is an effect originating from the frequency dependence of the refractive index of light in dielectric media. The time varying field of an electromagnetic wave propagating along the axis z of an optical fibre in the x or y directions can be described as

$$\vec{E}(x,y,z,t) = \frac{1}{2}\left\{E\left(x,y,z,t\right)\cdot\exp\left[i\left(\beta z-\omega t\right)\right]+c.c\right\} \tag{2.1}$$

where $\{E(x,y,z,t)$ represents the envelope of the waveform, β the propagation constant, ω the frequency of the carrier and $c.c$ the complex conjugate. The assumption behind Eqn. 2.1, which is sometimes referred to as the *slowly varying envelope approximation*, is that the envelope of the wave propagating in the z direction changes much slower than the period of the wave [33]. For spectrally broad signals, one can describe the frequency dependence of β as a Taylor series about a reference angular frequency ω_0

$$\beta(\omega) = n(\omega)\frac{\omega}{c} = \beta_0 + \beta_1(\omega-\omega_0) + \frac{\beta_2}{2!}(\omega-\omega_0)^2 + \frac{\beta_3}{3!}(\omega-\omega_0)^3 + \frac{\beta_4}{4!}(\omega-\omega_0)^4 + \dots \quad (2.2)$$

where

$$\beta_i = \frac{d^i\beta}{d\omega^i}\Big|_{\omega=\omega_0} \quad (2.3)$$

and c is the speed of light in a vacuum.

The lowest order wavelength dependent coefficient β_1 is inversely related to the *group velocity*, v_g, which is the speed at which the envelope of the wave propagates along the fibre and can be written as

$$v_g = \frac{d\omega}{d\beta} = \frac{1}{\beta_1} \quad (2.4)$$

The parameter β_2 is often referred to as the *group velocity dispersion parameter* (GVD), and in relation to the refractive index n can be written as

$$\beta_2 = \frac{1}{c}\left(2\frac{dn}{d\omega} + \omega\frac{d^2n}{d\omega^2}\right) \quad (2.5)$$

By minimising β_2, one can minimise the rate at which the various spectral components within a pulse disperse relative to each other during propagation. An alternative *dispersion parameter* D is more commonly used when fibre parameters are specified. D is related to β_2 as

$$D = -\frac{2\pi c}{\lambda^2}\beta_2 \quad (2.6)$$

Typically, there is a wavelength, referred to as the *zero dispersion wavelength* (ZDW), at which the GVD becomes zero. For fused silica, this is typically around 1.27 μm [33]. In nonlinear fiber optics, it is normally beneficial to use nonlinear fibers whose ZDW is close to the wavelengths of the interacting waves. To achieve this at telecom wavelengths (around 1550 nm), *dispersion shifted fibre* (DSF) is used. In DSF, the ZDW is tuned by a combination of doping, and engineering the device structure, such that a waveguide contribution to β_2 offsets the original material dispersion [34]. By convention, for wavelengths where $\beta_2 > 0$, i.e. $D < 0$, the dispersion is said to be *normal*, and for $\beta_2 < 0$, i.e. $D > 0$, *anomalous*. By shifting the ZDW to even longer wavelengths, it is possible to obtain fibres with negative D values in the C band; these fibres are often used to compensate for accumulated dispersion following propagation in standard single mode fibre, and are referred to as *dispersion compensating fibre* (DCF).

The series in Eqn. 2.2 has been written up to the fourth order as the β_4 term can have significant impact in determining the properties of parametric devices hosted in low dispersion and low dispersion slope fibres [35].

2.2.2 Polarization Mode Dispersion

In real fibres, cylindrical asymmetry due to random variations in the core shape as well as stress-induced anisotropy cause the existence of two distinct polarization states. The mode-propagation constant, β, is slightly different for the two states, causing relative dispersion between the two polarizations. The difference between the refractive indices experienced by the two polarization states is called *birefringence*.

When a polarized beam is launched down an optical fibre, the two components of the signal (resolved along the two principal polarization states) experience different propagation delays due to the birefringence, causing a phenomenon referred to as *polarization mode dispersion* (PMD) [33]. The instantaneous difference between the delay of the two components is called the *differential group delay* (DGD). In long transmission fibres, the birefringence varies randomly along the fibre length. It is also not static, being sensitive to temperature and stress, and as a result, the output polarization and DGD in an installed fibre link will vary with time, albeit slowly (timescales measured in hours to days [36]). The relationship between the accumulated DGD, $\Delta\tau$, and the PMD parameter, D_{PMD}, following propagation over a distance L, is given by [33]

$$\Delta\tau = D_{PMD}\sqrt{L} \tag{2.7}$$

PMD is often cited as a limiting factor in the performance of high speed (>40 GHz) WDM systems, with typical values of 0.1 - 1 ps/$\sqrt{\text{km}}$ [33]. With the advent of real-time coherent systems however, compensation for dispersion and PMD can be done at the receiver [37], overcoming this obstacle.

If polarized beams need to be propagated along an optical fibre stably, polarization maintaining (PM) fibres are typically used. These have a deliberately high built-in birefringence, making the overall birefringence largely insensitive to small changes caused by stress or temperature fluctuations. This is usually done by inducing a permanent internal stress along one of the transverse axes of the fibre core [38].

2.2.3 Effective Length

The *effective length* accounts for the attenuation α of the transmission medium when studying nonlinear effects. The effective length L_{eff} of a fibre of loss α, is calculated from the real length L as

$$L_{eff} = \frac{1}{\alpha}\left(1 - \exp\left(-\alpha L\right)\right) \tag{2.8}$$

When calculating the impact of nonlinearity, it is necessary to substitute the real length with the effective length.

2.2.4 Nonlinear Refraction

Nonlinear refraction refers to the dependence of the material refractive index n not just on a linear frequency dependent term, $n_0(\omega)$, but also on the local intensity, I, of the electric field [39]

$$n(I) = n_0(\omega) + n_2 I \tag{2.9}$$

This effect is induced by the third order susceptibility, χ^3, of the dielectric medium. During analysis of electromagnetic propagation in optical fibres, a commonly used parameter is the *nonlinear coefficient*, γ , which incorporates the nonlinear index n_2 and the effective area, A_{eff}, of the propagating mode. The effective area is defined to account for the fact that the propagating field (in single mode fiber) is not constant in field across the fiber core, but rather is largest near the fiber axis, and also extends into the cladding, meaning that the intensity can not be accurately calculated simply by dividing the power by the core area. The effective area can either be calculated by using simulations or directly measured, provided in both cases that the other fibre parameters are known [40], and once this is done, γ can then be calculated as [33]

$$\gamma = \frac{2\pi n_2}{\lambda A_{eff}} = \frac{\omega n_2}{c A_{eff}} \tag{2.10}$$

The intensity dependence of n is responsible for a number of nonlinear effects, e.g. those described in the following two sub-sections.

2.2.4.1 Self Phase Modulation

During propagation, the $\vec{E}$ field experiences a nonlinear phase shift $\phi_{NL(SPM)}$ induced by its own intensity, which can be quantified as

$$\phi_{NL(SPM)} = \gamma P L_{eff} \tag{2.11}$$

where P is the optical signal power and L_{eff} the effective propagation length. Self phase modulation (SPM) is commonly used for many nonlinear optical processes such as soliton generation and the spectral broadening of ultra short pulses [33].

2.2.4.2 Cross Phase Modulation

If a signal, $\vec{E}_1$, is launched into a fibre together with another at either a different wavelength, polarization or propagating in the opposite direction, $\vec{E}_2$, the signal $\vec{E}_1$ experiences a nonlinear phase shift $\phi_{NL(XPM)}$ induced by the intensity of $\vec{E}_2$, a phenomenon known as cross phase modulation (XPM). For co-propagating waves, this phase shift is equal to

$$\phi_{NL(XPM)} = 2r \cdot \gamma P L_{eff} \tag{2.12}$$

where P is the power of $\vec{E}_2$ and r is a polarization dependent term of value 1 if $\vec{E}_1$ and $\vec{E}_2$ are linearly co-polarized and 1/3 when orthogonally-polarized. Cross phase modulation has been widely exploited as well, in switching and retiming applications [41], as well as nonlinear phase matching in parametric amplifiers [13] to name but a few examples.

It is important to note that Eqn. 2.12 is usually only valid for continuous wave signals. When the interacting beams are comprised of a pair of pulses, it is possible for dispersion to cause them to separate in time, a process termed as *walk-off*. In that case calculations of the nonlinear phase shift should take into account the real interaction length, which may be significantly less than L_{eff}.

2.3 Parametric Amplification

Parametric amplification is a phenomenon by which a weak wave, termed the *signal*, is amplified by a stronger wave, termed the *pump*, and in the process a third wave termed the *idler*, equally detuned in frequency from the pump as the signal, is generated. The term 'parametric' in this case is a legacy of the older field of radio engineering. Parametric amplification is achieved without energy storage in the amplifier medium, as compared to the amplification process in an EDFA.

Optical parametric amplification requires a nonlinear process to initiate the direct transfer of energy from pump to signal. This can be performed using second order nonlinearity in a medium such as a KTP crystal [42] or third order nonlinearity in optical fibre [43]. In optical fibre, the parametric process most commonly used for amplification is FWM.

2.3.1 Four Wave Mixing

When two waves with frequencies ω_1 and ω_2 interact inside a nonlinear medium, the resulting beating in intensity at the difference frequency, $\Delta\omega = |\omega_1 - \omega_2|$, nonlinearly modulates the refractive index, and consequently the propagating waves, resulting in the generation of new frequency components (modulation sidebands) at frequencies $\omega_3 = \omega_1 - \Delta\omega$ and $\omega_4 = \omega_2 + \Delta\omega$ [44]. Four wave mixing is subject to energy conservation

rules, such that $\omega_3 + \omega_4 = \omega_1 + \omega_2$. In addition, linear momentum must be conserved, and as such $\phi_3 + \phi_4 = \phi_1 + \phi_2$, where ϕ_j is the phase of wave j. The new frequency components are called the idlers. This process leads to signal gain, and FOPAs exploit this mechanism. To maximise the efficiency of the parametric process, it is necessary to maintain the phase relationship between the original waves and the idlers, something that may be altered during propagation by dispersion. Nonlinear phase matching is a technique to maximise parametric efficiency by using nonlinear refraction to offset dispersion, and is discussed in the following section.

2.3.2 Nonlinear Phase Matching

As the waves propagate down a fibre, it is possible for the energy transfer to be from the signal and idler to the pump(s) or vice versa, depending on the waves' relative phases. The direction of energy transfer depends on the phase relationship between the propagating waves and the induced polarization of the bound electrons in the medium [43]. If ϕ_s, ϕ_i, and ϕ_p are the absolute phases of the signal, the idler and the pump(s) respectively after propagating a distance z along the fibre, the *relative phase* can be defined as

$$\phi_{rel}(z) = \phi_s(z) + \phi_i(z) - 2\phi_p(z) \tag{2.13}$$

If $\phi_{rel}(z) \geq 0$, the energy transfer is from the pump(s) to the signal-idler pair, while if $\phi_{rel}(z) \leq 0$, the energy transfer is from the signal-idler pair to the pump(s). Temporarily neglecting the dispersion effect, the relative phase is modified with distance due to nonlinear pump induced XPM and SPM. Thus, the relative phase can be re-written as

$$\phi_{rel}(z) = \phi_s(0) + \phi_i(0) - 2\phi_p(0) + \Delta\beta_{NL} z \tag{2.14}$$

where the nonlinear phase mismatch $\Delta\beta_{NL} = 2\gamma P$ and P is the total pump power. In the presence of dispersion, an additional linear phase mismatch term can be defined as

$$\Delta\beta_L = \beta_s + \beta_i - 2\beta_p \tag{2.15}$$

where β_s, β_i and β_p are the mode propagation constants of the signal, idler and pump respectively. The relative phase then becomes:

$$\phi_{rel}(z) = \phi_s(0) + \phi_i(0) - 2\phi_p(0) + (\Delta\beta_L + \Delta\beta_{NL})\, z \tag{2.16}$$

The relative phase varies linearly with propagated distance at a rate determined by the total phase mismatch κ, given by

$$\kappa = \Delta\beta_L + \Delta\beta_{NL} \tag{2.17}$$

If the magnitude of κ is greater than zero, an oscillation in the gain of the signal is observed, which is detrimental to amplifier performance. To optimise a FOPA, one would like to minimize the total phase mismatch and maximize the signal gain. In FOPAs, a convenient way of doing this is by locating the pump in the anomalous dispersion regime and (only) one of the signal or idler in the normal regime, such that the ensuing negative $\Delta\beta_L$ cancels out the positive $\Delta\beta_{NL}$ [13]. This is referred to as *nonlinear phase matching*.

2.3.3 Phase Sensitive Amplification

FOPAs are *phase sensitive* (PS) when both the signal and the idler fields are present at the amplifier input and are phase locked to each other. In this case, the terminology signal and idler is retained only for convenience, in reality they are simply two independent waves with the same frequency detuning from the average pump frequency. The PSA behaviour can be explained physically as a result of the interference between the fields generated parametrically and the signal/idler fields already present at the amplifier input. In Chapter 3, PSA in FOPAs will be reviewed in more detail.

2.4 Scattering Effects

A number of scattering mechanisms in optical fibres exist that have an important impact on the performance of fibre optic devices. Some of these mechanisms are reported in the following sub-sections.

2.4.1 Rayleigh Scattering

Rayleigh scattering is due to the elastic scattering of photons by non propagating density fluctuations within the glass fibre structure, fluctuations that result from entropy (intrinsic disorder) in the molecular organization. The degree of Rayleigh scattering scales as λ^{-4} and limits the minimum losses achievable in state of the art fibre fabrication [45]. No energy is transferred from the photons to the scattering medium, meaning that the scattered light is at the same frequency as the incident light.

2.4.2 Stimulated Raman Scattering

Stimulated Raman scattering (SRS) is an inelastic scattering mechanism that originates from the interaction of propagating light with high frequency vibration modes (optical phonons) of the molecules of the transmission medium [39]. The scattered light is downshifted by the energy of an optical phonon. The resulting frequency shifts are very large,

typically strongest around 13 THz [33], although Raman effects can be observed over a broad frequency range. Raman effects will largely be ignored during the analytical work in this thesis due to their negligible effects on parametric gain [43] at the bandwidths of interest (with signals between 1530nm to 1560nm).

2.4.3 Stimulated Brillouin Scattering

When a high intensity source, usually called the pump, is coupled into a fibre, inelastic scattering of the forward propagating pump radiation sometimes occurs due to thermally generated acoustic phonons via a Bragg diffraction mechanism [39]. The scattered backward propagating light, termed the Stokes wave, is frequency downshifted by a material dependent amount, typically around 10 GHz [33]. Interference between the pump and Stokes wave sets up a standing wave and the resulting high electric field intensity gradients reinforce the acoustic wave due to electrostriction. This leads to an increase in both the reflected and acoustic waves until a steady state is reached. Beyond this point virtually any extra pump power coupled into the fibre input is converted into the backward travelling Stokes wave.

Suppressing SBS is one of the major challenges in designing high gain FOPAs, as unmitigated it severely limits the pump power that can be coupled into a fibre. SBS is typically characterized by the pump threshold power above which the SBS process becomes self reinforcing. SBS is a resonant narrowband mechanism (gain bandwidths typically around 20 - 50 MHz in silica) [33]. It is also a nonlinear process, and is therefore enhanced by increasing the interaction length or pump power. The majority of the methods that exist to suppress SBS rely on either increasing the pump bandwidth such that the pump spectral density reduces, or reducing the interaction length, for example by either physically separating various sections of the fibre using isolators, or modifying the fibre properties in a distributed fashion, broadening the effective Brillouin gain bandwidth and reducing the peak gain. Some of these techniques for increasing this threshold include [13]:

1. Pump phase modulation: SBS threshold increase is proportional to ν_p/ν_B, where ν_p is the pump spectral width after modulation, and ν_B the Brillouin gain bandwidth. While high SBS suppression is possible, the method is expensive and makes phase locking complicated.

2. Inline isolators: Adding N inline isolators provides an N-fold increase in the SBS threshold, although care must be taken to ensure that if the isolators are pigtailed the connecting fibres do not distort the FOPA gain spectrum.

3. Strain distribution: Applying varying strain along the length of fibre can provide over 10 dB SBS threshold enhancement. This can perturb the dispersive properties of the fibre, although it can conversely be used to optimise dispersion [46].

4. Al_2O_3 core doping: State of the art demonstrations today allow for around 6 dB increase in threshold, although this increases fibre losses significantly.

5. Temperature gradient: Approximately 3 dB threshold increase can be obtained per 100°C.

2.5 Generalised Nonlinear Schrödinger Equation

2.5.1 The NLSE

The Nonlinear Schrödinger Equation (NLSE) is the typical starting point for both analytical and numerical studies of the propagation of electromagnetic fields in optical fibre. This classic equation is derived from Maxwell's equations. For propagation in single mode fibre such as that typically used in FOPAs, one can separate the temporal and longitudinal evolution of the electric field, as follows [33].

$$\vec{E}(x,y,z,t) = \vec{F}(x,y)\vec{A}(z,t) \tag{2.18}$$

In Eqn. 2.18, $\vec{F}(x,y)$ describes the mode field distribution of the fundamental fibre mode and $\vec{A}(z,t)$ the propagating envelope of the field. At this stage the slowly varying envelope approximation, which assumes that the envelope of the field varies slowly compared to the field period, can be employed to simplify the mathematics. The NLSE is a differential equation describing the propagation of this slowly varying envelope under the influence of the earlier described linear and nonlinear effects, and can be written as

$$\frac{\delta A}{\delta z} = i\gamma \left|\vec{A}\right|^2 A - \left(\frac{\alpha}{2}A + i\frac{\beta_2}{2}\frac{\delta^2 A}{\delta t^2} - i\frac{\beta_3}{6}\frac{\delta^2 A}{\delta t^2}\right) \tag{2.19}$$

In the numerical simulations in this thesis, all the effects listed in Eqn. 2.19 are included. While β_4 is an important parameter for ultra wideband parametric amplifiers, the systems used in the PSA and regeneration work here typically occupied less than 20 nm spectral span, therefore accounting for β_4 was not crucial.

2.5.2 The Split-Step Fourier Method

The NLSE can be solved numerically using the Split Step Fourier Method (SSFM). In the SSFM, the NLSE describing the electric field is solved by discretely calculating the propagation over short steps in which the linear and nonlinear terms can be approximated to be independent of each other. Eqn. 2.19 can be written in the form

$$\frac{\delta \vec{A}}{\delta z} = \left(-\hat{D} + \hat{N}\right)\vec{A} \tag{2.20}$$

where $\hat{D} = \left(\frac{\alpha}{2} + i\frac{\beta_2}{2}\frac{\delta^2}{\delta t^2} - i\frac{\beta_3}{6}\frac{\delta^2}{\delta t^2}\right)$ is the differential operator comprising the dispersive and attenuation effects, and $\hat{N} = i\gamma\left|\vec{A}^2\right|$ the nonlinear refractive effects. If the step along which the NLSE is being solved is of length h, then an approximate solution for the signal field following propagation is

$$\vec{A}(z+h,t) \approx \exp\left(h\hat{D}\right)\exp\left(h\hat{N}\right)\vec{A}(z,t) \tag{2.21}$$

To solve Eqn. 2.21 , the nonlinear contribution to the propagation evolution is first solved in the time domain giving

$$\vec{B}(z,t) \approx \exp\left(h\hat{N}\right)\vec{A}(z,t) \tag{2.22}$$

Following this, the linear contribution is accounted for by transforming into the spectral domain such that

$$\tilde{\vec{B}}(z+h,\omega) \approx \exp\left(h\tilde{\hat{D}}(i\omega)\right)\tilde{\vec{B}}(z,\omega) \tag{2.23}$$

where $\tilde{\vec{B}}(z,\omega)$ and $\tilde{\hat{D}}(i\omega)$ are the Fourier transforms of $\vec{B}(z,t)$ and $\hat{D}$ respectively. Finally, the solution is provided in the time domain by performing the inverse Fourier transform

$$\exp\left(h\hat{D}\right)\vec{B}(z,t) = \mathcal{F}^{-1}\left(\exp\left(h\tilde{\hat{D}}(i\omega)\right)\tilde{\vec{B}}(z,\omega)\right) \tag{2.24}$$

This process can then be iterated over many small steps to derive high precision approximations of field propagation along the fibre path being studied.

The simulation work carried out in Chapter 3 utilises a generalized analytical solution describing FOPA gain derived from Eqn. 2.24, the derivation of which is shown in Section 3.3.2. That analytic solution is useful for quickly estimating the gain and bandwidth of parametric amplifiers, but the accuracy is significantly degraded in the presence of high losses, high pump depletion and large absolute signal gains. As such the remaining modeling work as presented was carried out by using VPI Transmission Maker 8.0 which implements a commercial Split Step Fourier solver algorithm. Such modeling tools have their limits though; this work utilised narrow linewidth lasers (sub 100 kHz) but modeling such long timescales requires vast amounts of computational time, hence in the simulations the laser linewidths are effectively treated as zero.

2.6 Optical Injection Locking

Optical injection locking (OIL) refers to a technique by which the frequency and phase properties of a laser, termed the *slave*, are forced to follow to those of another laser, termed the *master*, by injecting some light from the master into the slave [47]. The injected light distorts the lasing dynamics within the laser cavity, such that the master

frequency experiences preferential resonant gain, even if the natural frequency of the slave laser was elsewhere.

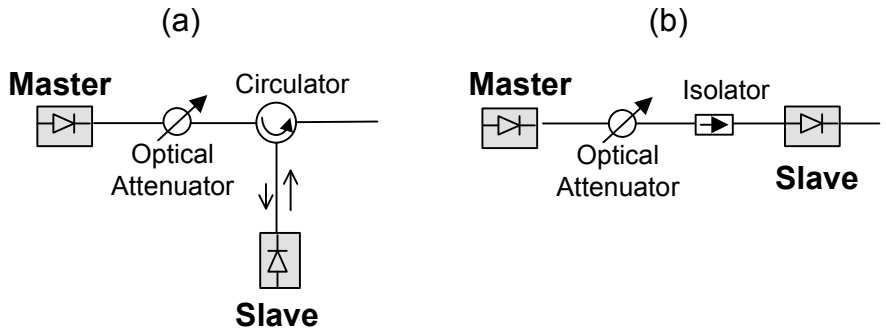

FIGURE 2.1: Optical injection locking of semiconductor lasers - (a) Reflection style, (b) Transmission style.

Fig. 2.1 shows how OIL of semiconductor lasers is typically implemented. In reflection style OIL, Fig. 2.1(a), light from the master is coupled into the slave laser cavity using the same facet from which the slave laser light is coupled out. This requires a circulator to separate the slave output from the master input. An alternative is to use transmission style OIL, Fig. 2.1(b), in which light from the master is injected into the slave cavity via one of the slave's facets, while the slave output is extracted from the other. In both cases the polarization of the master needs to be aligned to the principal polarization axis of the slave laser. Reflection style OIL is usually preferable as it only requires coupling optics on one of the slave laser facets, and is the technique used throughout this thesis.

The dynamic characteristics of the OIL process are rather complex, but generally speaking, depend on a combination of the injected master power/polarization, as well as the state of the slave cavity [48]. As such the frequency response of the OIL process can be tailored using those properties. Fig. 2.2 shows the OIL frequency response for a discrete mode semiconductor laser from Eblana Photonics as measured by Stylianos Sygletos, University College Cork. Similar lasers were supplied by Eblana Photonics to be used in the regeneration work in Chapters 5 and 6. The lasers had output power of approximately 6 dBm.

For these lasers, at weak injection levels (such as -21.5 dBm in Fig. 2.2), OIL transfers phase modulation from master to slave, but this is a very narrowband mechanism, with 3 dB width approximately 1 GHz. There is very strong suppression of amplitude fluctuations present on the master, although input phase fluctuations lead to some weak (-20 dB) amplitude changes on the slave output. Amplitude fluctuations on the master cause some phase changes on the slave, but this is a narrowband process with similar bandwidth to the phase transfer characteristics, albeit significantly weaker. In general, the injection locked laser during weak injection can be regarded as performing a low pass filtering function on the optical phase of the master, and as a limiting amplifier in amplitude.

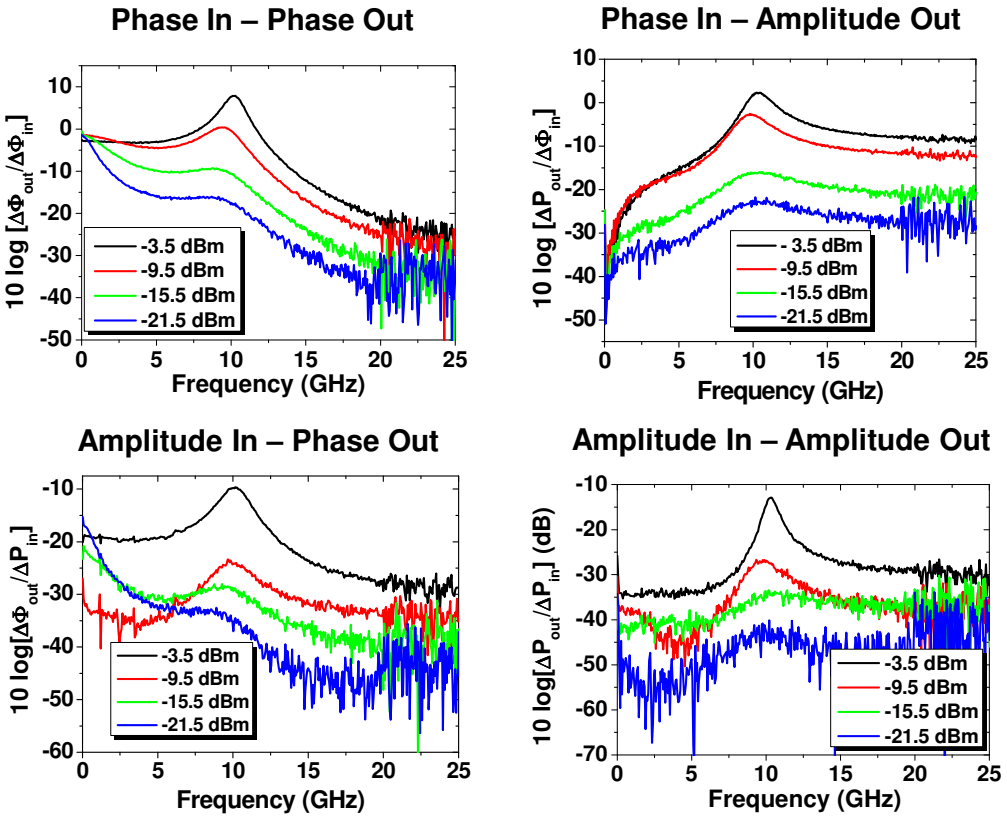

FIGURE 2.2: OIL Transfer function for Eblana Photonics *Discrete Mode* semiconductor laser.

At strong injection levels (such as -3.5 dBm in Fig. 2.2), the OIL dynamics are significantly altered and a strong resonance can be seen emerging (at approximately 10 GHz for these lasers). Phase fluctuations are transferred from master to slave over a much wider bandwidth than in the weak injection case, and any fluctuations close to the resonance are enhanced significantly. There is also a strong phase to amplitude transfer at the resonance frequency.

For the regeneration work in this thesis the weak injection regime was used, and this is the regime of choice in most other applications of injection locking. The strong OIL regime does have its uses though, such as enhancing the resonant frequency of semiconductor lasers to >100 GHz [49], useful for high speed communications with directly modulated lasers.

2.7 Conclusion

This chapter gives a theoretical overview of the main topics that need to be known to allow a detailed understanding of the experimental work in this thesis. Chapter 2 provides a basis for the theoretical aspects of the work. Key effects during signal propagation in

optical fibres are presented, including dispersion and nonlinear refraction. Fibre optical parametric amplification is introduced, as well as the phase matching technique that allows efficient parametric amplification by careful selection of the pump(s) wavelengths relative to the fibre zero dispersion wavelength. This is followed by a mention of some of the inelastic scattering mechanisms in fibre of relevance to parametric amplifier design, particularly stimulated Brillouin scattering (SBS). The Nonlinear Schrödinger Equation (NLSE) is introduced and its solution by use of the Split Step Fourier Method (SSFM) described. This was used to perform numerical simulations of the parametric devices used for amplification and regeneration, as described in later chapters. Finally, the process of injection locking of semiconductor lasers is briefly introduced. Injection locking plays a key role in the phase sensitive regeneration demonstrations presented in this thesis.

Chapter 3

Phase Sensitive Amplification

3.1 Introduction

Phase sensitive optical amplifiers exhibit gain characteristics that depend on the phase of the input optical signal relative to some local optical reference. The theory of PSAs is more than five decades old, and interest in them first stemmed from a semi-classical realisation that knowledge of signal phase allows signal measurements to be made more precisely than the Uncertainty Principle dictates [50], and later from a more in-depth analysis by Caves [51] that showed how this could be used for noiseless amplification. Research efforts into PSA increased significantly due to the new knowledge of their ability to *squeeze* the characteristics of any input light causing fluctuations below the quantum limit in one of the two phase quadratures; an excellent review by Slusher and Yurke [52] highlights the diverse applications of squeezed light in communications and sensing. Second order nonlinearity in bulk crystals was used to demonstrate degenerate phase sensitive amplification, both for squeezing [52] and amplification below the 3 dB quantum noise limit [17].

Practical PSAs deployed within optical networks would allow significant benefits - increased receiver OSNR allowing more spectrally efficient communications, increased amplifier spans and interesting photon correlation characteristics of possible interest for quantum communications. The ability to provide different gains to the two phase quadratures can also be used for all-optical signal processing, including phase regeneration and signal sampling/characterisation. Performing PSA using third order nonlinearity in optical fibers rather than in second order crystals was a first step towards practical network applications due to increased robustness, improved power efficiency and ease of system integration. Marhic et. al. successfully demonstrated the first degenerate FOPA by 1991 [53], but progress in the field was quite limited up until the demonstration of amplification with 1.8 dB NF by Imajuku et. al. in 1999 [54]. Further experimental work by Tang et. al. showed that phase sensitive gain could be obtained

over wide bandwidths [55, 56], although these results were not accompanied by noise figure measurements.

Prior to the start of PHASORS, PSAs were generally regarded as interesting, but impractical. They require precise phase-locking between the pump and signal waves to obtain stable low noise amplification, an issue that was sidestepped in the early demonstrations either by locally generating the pump and signal fields and ensuring that they never lose coherence [53], or by using phase modulation free beams that can be directly synchronised using techniques such as injection locking [57] and optical phase locked loops [58]. In addition, SBS was clearly identified as a limiting factor in FOPA performance by Imajuku et. al. [18], hence the need for the development of new SBS suppressed HNLF designs. PHASORS sought to bring together various groups of expertise to collectively tackle these challenges and develop practical PS-FOPAs exhibiting flat gain over at least 20 nm. This chapter documents the steps towards achieving this target, including an initial understanding of low noise amplification as a concept, development of a theoretical modelling capability for PS-FOPAs, detailed characterisation of wideband PS-FOPAs, and several experimental demonstrations of PS-FOPA.

3.2 Background

3.2.1 Amplifier Noise Figure

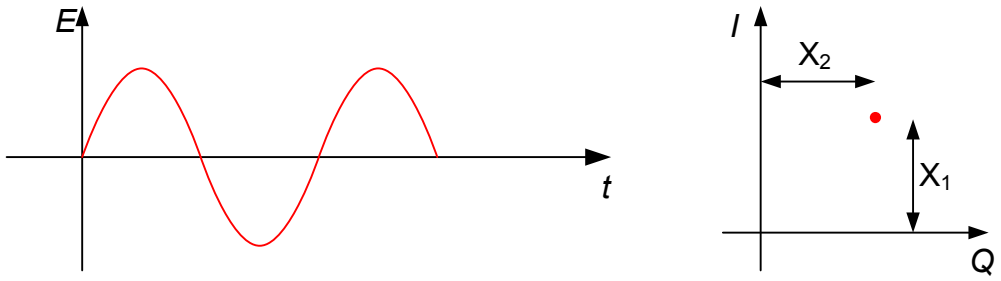

FIGURE 3.1: Representation of the noiseless $\vec{E}$-field.

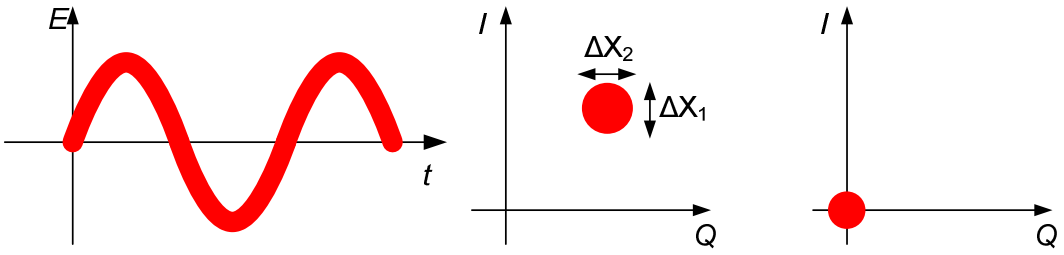

FIGURE 3.2: Representation of a real time $\vec{E}$-field, classical signal, and vacuum state.

The electric field component of electromagnetic waves can be represented either by a time varying intensity plot, or in the complex form in which the magnitudes of the in-phase and quadrature components, X_1 and X_2, are plotted, as shown in Fig 3.1. The power of the wave, which is proportional to the square of intensity, is given by $E^2 = X_1^2 + X_2^2$, while its phase $\phi = tan^{-1}(X_1/X_2)$. In reality, the inherent *uncertainty* in position and momentum of photons means that there are always fluctuations in the values of X_1 and X_2 [51]. As a result, a better representation of the electric field is as shown in Fig. 3.2.

Rather than being perfect, uncertainty means that the waves have fluctuations in both I and Q quadrature components. As such they are best depicted on the constellation diagram as circles, rather than points. The standard deviations of these fluctuations are ΔX_1 and ΔX_2. These fluctuations can be thought of as noise, and the noise power $\Delta E^2 = \Delta X_1^2 + \Delta X_2^2$. The area of the circle is consequently a good measure of the noise power in the wave. There is a minimum uncertainty possessed by every electromagnetic wave, and therefore the circle can not be shrunk to a point, not even if the wave is attenuated to the point where its mean intensity is zero - this is called a *vacuum* state. The quality of a signal is given by the *signal-to-noise ratio* (SNR), $E^2/\Delta E^2 = (X_1^2 + X_2^2)/(\Delta X_1^2 + \Delta X_2^2)$.

Because classical measurement devices (such as photodiodes) are very noisy in relation to their quantum counterparts, optical amplification is required to meet the receiver power requirements in optical communications links. Optical amplifiers can be classed into *linear* and *nonlinear* categories. With linear amplifiers, the output power is a constant multiple of the input power, with this multiple (the gain) being independent of the input power. With nonlinear amplifiers, the gain is a function of input power. All real amplifiers are nonlinear; linearity is only observed by constraining the input powers to a defined range. Note that linearity is a characteristic of the *gain*, not the *gain mechanism*, and therefore amplifiers based on optical nonlinearity as the gain mechanism, such as the FOPA, can still be made to operate linearly, for all intents and purposes. Linear amplifiers are characterized by their *gain*, as well as *noise figure* (NF).The noise figure of a linear amplifier is the ratio of the SNR before and the SNR after the amplifier, i.e. $(NF) = SNR_{in}/SNR_{out}$.

3.2.1.1 Quantum Noise Limit

For conventional PI amplifiers (such as EDFAs and PI-FOPAs) with gain G, where $G \geq 1$, there is a minimum NF derivable from Heisenbergs Uncertainty Principle [51]:

$$NF_{PIA} \quad \geq \quad \left|2 - \frac{1}{G}\right| \tag{3.1}$$

For large values of G, the NF tends to 2 (or 3 dB in logarithmic terms). This is often referred to as the classic 3 dB *quantum noise limit*. The origin of this minimum NF is the

quantum nature of both the signal and the amplifier. The internal mechanisms (modes) of the amplifier interact with the input signal to generate gain. These modes are always subject to a certain amount of fluctuations in phase and amplitude (uncertainty), which are added to the signals during amplification [51]. Taking the FOPA as an example, the signal experiences gain through an interaction involving the idler, which will add its quantum fluctuations to those already present in the signal at the amplifier input [17]. Note that there will always be a minimum amount of energy present at the idler input, corresponding to vacuum fluctuations [51]. In the EDFA, the gain mechanism is accompanied by a spontaneous emission process that adds extra noise to the amplified signals [51].

In phase sensitive amplifiers, the gains experienced by the I and Q quadratures are different, and can be denoted as G_1 and G_2 respectively. The minimum noise figure for such an amplifier (provided that at least one of G_1 and G_2 is greater than or equal to 1) is then given by [51]

$$NF_{PSA} \quad \geq \quad \left| 2 - \frac{1}{G_1 G_2} \right| \tag{3.2}$$

By designing the amplifier such that $G_2 = {G_1}^{-1}$, the NF can be made to equal 1 (0 dB). It is important to question why this condition does not violate the Uncertainty Principle. The answer lies in the fact that attenuation intrinsically adds noise to quantum noise limited signals. It can be shown that applying an attenuation of G^{-1} to a shot-noise limited signal is equivalent to a noise figure of G [15], and therefore the PSA is able to selectively add all its noise to the de-amplified quadrature, and therefore information in the orthogonal quadrature can be amplified perfectly. The better noise performance comes at the cost of the de-amplified quadrature not being available to transmit information. While this as a result might be seen to offer no overall benefit, there are systems in which information is encoded in one quadrature only to make detection easier, in which case the benefits of PSA amplification may be extracted.

3.2.1.2 Noise Figure of Cascaded Links

Communications links typically contain cascades of amplifiers and lossy sections. Given that single PSAs have a 3 dB NF advantage over PIAs , what is the net benefit in a chain of multiple amplifier + loss sections?

There are two broad classifications of gain-equalised cascaded amplifier links (see Fig. 3.3). In *type A* links, every lossy section is pre-compensated by amplification, while in *type B* links the compensation happens after the loss. The aggregate noise figure for such cascades has been studied extensively [15, 59]. For the case of a chain of n amplifier + loss spans where all amplifiers have identical noise figure F, then the aggregate NFs are

$$NF_A = 1 + nF(1 - \frac{1}{G}) \tag{3.3}$$

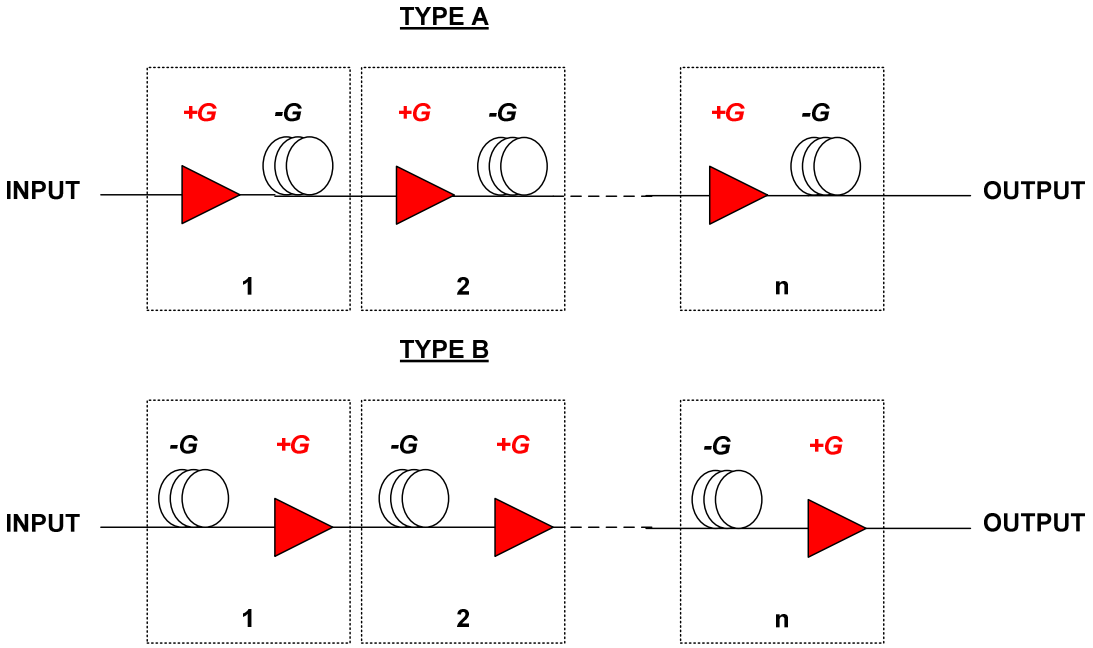

FIGURE 3.3: Classes of gain equalised amplifier+loss cascades.

$$NF_B = 1 + nFG(1 - \frac{1}{G}) \tag{3.4}$$

If $n \gg 1$ and $G \gg 1$, from Eqns. 3.3 and 3.4 it can be deduced that improving the NF of each amplifier by M dB leads to an M dB improvement in the overall NF for both type A and type B links. As such substituting quantum limited amplifiers with phase sensitive amplifiers in a long, multi-span link yields on overall 3 dB NF improvement. This additional margin can be used in a number of ways. First, from Shannon's communication theorem [60], 3 dB SNR improvement is sufficient to increase the information carrying capacity of the link by 1 bit/s/Hz, and therefore the modulation format of signals in the link for a fixed receiver BER could, as an example, be upgraded from 3 bit/symbol 8-PSK to 4 bit/symbol 16-PSK with no penalty (in principle). The situation in a real link is more complicated because of the presence of deleterious nonlinear interactions during transmission. A simple numerical comparison is shown here by simulating a single 10 Gbit/s DPSK channel, propagating down a 3000 km dispersion compensated link, evaluated using the split-step method implemented with commercial software, *VPI Transmission Maker*. The link configuration is shown in Fig. 3.4, and compares the use of classical amplifiers of NF 3.5 dB with sub-quantum amplifiers of NF 0.5 dB. Note that a blackbox amplifier model used, and therefore the simulation is not specific to any particular amplifier technology. The estimated BER at the link output as the launch power is varied is shown in Fig. 3.5.

From Fig. 3.5, it is visible that the span using the 0.5 dB NF amplifiers provides better performance at almost all launched power levels. In the low launch power regime (around

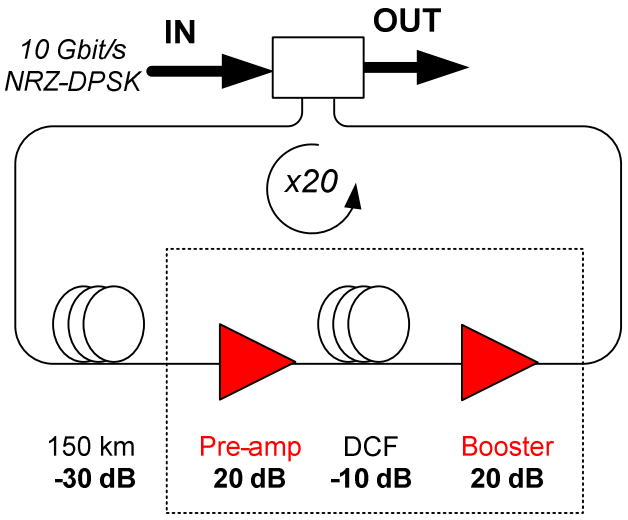

FIGURE 3.4: Numerical simulation of a type B link.

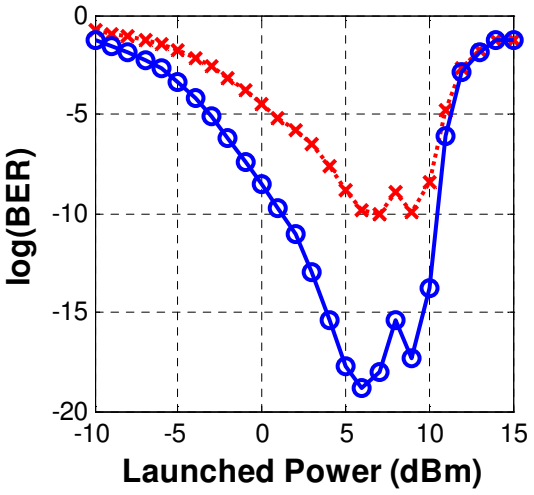

FIGURE 3.5: Launch power vs BER for simulated type B link, blue circles show link with 0.5 dB NF amplifiers, red crosses show 3.5 dB NF amplifier link.

-5 dBm), the link is dominated by linear noise, predominantly quantum noise from the lossy fibre sections and the amplifier added noise, and the 3 dB advantage of the 0.5 dB NF link can be observed. As power levels rise further, nonlinearity starts to become a significant impairment, providing a lower bound on the measured BER. However, the lower NF still demonstrates better BER performance. The reason for this is that most of the nonlinear impairment arises from Kerr induced interactions between noise and the signal, and as a result the 0.5 dB NF link in which less noise is generated is less degraded by nonlinearity.

In order to implement a fully non-degenerate PSA link, both signal and idler fields would have to propagate down the channel, bearing identical information, and with

equal power. Tong et. al. [59] have argued that in the case of non-degenerate PSAs, the overall link improvement can be 6 dB compared to using PIAs. This conclusion is reached if the NF is measured by comparing the SNR of the signal before and after the link, with a -3 dB NF suggested as being possible for a type A link. However, it is obvious that this argument is flawed even without knowing the details of the amplification mechanism in non-degenerate PSAs - a negative NF implies that more information is received at the output of the link than was present at its input. This incorrect conclusion is drawn by neglecting the power of the idler beam in the SNR calculation - if both signal and idler powers coherently combined are taken to constitute the amplifier input (as is the physical case), then the overall link improvement for PSA over PIA links returns to a more plausible 3 dB. It is prudent to note that this 3 dB advantage comes at the expense of half the information carrying capacity of the link being unused because the signal and idler channels must be correlated.

3.3 Fibre Based Phase Sensitive Amplification

3.3.1 Interferometric Fiber Based PSA

The first demonstrations of PSA in optical fiber relied on interferometric techniques [53, 54]; Marhic et. al. (1991) mention the reasons for this preference over non-degenerate four wave mixing (NDFWM), "*Although high parametric gains have been achieved in fibres by NDFWM, the scheme suffers from limitations due to dispersion, such as restricted choice of wavelengths and limited speed ... Also, NDFWM requires the use of at least two different frequencies, thereby complicating experiments.*"

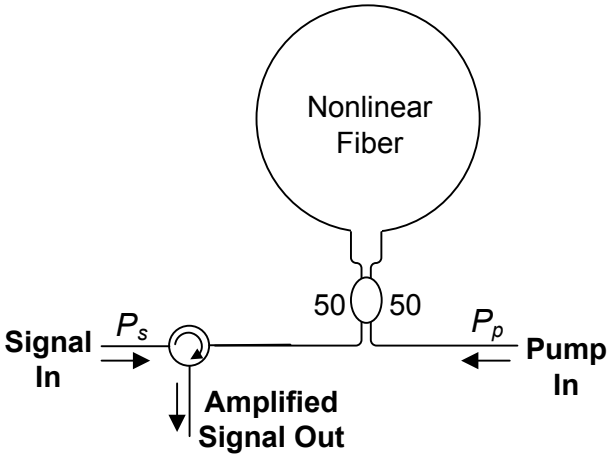

FIGURE 3.6: Interferometric fiber based PSA schematic

Fig. 3.6 shows the setup for a typical interferometric PS-FOPA, based around a Sagnac interferometer. A 3 dB splitter is used to combine a strong pump with a signal, both

of which are phase locked at the same frequency. The outputs of the splitter are then coupled either into the opposite ends of a nonlinear fiber, allowing the combined beam from each splitter port to travel separately from that emerging from the other splitter port. Following a nonlinear interaction in the fiber, the two beams are recombined in the splitter, and an amplified version of the signal can be seen to emerge from the same splitter input port as the signal, and can be retrieved using a circulator as shown. A modification to this setup would be to send the two combined outputs through separate fibers and have a second 3 dB splitter to separate the signal and pump, effectively creating a nonlinear Mach-Zender interferometer, but this requires two length matched nonlinear fibers and is susceptible to acoustic and thermally induced phase pertubations, hence is more unstable.

The gain expression for this device can be found in a straightforward fashion. Assuming P_s and P_p to be the input signal and pump powers respectively, γ to be the nonlinear coefficient of the fiber, L to be the effective length of the fiber and ϕ to be the phase difference between signal and pump at the splitter, then the output signal power P_S can be found as [53, 61]

$$\begin{aligned} P_S(\phi) = P_s \cos^2\left(\Phi_{NL}\cos\left(\phi\right)\right) + P_p \sin^2\left(\Phi_{NL}\cos\left(\phi\right)\right) \\ - \sqrt{\left(P_p P_s\right)}\sin\left(\phi\right)\,\sin\left(2\Phi_{NL}\cos\left(\phi\right)\right) \end{aligned} \tag{3.5}$$

where

$$\Phi_{NL} = \gamma L\sqrt{P_s P_p} \tag{3.6}$$

Note that Eqn. 3.5 assumes that dispersion is negligible (a valid assumption for narrow-band signals) and that the losses in the fiber are small. If $P_p \gg P_s$ and $\Phi_{NL} \ll 1$, then the small angle approximation can be applied to Eqn. 3.5, giving

$$\begin{aligned} P_S(\phi) = P_s\left(1 - \frac{{\Phi_{NL}}^2}{2}\cos^2(\phi)\right) + P_p{\Phi_{NL}}^2\cos^2(\phi) \\ - 2\Phi_{NL}\sqrt{\left(P_p P_s\right)}\sin\left(\phi\right)\cos(\phi) \end{aligned} \tag{3.7}$$

It is clear from Eqn. 3.7 that the signal gain will vary with phase ϕ with 2π periodicity. The solutions for the maximum and minimum gain, G_1 and G_2 respectively, are well known to be [61]

$$G_1 = 1 + 2\Phi^2 + 2\Phi\sqrt{1+\Phi^2} \tag{3.8}$$

$$G_2 = 1 + 2\Phi^2 - 2\Phi\sqrt{1+\Phi^2} \tag{3.9}$$

where

$$\Phi = \frac{\gamma L P_p}{2} \tag{3.10}$$

Because $G_1 \cdot G_2 = 1$, from Eqn. 3.2 it can be calculated that the NF for such an amplifier would be 0 dB. This of course is only a semi-classical derivation, for a more detailed quantum-mechanical analysis see Shirasaki et. al. [62]. Note that the maximum gain

varies with $(\gamma L P_p)^2$; this will be referred to shortly while comparing interferometric and non-interferometric PSAs.

3.3.2 Non-Interferometric Fiber Based PSA

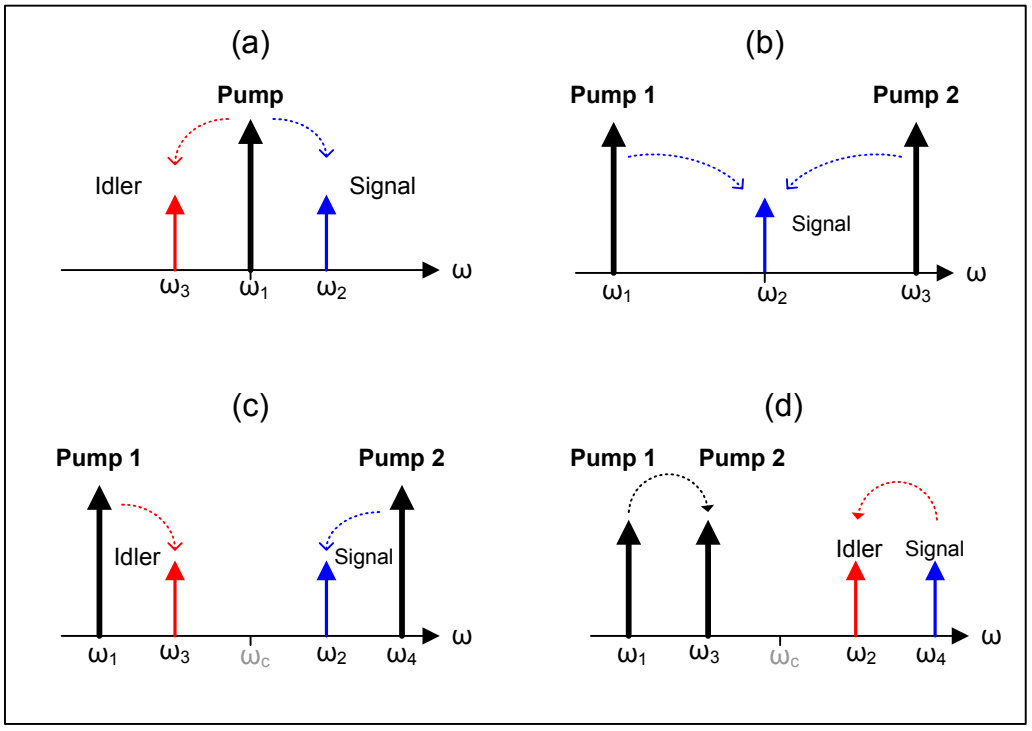

FIGURE 3.7: Phase sensitive FOPA configurations: (a) non-degenerate single pump, (b) degenerate dual pump, (c) non-degenerate dual pump, (d) dual pump wavelength exchanger.

There are four possible FOPA configurations for all optical network applications. In the non-degenerate single pump (1P) FOPA, two photons, one at each of the signal and idler wavelengths, are created following the annihilation of two pump photons, Fig. 3.7a. In the degenerate dual pump (2P) FOPA , two photons, one from each pump, are annihilated as the signal gains two photons, Fig. 3.7b. In the non-degenerate 2P FOPA, each pump loses a photon while the signal and idler simultaneously gain one, Fig. 3.7c. Finally, a modification of the non-degenerate 2P FOPA is the dual pump wavelength exchanger [63]. In this device, the signal/idler naming conventions are maintained only for convenience; in fact the signal serves to pump the idler and vice versa, Fig. 3.7d. The efficiency of all these parametric processes, particularly wavelength exchange, is very sensitive to the location of the central frequency relative to the zero dispersion wavelength.

The solutions to the coupled equations linking the pump, signal and idler in a non-degenerate FOPA have been studied analytically in [44, 64]. For a non-degenerate single

pump PS-FOPA, assuming a fiber of effective length L and nonlinear coefficient γ, input signal and idler power P_s and P_i respectively, and pump power P_p, then neglecting pump depletion, the FOPA signal gain G can be found as

$$G = \cosh(gL) + \frac{i}{g}\left(\frac{\kappa}{2} + r\eta\exp(-i\phi_{rel})\right)\sinh(gL) \tag{3.11}$$

Where $\eta^2 = \frac{P_i}{P_s}$, $r = 2\gamma P_p$, the phase mismatch κ is as defined in Eqn. 2.17, the relative phase ϕ_{rel} is as defined in Eqn. 2.14 (for $z = 0$), and the parametric gain coefficient $g = \sqrt{r^2 - \frac{\kappa}{2}^2}$. If the FOPA is perfectly phase matched, i.e $\kappa = 0$, and $\eta = 1$, then Eqn. 3.11 reduces to

$$G = \cosh(2\gamma P_p L) + \exp\left(-i\left(\phi_{rel} + \frac{\pi}{2}\right)\right)\sinh\left(2\gamma P_p L\right) \tag{3.12}$$

The maximum and minimum values of G (i.e. G_1 and G_2 respectively) are found by substituting $\phi_{rel} = -\pi/2, \pi/2$ into Eqn. 3.12, and using the identities linking exponential and hyperbolic functions, leading to

$$G_1 = \exp(2\gamma P_p L) \tag{3.13}$$

$$G_2 = \exp(-2\gamma P_p L) \tag{3.14}$$

Once again, $G_1 \cdot G_2 = 1$, and from Eqn. 3.2 it can be calculated that the NF for such an amplifier would be 0 dB. This solution is generally valid up to pump depletion levels of around 50% [13].

Code was written in MATLAB to implement this solution to show some key non-degenerate FOPA characteristics. Unless stated otherwise the parameters used are ZDW 1542 nm, dispersion slope 0.02 ps/nm^2/km, nonlinear coefficient 11.7 /W/km and length 150 m. For the 1P-FOPA the pump was at 1553 nm, while for the 2P-FOPA the pumps were at 1545 nm and 1561 nm. The model neglects fibre losses which thanks to advances in conventional HNLF design and fabrication are typically very low; for losses of 2 dB/km (which are often bettered in conventional Ge-doped silica HNLF), the effective length (as calculated using Eqn. 2.8) would be 143 m which is very close to the true 150 m length, justifying this simplification.

As discussed previously, when both signal and idler are present at the FOPA input, the behavior is phase sensitive and the gain varies as a function of the relative input phase (with a period of 2π). The difference between the maximal gain and maximal attenuation (~38 dB for a pump power of 2W as shown in Fig. 3.8) will be referred to as the phase sensitive swing.

The maximal gain is equal to the maximal attenuation if the signal and idler intensities are equal at the amplifier input. An increase in the pump power leads to higher gains, while the absolute relative input phase for which the maximum is achieved changes, Fig.

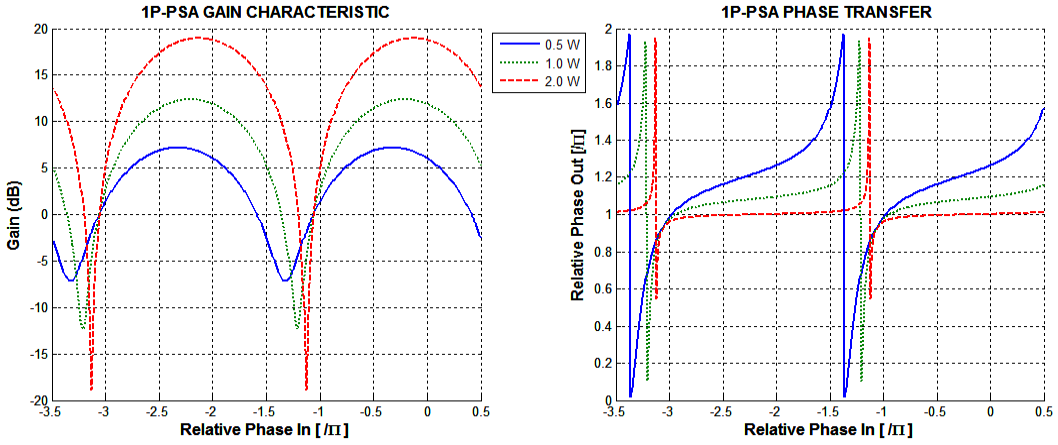

FIGURE 3.8: Simulated gain and phase transfer characteristics of 1 pump non-degenerate PS-FOPA showing phase dependent gain and step phase transfer function at high gain.

3.8. As expected, the maximum attenuation also increases, while the associated dip in the gain-versus-phase characteristic is narrower, leading to a stricter phase stabilization requirement in order to achieve the maximum de-amplification. The phase transfer characteristic shows an important property of PS-FOPAs at high gains (PS swing $>$ 10 dB), they have a flat relative phase transfer characteristic. This suggests that PS-FOPAs can be used for performing phase regeneration. Similar characteristics can be derived for the 2P PS-FOPA case.

3.3.3 Comparison Between Interferometric and Non-Interferometric PS-FOPA

The expressions for the maximum gain of the interferometric PS-FOPA, Eqn. 3.8, and that of the phase-matched non-interferometric non-degenerate PS-FOPA, Eqn. 3.13 show that in the case of the former, the gain scales quadratically with pump power as compared to exponentially in the latter. As an example, for a fiber of nonlinear coefficient 12 /W/km and effective length 200 m (values chosen to correspond to parameters of OFS Ge-doped silica HNLF available in the lab for experiments), the expected gains in interferometric and non-interferometric mode are shown in Fig. 3.9.

For these parameters, achieving 20 dB gain would require 4 W of pump power in the interferometric PSA, as compared to 1 W in the non-interferometric. In addition, the interferometric PSA is inherently single channel, while the non-interferometric device can operate with multiple signals provided that corresponding idlers are presented at the device input. With all this in mind, non-interferometric PSA was chosen as the preferred choice for PHASORS, and any reference to PS-FOPA hereon refers to the non-interferometric configuration.

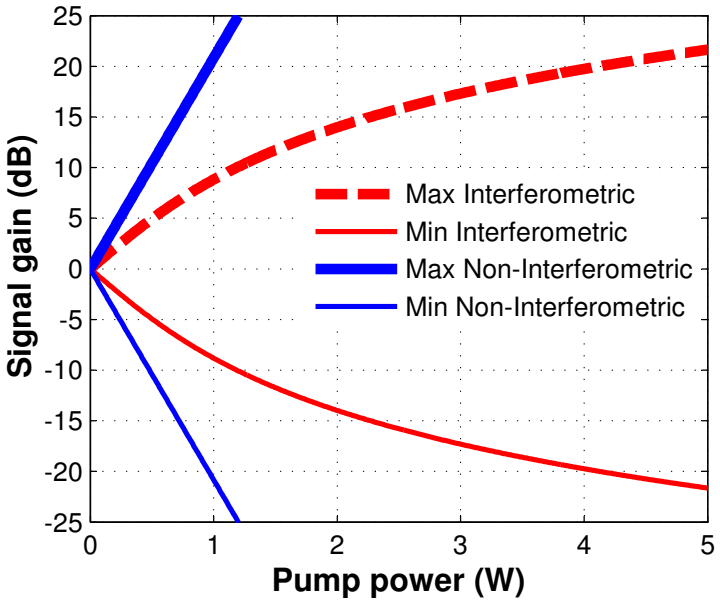

FIGURE 3.9: Comparison of gain characteristics in single pump PS-FOPA based on interferometric and phase matched non-interferometric approaches.

3.4 Wideband Experimental PS-FOPA Characterisation

Having chosen the non-interferometric PSA as the configuration of choice for further investigations into PSAs, it was necessary to develop an experimental testbed to investigate practical issues regarding the suitability of components developed by consortium partners for incorporation in a PSA, understand the practical limits to PSA performance, and to develop simple but proven theoretical modelling tools for these subsystems.

A non-interferometric PS-FOPA requires the injection of three or four waves: one or two pumps, and a signal-idler pair to be amplified/de-amplified. Several different signal-idler pairs can be phase-sensitively amplified at the same time and, thus, is in principle compatible with WDM systems. Note that transmission of both signal and idler in separate channels means that twice as much bandwidth is required as compared to a system based on PIAs. The interacting waves need to be phase-locked to observe the phase sensitive behavior. Such phase-locked waves can be derived by using electro-optic modulation (EOM) of a narrow linewidth optical source, producing multiple sidebands locked to the carrier [65]. However, current EOM technology limits the bandwidth achievable via this technique to a few 100 GHz at best.

A wideband PSA can also be created by cascading two FOPAs, generating a phase-locked but conjugated idler in the first FOPA, and achieving PSA operation in the second one. This was first demonstrated in [55] using a short dispersive fibre to introduce a

wavelength-dependent relative phase shift[1]. This cascaded FOPA concept is introduced here, and its suitability for wideband PSA demonstrations without needing to perform sophisticated phase locking will soon be apparent.

3.4.1 Cascaded PS-FOPA Concept

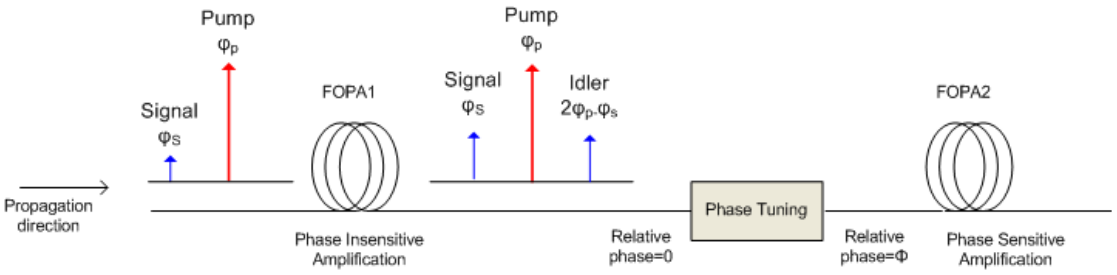

FIGURE 3.10: Cascaded PS-FOPA demonstration; in FOPA1 phase uncorrelated pump and signal are mixed to generate an idler that is phase locked to the pair of them, in FOPA2 a PS interaction between all three waves can be observed.

To easily observe the PS interaction in the time domain it was necessary to stabilize the relative phase of the interacting waves for the whole duration of the observation; this could be done using the cascaded PS-FOPA approach as discussed above [55] and is illustrated in Fig. 3.10. The idea is to inject a pump and a signal into a first HNLF thereby generating a phase conjugated idler. The relative phase between pump, signal and idler is then altered in a controlled way before all three waves are coupled into a second HNLF, in which they now interact in a PS manner. Note that the output relative phase of the first stage FOPA is always stabilized regardless of phase fluctuations between signal and pump, since all the waves travel in the same path . It is therefore locked at the input to the second stage. By changing the phase of one or more of the waves, the relative phase, ϕ_{rel}, at the input of FOPA2 can be set to an arbitrary value. The first demonstrations of PSA using this technique relied on using dispersion between FOPA1 and FOPA2 to induce a wavelength dependent relative phase modulation [55]. In the following section a similar experiment is reported, where a programmable filter (Opt. Proc., Finisar Waveshaper 4000E) was used in order to conveniently and controllably vary the input relative phase.

3.4.2 Cascaded PS-FOPA Experimental Demonstration

At the point in time in which these first detailed PSA studies were carried out, there were no low dispersion SBS suppressed fibers available from the project partners to

[1]The same method was later used by PHASORS partners at the University of Chalmers [66, 67] to demonstrate a sub-quantum limit NF of the PSA stage. However, it should be noted that the NF of the combined system is limited by the 3 dB quantum limit of the PIA stage.

work with. Consequently, the choice of experimental setup had to be compatible with conventional SBS suppression techniques, and the most convenient of these is pump phase modulation. The cascaded FOPA was therefore an ideal approach because it is possible to phase modulate the pump before the first stage and still observe PSA in the second.

Having carried out a few preliminary experiments using two FOPAs with the Waveshaper between them, a decision was made to collaborate with the partners at the University of Chalmers on an experiment that was directly relevant both to Southampton, as a basis for the phase regeneration work carried out later on, and to Chalmers for the low noise PSA work. At the time, there was a developed testbed for phase insensitive FOPAs at Chalmers, with an SBS suppression setup optimised to couple more than 4 W of power into 200 m silica HNLFs, and with pump wavelengths optimised for the fiber samples at hand. A joint set of experiments was an opportunity to leverage both groups' knowledge. These experiments were performed in Chalmers, and their results are described here. The measurements and data analysis were performed jointly in April 2009 with Carl Lundström, a PhD student in the group of Prof. Peter Andrekson at the University of Chalmers.

3.4.2.1 Experimental Setup

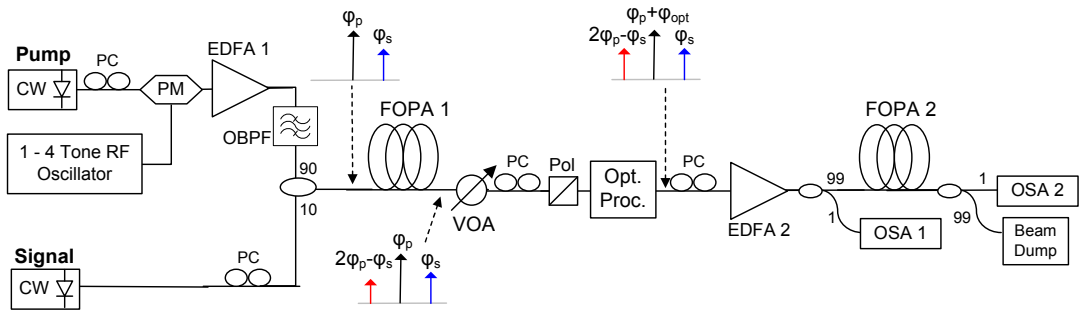

FIGURE 3.11: PSA setup based on cascaded PS-FOPA. PM: phase modulator, PC: polarization controller, OBPF: optical bandpass filter, VOA: variable optical attenuator, OSA: optical spectrum analyzer.

The experimental setup is shown in Fig. 3.11. A tunable laser (TL) set at 1553.0 nm was used as a pump source. Unless stated otherwise the pump was phase modulated with four RF tones at approximately 100, 300, 900 and 2700 MHz, increasing the pump linewidth up to 10 GHz to suppress SBS. The pump was then amplified to 3.8 W in EDFA1, and filtered by a 2 nm-bandwidth optical filter to suppress ASE. A second tunable laser was used as the signal source and the pump and signal were combined via a 10 dB coupler into FOPA1, where a conjugated idler was generated by FWM. FOPA1

was implemented using a 150 m long HNLF, with a nonlinearity coefficient of 10 /W/km and ZDW 1542 nm.

The output, consisting of three phase locked waves, was then passed through a 10 dB coupler, a polarizer and a variable optical attenuator (VOA). The polarizer provided a polarization reference for all three waves going into FOPA2 and ensured that the signals were aligned with the principal axis of EDFA2 in order to minimize the DGD accumulated in EDFA2 (measured at approximately 0.5 ps/nm). After the polarizer, the waves were subsequently passed through the Waveshaper in which the desired relative amplitudes and phases could be set. Note that by setting the idler channel attenuation to the device upper limit (35 dB) PI operation of FOPA2 could be obtained. The processor also allowed for very narrow filtering of the pump wave, removing any residual ASE.

The three waves were then amplified by EDFA2 up to 2 W, with the pump signal completely dominating the power, and injected into FOPA2. FOPA2 was implemented with a 250 m HNLF with nonlinear coefficient of 11.7 /W/km and a ZDW of 1542 nm. The input and output from FOPA2 were monitored on two optical spectrum analyzers (OSAs) via two 20 dB tap couplers.

3.4.2.2 Experimental Results

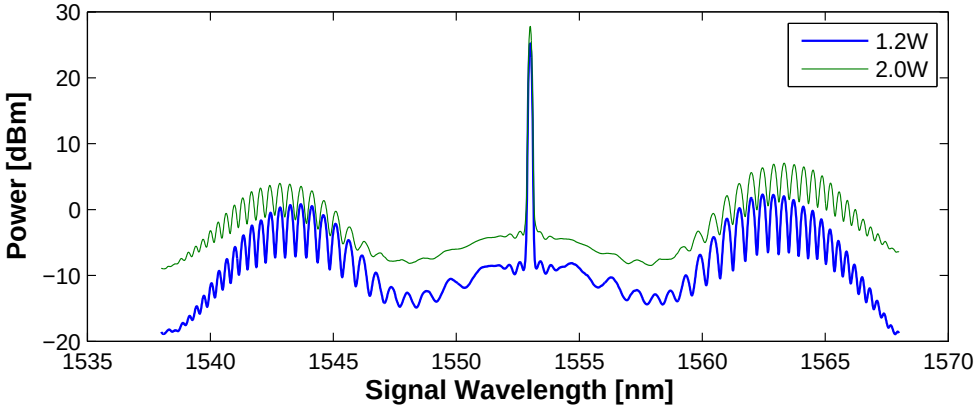

FIGURE 3.12: FOPA2 output spectra when pump and ASE from FOPA1 are coupled into FOPA2 without mid-stage filtering.

With the signal laser off and the Waveshaper configured so as to couple the parametrically amplified residual ASE from FOPA1 into FOPA2, it was possible to quickly characterize the system in terms of bandwidth, peak gain, and with limited accuracy, phase sensitivity. Fig. 3.12 shows output spectra from FOPA2 using pump power levels of 1.2 W and 2 W in FOPA2 (the pump power in FOPA1 was kept constant). Symmetric gain peaks can be seen around 1563 and 1543 nm, with the bandwidth being slightly more with the stronger pump. The ripple in the curves is a clear sign of PSA, with dispersion from the optical elements placed between the two FOPAs (fiber pigtails, EDFA

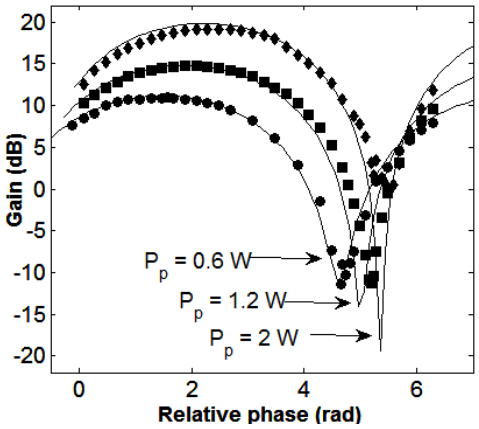

FIGURE 3.13: PSA gain at varying pump powers with signal and idler powers equalized. Solid lines are theoretical fits.

etc) causing a wavelength dependent relative phase modulation [55]. As the dispersion-induced phase scales quadratically with the frequency separation between signal and idler, the periodicity of the rippling increases with wavelength detuning from the pump.

Fig. 3.13 shows the variation of gain as a function of the relative phase for a signal at 1 nm detuning from the pump at three different pump power levels, 0.6, 1.2 and 2 W respectively. The signal and idler powers were equalized and kept 30 dB lower than the pump. At lower pump power, and consequently lower gain (circles), the maximal amplification was the same as the maximal attenuation (11 dB at 0.6 W pump power). However, as the pump power increased, this behaviour was lost. Theoretical fits were determined (as shown) by the SSFM method in Matlab, with an estimated 1 dB insertion loss between EDFA 2 and FOPA 2.

To study the sensitivity of the PSA to the signal and idler power ratio, the idler was systematically attenuated and the phase dependent gain on the signal recorded, as shown in Fig. 3.14. As expected from Eqn. 3.11, as the signal becomes significantly greater than the idler, the maximal gain and attenuation decrease and approach the gain of the PIA. Furthermore, the maximal attenuation drops off much faster than the maximal gain. It is worth noting that in Fig. 3.14 a signal/idler relative fluctuation of 1dB from the 0 dB optimal point would lead to a 7.5 dB reduction in the PS swing, of which 7 dB would be due to reduced PSA attenuation, and only 0.5 dB due to reduced maximal PSA gain. Such a fluctuation would have an impact on the device NF due to the subsequent reduction in phase squeezing.

The pump power was then varied and the phase dependent gain recorded as shown in Fig. 3.15 for a signal at a 1 nm detuning from the pump. As the pump power increased, the maximum phase sensitive gain increased by approximately 1.5 dB/dB, and the maximum phase sensitive attenuation by -1.2 dB/dB. The difficulty in achieving the theoretical maximal attenuation further highlights the limited maximal attenuation demonstrable

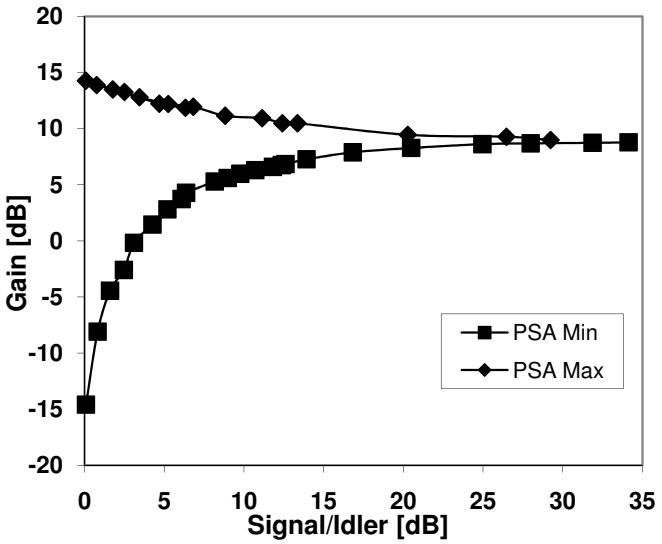

FIGURE 3.14: PSA gain as the signal-to-idler power ratio is varied. The lines are respective results of simulations using the same parameters as in the experiment. Pump power is 1.2 W and two pump modulation tones were used.

with this experimental technique. The difference between the maximal phase sensitive and the phase insensitive gain is also seen to approach 6 dB beyond a pump power of 0.8 W. Furthermore, the maximum difference PS swing achieved was 30 dB. While a higher figure of 35 dB had been previously demonstrated [27] using a Bismuth oxide fibre, the real fibre gain was not stated.

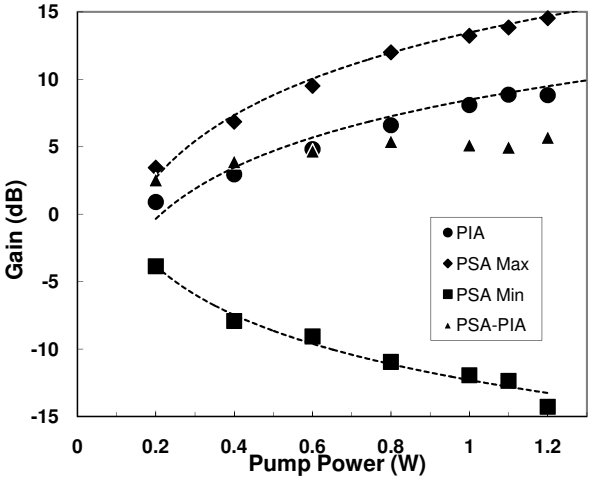

FIGURE 3.15: Measured PIA (circles), PSA maximum (diamonds), PSA minimum (squares) and difference between PIA and PSA maximum (triangles) gains of FOPA2 versus pump power. Two pump modulation tones were used.

An investigation of the gain saturation properties of the PSA was carried out by increasing the signal/idler power, while keeping the input pump power constant at 1.2 W (still at 1 nm detuning from pump). The resulting FOPA2 gain is shown in Fig. 3.16,

with a measured PSA dynamic range of about 23 dB. Since the maximum gain achievable for the PSA case is higher, it saturates before the PIA gain as can be seen by the reduction in the PSA-PIA gain difference (triangles in Fig. 3.16) from the theoretical maximum of 6 dB. Additional measurements revealed no saturation for the minimum phase sensitive gain as would be expected. By moving the signal wavelength to 1563.8 nm, which corresponded to the PSA gain peak, and increasing the pump power to 2 W, 33 dB of maximal PSA gain was achieved, albeit at the expense of a reduced PSA swing (6 dB rather than the theoretical 66 dB). This discrepancy between the expected and measured PSA swing is in some ways consistent with what was observed for the lower gain measurements earlier, although it was surprising that the difference was so big- perhaps the attenuation measurement was compromised by SBS.

Fig. 3.17 shows the measured characteristics of the PIA gain, maximum PSA gain and maximal PSA attenuation of FOPA2 as the signal and idler wavelengths were detuned from the pump. The maximum PSA gain increased with signal wavelength detuning up to 19 dB at the gain peak for a pump power of approximately 1.2 W. The PS swing was highest closest to the pump, and reduced steadily as the signal wavelength approached that of the PSA gain peak.

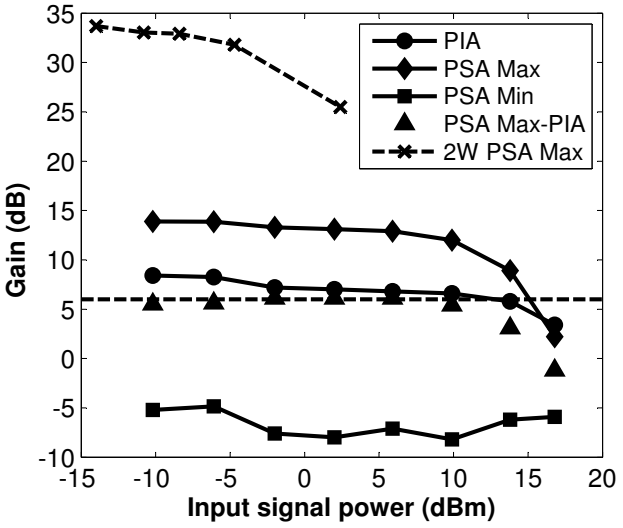

FIGURE 3.16: Measured PIA (circles), PSA maximum (diamonds), PSA minimum and difference between PIA and PSA maximum (triangles) gains of FOPA2 versus input signal power at 1nm detuning and 1.2W pump. Dashed line shows PSA gain at the gain peak with 2W pump.

3.4.2.3 Origin of Compromised Attenuation

In this set of experiments there appeared to be a limit to the maximal attenuation achievable either by varying signal phase, wavelength or pump power. This could have been due to any of a combination of phenomena. Firstly, as the maximal gain increases

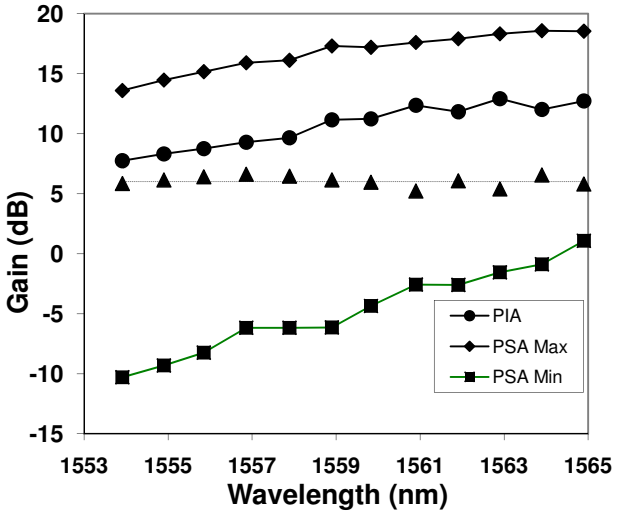

FIGURE 3.17: Measured PIA gain (circles), PSA maximum gain (diamonds), PSA maximum attenuation (squares) and difference between PIA and PSA gain (triangles) gains of FOPA2 as a function of the signal wavelength with pump power of 1.2 W.

the tolerance required to achieve maximal attenuation becomes stricter as can be seen by the narrowing of the dip in Fig. 3.12. Secondly, the use of pump dithering to suppress SBS meant that the pump and idler had linewidths on the order of 10 GHz. This rapid variation in wavelength is translated to a rapid variation in phase through dispersion, and thereby potentially distorts the relative phase. The tolerance to relative phase variations is lower closer to the gain peak (this can also be noted in the ripples in Fig. 3.12, which increase as the signal wavelength detuning increases). In addition, the PMD in EDFA2, which was estimated to be around 0.5 ps/nm, will certainly have meant that the polarization states of the various waves relative to each other at the input to FOPA2 will have varied as the detuning was increased, leading to compromised phase dependent gain. Also, as the spacing in wavelength from the pump increases, longitudinal ZDW fluctuations act to randomly detune the relative phase between the propagating waves from that precise value required for maximal attenuation [68].

3.4.3 Modified PS-FOPA With Dual Pump Capability

Analysis of the results from the joint experiments at Chalmers, as discussed previously (Section 3.4.2.3), left a number of questions unanswered, particularly with regard to achieving symmetrical PS gain and attenuation. On returning to Southampton, an in-house testbed was developed, seeking to address some of these issues, as well as extend the investigations to dual pump PSA operation. The 2P PS-FOPA was of relevance because a literature survey had indicated that this would be a good starting point from which to develop a DPSK regenerator.

The new setup, being a cascaded FOPA, had some similarities to that shown in Fig. 3.11. An additional modification was the addition of a second pump laser so that the properties of 2P PSAs could be investigated. A PM EDFA replaced the existing EDFA at the input of the PSA stage to minimize PMD and its detrimental impact. The 90-10 coupler which was previously used to combine the pump and the signal was replaced by a circulator and grating filter configuration [69] in order to filter the ASE noise coming from the EDFA and at the same time to improve by about 8 dB the insertion loss experienced by the signal. By independently modulating the two pumps using complementary electrical drive signals generated using a single RF comb and a 90° RF splitter (see Appendix A for more details), it was also possible to minimize the spectral broadening effect on the idler following FOPA1. Finally, a high speed DPSK modulator was added to the signal path to observe the PSA's effect on wideband data signals. The pump power(s) and wavelength(s) were then optimized to try and obtain up to 10 dB PSA maximal gain, which would correspond to a 20 dB PS swing.

3.4.3.1 Experimental Setup

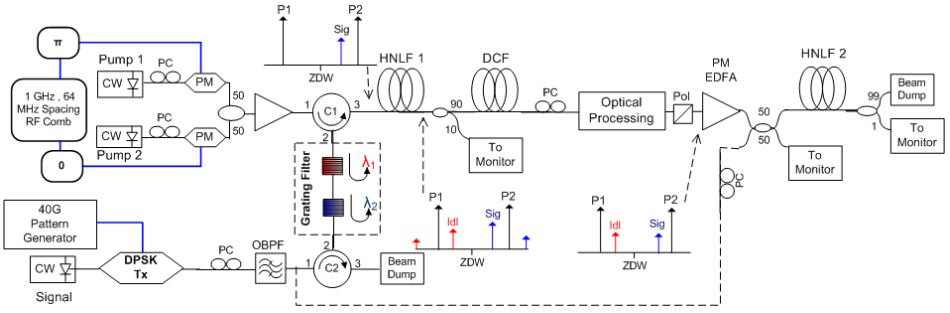

FIGURE 3.18: Improved inline PSA with added polarization and dispersion management., CW: tunable laser source, PC: polarization controller, PM: phase modulator, Pol: Polarizer, OBPF: optical bandpass filter.

This improved experimental setup for 1P and 2P PSA configurations is shown in Fig. 3.18. Two tunable lasers were counter-phase modulated using a 1 GHz RF comb of 64 MHz spaced lines to suppress SBS before being combined in a 3 dB coupler and amplified to provide pumps at 1540 and 1560.5 nm. Alternatively, one of the lasers was turned off and the other tuned to 1550 nm to convert to the 1P equivalent. The pump(s) were then launched into port 1 of circulator C1 and reflected off a single (dual) window 0.5 nm FWHM fibre grating filter to reject any out-of-band ASE. A third tunable laser was externally modulated to provide a 40 Gbit/s DPSK signal that was coupled into port 1 of circulator C2. Since the signal wavelength was different as compared to the pump(s), it was transmitted through the grating and, thus, coupled together with the pump(s) emerging from circulator C1 port 3 with a pump insertion loss <1 dB.

The pump(s) and signal were launched into HNLF 1 to generate an idler, which was phase locked to the signal and pump(s). The HNLF was 500 m long with a nonlinear coefficient of 11 /W/km and a ZDW of 1555 nm (OFS Fitel, Denmark). This was followed by a few meters of dispersion compensating fibre (DCF) to compensate for the dispersion between HNLFs 1 and 2, a Waveshaper to control the signals relative phase and amplitude, a polarizer to ensure uniform polarization alignment and a PM EDFA to boost the signals up to 0.5 W with the pump(s) dominating the power. The amplified waves were then coupled into HNLF 2 via a 3 dB coupler where they experienced PS amplification. HNLF 2 was 220 m long with nonlinear coefficient 11/W/km and ZDW 1550 nm. The second port of the coupler was used to launch the data signal from the transmitter directly into HNLF 2 to allow measurements of the absolute PI amplification by comparing the output of HNLF2 on an OSA with the pump on and off respectively. While HNLF 2 was not PM, it was assumed that this was not crucial as the fiber was not specified as having significant PMD.

3.4.3.2 Experimental Results

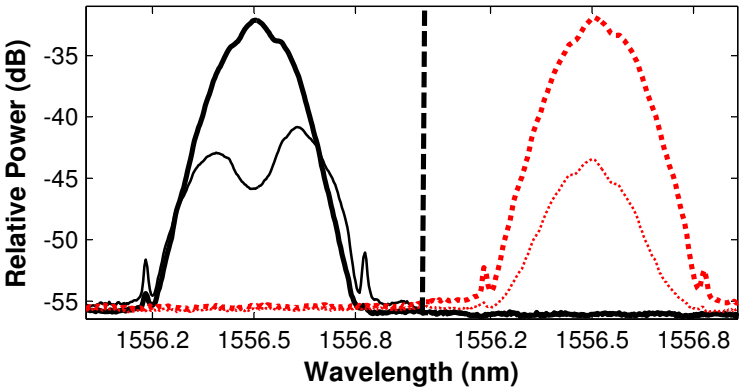

FIGURE 3.19: Spectral traces of a 40 Gbit/s DPSK signal at 2P-PSA output. Black solid thick (thin) line - No compensation PS maximum (minimum), red dashed thick (thin) line - compensated PS maximum (minimum).

Fig. 3.19 shows the impact of mid-stage dispersion compensation on a 40 Gbit/s DPSK signal when 2P-PSA configuration was considered. Although not shown, similar results were achieved for 1P-PSA. From these optical spectra, it is clear that amounts of dispersion corresponding to just a few metres of SMF between the PIA (HNLF 1) and PSA (HNLF 2) can greatly distort the transmitted data signals due to the quadratic wavelength dependence of the added phase within the signal bandwidth. This distortive effect in the spectral amplitude envelope is visibly more severe when attempting to achieve maximum PS de-amplification across the entire spectrum, due to the PSA amplitude transfer function which is steepest during de-amplification. Mid-stage dispersion compensation allows this problem to be alleviated. Note that similar minimum attenuation

at the very centre of the spectrum is achieved for compensated and uncompensated systems, implying that dispersion does not affect narrowband PSA behavior and thus could not have been the cause of compromised attenuation as proposed in Section 3.4.2.3.

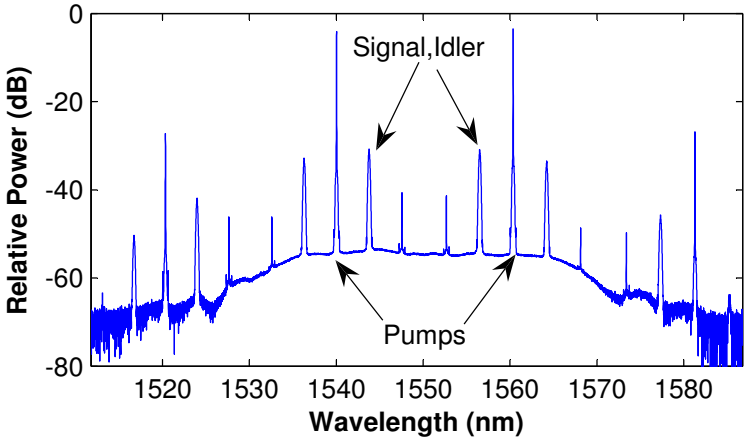

FIGURE 3.20: 2P PS-FOPA output spectra showing unwanted broadband secondary mixing products, when the signal's relative phase is optimized for maximum gain.

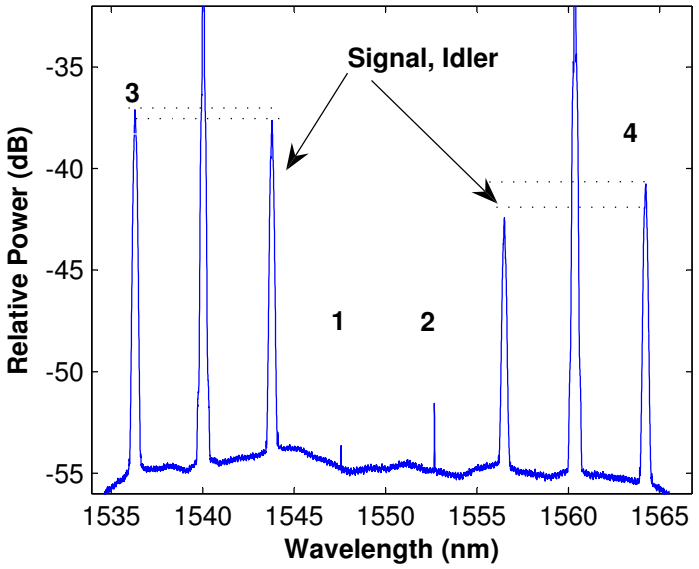

FIGURE 3.21: Impact of second order mixing products, labelled 1 - 4, generated in 2P PI-FOPA.

Figs. 3.20 and 3.21 highlight the presence of extra sidebands in 2P FOPAs. This is due to the coexistence of single pump interactions between the signal, idler and pumps at the FOPA input. These affect the PS operation, particularly during PS attenuation, and this is more severe for the case of maximal attenuation. The sidebands labelled 3 and 4 in Fig. 3.21 are generated at an early stage in HNLF 2, experience PIA and eventually become

larger than the signals, and start to affect the amount of signal attenuation achievable, adding noise to the signals in the process. These extra interactions compromise the NF obtainable with 2P FOPAs [19, 70, 71].

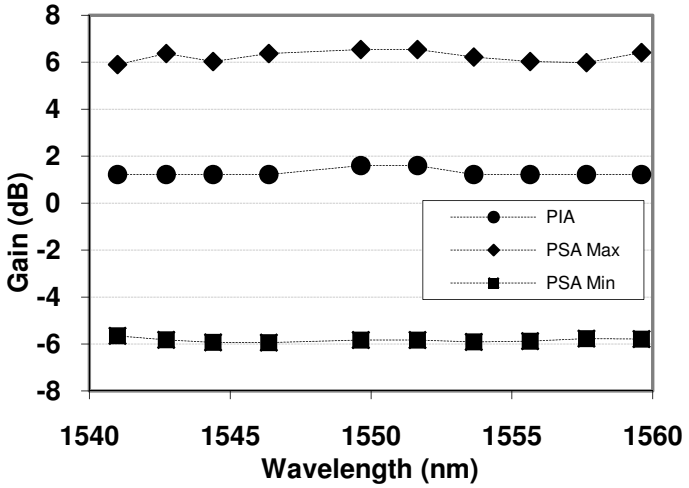

FIGURE 3.22: 1P PS-FOPA gain over 20 nm for a 0.5 W pump at 1550 nm.

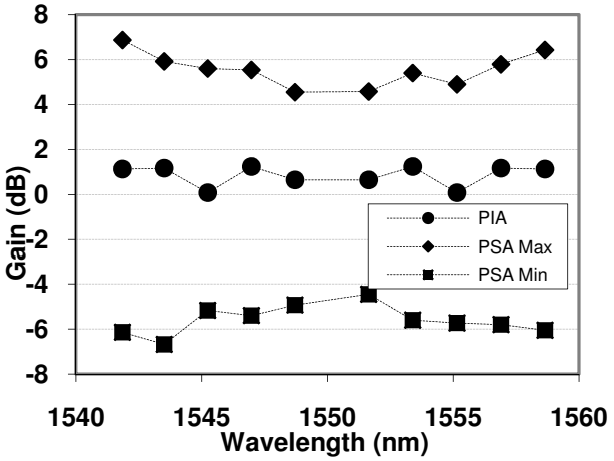

FIGURE 3.23: 2P PS-FOPA gain over 20 nm for pumps at 1540 and 1560.5 nm, a total power of 0.5 W.

Figs. 3.22 and 3.23 show the PS maximal gain, maximal attenuation and PIA gain achieved for 1P and 2P PS-FOPA for the same power level of 0.5 W and centre wavelength. The PI-FOPA gain in both cases was around 1 dB, with the maximal PS gain being 4 to 5.5 dB higher. The 1P PS-FOPA gain spectrum was flat due to the pump proximity to the fibre ZDW. In the 2P PS-FOPA case the gain variation was approximately 2.5 dB. The 2P PI-FOPA gain was around 1 dB close to the pump wavelength but decreased as the signal wavelength was further detuned from the pump wavelength. Similar behavior was observed for the PSA attenuation curves. Note that the maximal

gain and attenuation were approximately equal and opposite as expected theoretically over the full 20 nm operating bandwidth assessed for all the three cases.

Despite the modifications to the setup there were still limits to the attenuation that could be achieved experimentally, with measured peak PS swing of about 20 dB (comprising 13 dB gain and 7 dB attenuation) with the single pump configuration of this new setup. It may have been that the issue, rather than being purely with the PS-FOPA, was with the measurement technique, which relied on an OSA with a limited spectral, and consequently low temporal, resolution. Frequency or phase jitter, due to the finite pump linewidth for example, may have caused the gain to fluctuate faster than the acquisition time of the OSA, which would have caused an average power measurement higher than the instantaneous minimum signal power.

3.5 Phase Sensitive Amplification of Optical Combs

3.5.1 Introduction

Having investigated the wideband capabilities of PS-FOPAs, thought went into investigating application spaces other than phase regeneration and low noise amplification of telecom signals, both of which were already defined as PHASORS objectives. The performance of FOPAs today has been significantly improved by the advances in HNLF design, as well as improved pump sources offering high coherence and high power (especially when combined with pump pre-amplification in a DFA or Raman amplifier). Improvements in the achievable tolerance in the distributed physical characteristics of HNLF allow phase matching over long distances (on the order of hundreds of meters), allowing much broader gain bandwidths than DFAs, as well as engineerable operating windows across the IR spectrum [72] . High coherence pump sources also enable PS-FOPA operation, allowing both a NF below the 3 dB quantum limit when operated as linear devices [67], and the possibility of sophisticated signal processing functions such as phase regeneration when designed to be nonlinear [26]. Finally, by boosting pump power sufficiently FOPAs can provide very high signal gains with over 40 dB demonstrated [13].

Despite all these desirable characteristics, FOPAs as of 2011 do not offer an economically competitive alternative to DFAs, particularly for telecoms applications. This is due to a combination of many factors. DFAs are low cost and proven, having benefited from two decades of refinement in fibre and pump diode technology. DFAs [73] and FOPAs [74] have both been demonstrated to have quantum conversion efficiencies over 50%, but DFAs can achieve this figure for multi-channel WDM inputs, whilst higher levels of FWM, SPM and XPM in FOPAs make cross-talk free high quantum efficiencies in WDM operation hard to attain [13]. DFAs are also robust, have low susceptibility to stimulated Brillouin scattering SBS, and conveniently already cover the C and L band

portions of the low loss wavelength region in silica which are of most interest for current long haul optical communications. While many of these issues are being addressed by the fabrication of fibres with novel structure and composition [75] , it is interesting to assess the linear FOPA in a different light, as a device allowing multiple functionalities inherently suitable for the amplification of optical combs, particularly those derived from resonant cavity + modulator structures.

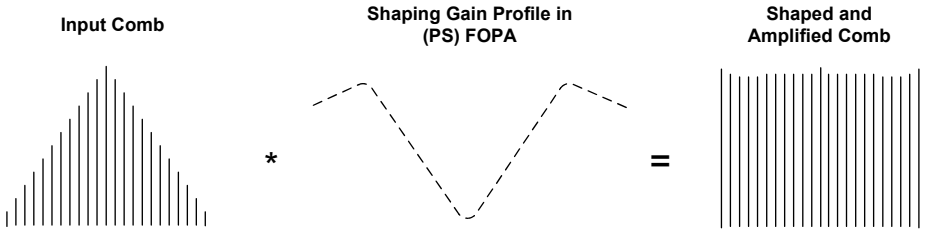

FIGURE 3.24: Illustration of aim of experiment - triangular comb amplification with intrinsically gain shaped parametric amplifier.

Optical combs provide an absolute reference in either the spectral or time domains, and as such have a vast range of applications in physical and life sciences [76]. In most comb generators, energy is transferred from a seed beam to a large number of frequency detuned comb lines, and energy conservation dictates that the individual comb lines consequently have low power and low SNR, which is further compromised whenever attempts are made to transmit the comb(s) through lossy media [77]. In addition, some combs, particularly those generated from resonant cavity structures [78] inherently have a spectral roll-off, with less power as the comb line detuning from seed carrier increases. Finally, the requirement to act as a reference means that combs are often required in spectral areas outside the telecom window. As a result, an ideal amplifier for optical combs should combine low noise with gain shaping (see Fig. 3.24) and a frequency translation capability. Here, a demonstration of how FOPAs allow all these features to be attained is made, and an attempt to objectively assess their ultimate suitability for this application follows.

3.5.2 Experimental setup

The setup is shown in Fig. 3.25. A narrow linewidth CW signal at 1550.92 nm seeded an optical frequency comb generator (OFCG) from Optocomb Inc. The OFCG comprises a phase modulator inside a high finesse Fabry Perot cavity driven with an internal 10 GHz RF clock. The output comb has a triangular 10 dB/nm spectral roll off, as well as a high insertion loss of approximately 30 dB. The comb was then passed through a reconfigurable filter (Finisar Waveshaper 4000E) which was used to switch between amplifying the full spectrum or only half of it, the necessity of which is discussed shortly.

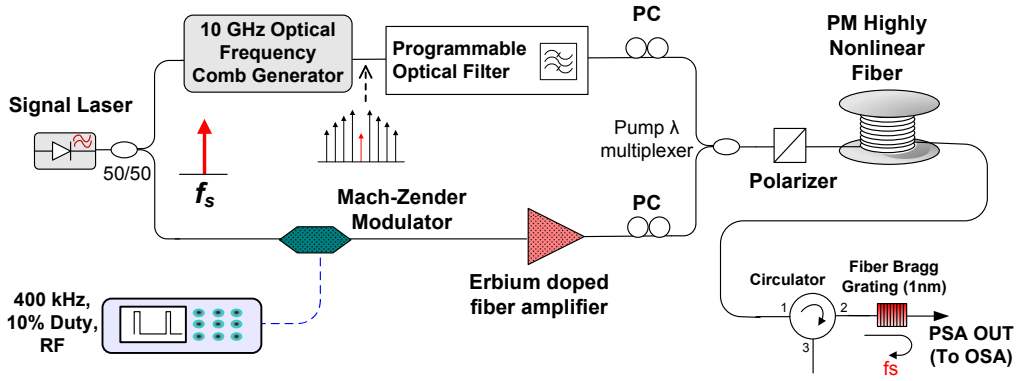

FIGURE 3.25: FOPA setup up to amplify input optical comb.

For a parametric comb amplifier, it is essential that the pump beam is locked in frequency to the comb, and for a comb spacing of Δf, at least a whole multiple of Δf away from the nearest comb line. In addition, the pump linewidth should be no more than that of the comb lines. This requirement is easily satisfied by injection locking a semiconductor laser to one of the comb lines. For simplicity though, a tap from the same laser as the comb seed was used as the pump.

The comb and pump were combined with a 100 GHz add-drop multiplexer at the pump wavelength. This suppressed comb lines within 50 GHz of the pump, although this could be reduced by using either a narrower multiplexer or a narrow grating. Polarization controllers and a polarizer ensured the comb and pump were co-polarized, and they were then launched into the fast axis of a 493 m PM HNLF (the FOPA), with fast axis ZDW 1544 nm, dispersion slope 0.029 ps/nm^2/km at 1550 nm and nonlinear coefficient 10.7 /W/Km (OFS Fitel, Denmark). The SBS threshold of this fibre was around 18 dBm, which was significantly lower than the desired launch pump power. While SBS suppression can be derived without degrading the effective pump linewidth in the parametric process by a number of techniques (as discussed in Section 2.4.3), for ease of implementation given the low dispersion fibres available, a decision was made to use a quasi-CW pump gated in an amplitude modulator at 400 kHz with a 10% duty cycle, effectively restricting the nonlinear Brillouin interaction to approximately 100 m. The comb power at the input to the FOPA was -40 dBm.

The FOPA was operable in both PI mode, in which case only the half of the comb with wavelength shorter than that of the pump was coupled into the FOPA, as well as in PS mode, in which the pump was located precisely in the middle of the symmetric comb spectrum. In PS mode, the gain experienced by each comb line depends on the instantaneous phase relationship between that comb line, the pump, and the comb line at the same spectral detuning but on the other side of the pump in frequency.

To maintain the PS-FOPA at optimal phase a feedback loop monitoring the PS-FOPA output is normally required to compensate for relative phase drifts resulting from thermal

and acoustic pickup. If n uncorrelated channels (such as multiple dispersed comb lines) are being amplified, n feedback loops (one per channel are required), an undesirable level of complexity. Instead, the OSA was set to perform multiple spectral sweeps of the output of the unlocked PS-FOPA while in maximum-hold mode. The resulting spectrum rapidly converges to that which would be measured if the pump and all the comb lines were phase locked at the PS maximum gain value. Conversely, operating the OSA in minimum-hold mode provides the PS-minimum spectrum.

3.5.3 Experimental Results

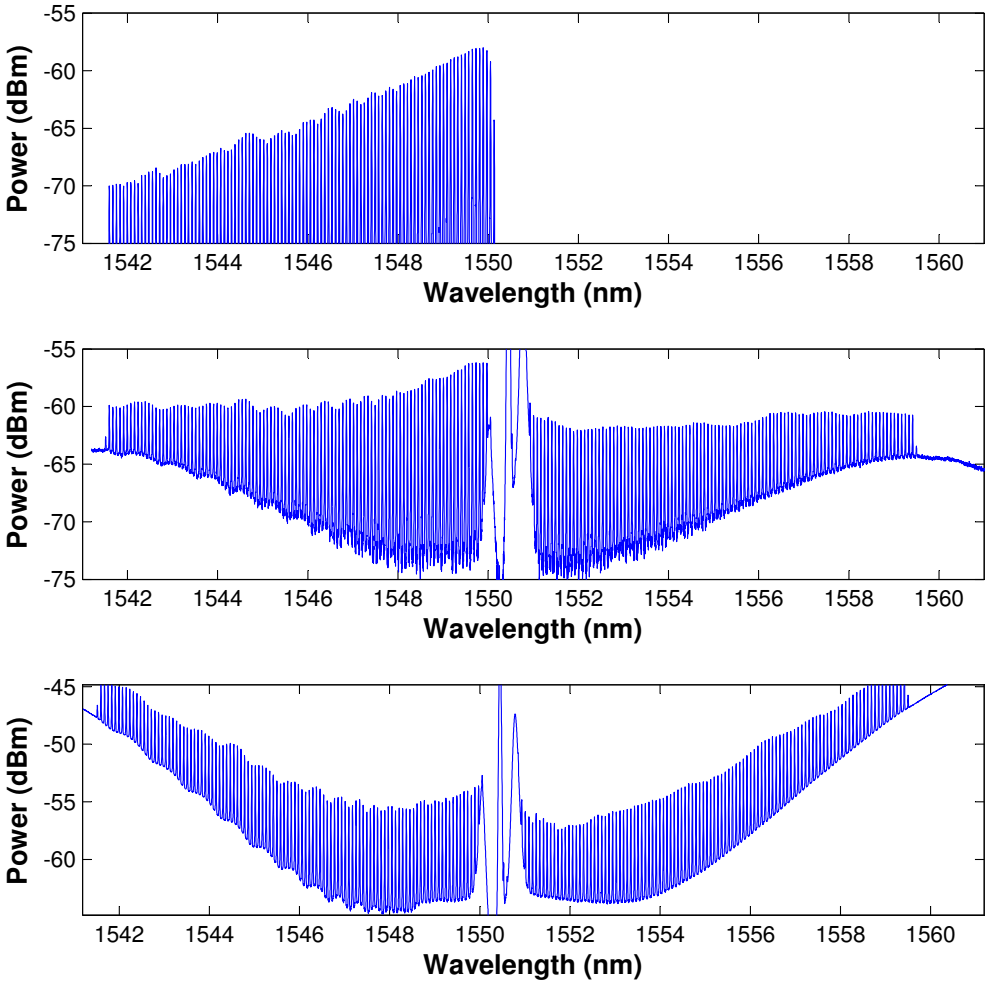

FIGURE 3.26: Output spectra in PI mode; Top - Pump off, Middle - Peak pump power 33 dBm, Bottom - Peak pump power 36 dBm.

The spectrum at the FOPA output with the pump off is shown in Fig. 3.26 (top). The OFCG provides a comb with -10 dB/ THz spectral roll-off as specified. The pump power was adjusted to ensure that the non-flat gain spectrum of the FOPA cancelled out the spectral roll-off of the input comb, i.e. obtain a +10 dB/ THz gain shape. Positive gain

slopes are easiest obtained by placing the pump in the anomalous dispersion regime, and the magnitude of the slope can be controlled by the pump power [13]. The output spectra with the pump turned on are also shown in Fig. 3.26 (middle and bottom). Note that the region between 1550 and 1551 nm should ignored as this is where the pump is filtered with some energy remaining. With peak pump power of 33 dBm, the comb line power variation at the output was reduced to under 1.5 dB variation over 8 nm ($\sim$ 1 THz). This is best observed by viewing the right side of the spectrum (wavelengths $>$ 1551 nm). The apparent deviation from this behaviour for short wavelengths is only an artifact of the 10% gating of the pump at the FOPA input, with the OSA measuring average power over both pump-on and pump-off cycles. Data was measured for average pump powers of 23 and 26 dBm, corresponding to 33 and 36 dBm pump peak powers approximately.

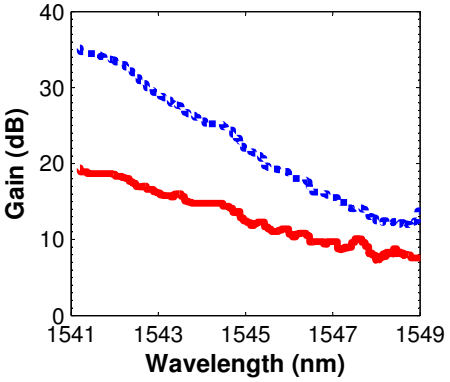

FIGURE 3.27: Single sided PI gain curves for 33 dBm (solid line) and 36 dBm (dotted line) peak pump powers.

Fig. 3.27 shows the gain measurement for single sided PI mode at 33 and 36 dBm peak pump power. The maximum gains obtained are 19 and 33 dB respectively. The slope of the curve at 33 dBm is very close to the + 10 dB/ THz target. In addition, in PI mode, the generation of idlers of the input comb lines means that the output spectrum is twice the width of the input, a useful benefit for the comb applications where a wide comb span is required, such as THz frequency generation.

Fig. 3.28 shows the output spectrum in the absence of the input comb. The noise present on the pump beam prior to the HNLF (residual ASE), as well as quantum noise generated in the FOPA, are amplified, and this is what limits the output comb SNR as observable in Fig. 3.26 (middle and bottom). Its impact should be less critical for higher input signal powers. Fig. 3.29 shows a narrow section of the spectrum when operated in PI and PS modes. The PS output shows both higher power and higher OSNR, as would be expected from the 6 dB OSNR advantage with non-degenerate PSAs. Comparing the two spectra reveals a maximum observed PS advantage or 4 dB (rightmost comb line).

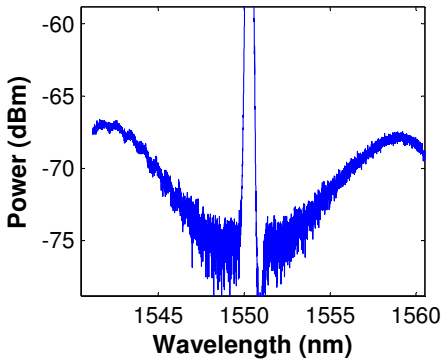

FIGURE 3.28: Output spectrum at 33 dBm peak power in absence of input comb signal.

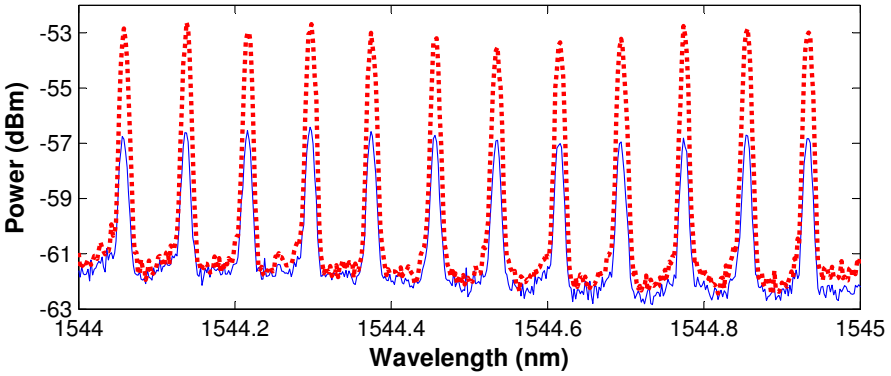

FIGURE 3.29: Magnification of comb lines amplified in PI (solid) and PS (dotted) showing a PS noise figure improvement greater than 3dB.

In simplistic terms, the 4 dB advantage of this particular PS-FOPA should be observed when benchmarked against any PI amplifier, such as a DFA.

3.6 Conclusion

PSA has been introduced as a technique to obtain amplification with a NF below the 3 dB quantum limit. The origin of this improved performance lies in the fact that the PSA only amplifies one of the two information quadratures, in a noiseless manner, while de-amplifying the other, consequently adding noise to it. As such no quantum mechanics laws are violated. This 3 dB NF improvement, if deployed in a multi-span amplifier chain would result in an overall 3 dB link margin improvement, which could be used to either extend the reach of the link, or allow the use of a denser signal constellation on the amplified quadrature.

PSA can be obtained using third-order nonlinearity in optical fiber by either interferometric or non-interferometric means. The non-interferometric approach has a significant advantage, in that when properly phase matched, its gain scales exponentially with pump power, as compared to quadratically with the interferometric scheme. Non-degenerate FOPAs allow PSA in 1P and 2P configurations if both signal and idler fields are present at the amplifier input. The interacting waves need to be frequency and phase locked, a task that can be challenging to perform. The inline cascaded FOPA, in which a first PI-FOPA is used to generate phase locked signal-idler pairs, followed by a second FOPA in which PSA takes place, is an easy way to demonstrate PS-FOPA properties. A demonstration of PS-FOPA was made using this technique, and used to study the gain characteristics of a PS-FOPA in linear and saturated modes of operation. In phase-matched PS-FOPAs, as with most nonlinear devices, increasing pump power linearly boosts the gain exponentially. Linear PS gain of up to 20 dB was recorded in experiments. While theory predicts that 20 dB peak gain should be accompanied by -20 dB maximal de-amplification, measuring high de-amplification values proved to be a challenge. The sensitivity of the PSA to signal-idler ratio was experimentally studied, and by boosting pump powers even higher, a peak PSA gain of 33 dB was attained, a record at the time, although this measurement was accompanied by severely degraded de-amplification (with only a 6 dB PSA swing seen).

An improved PSA configuration was devised in an attempt to demonstrate 2P PS-FOPA performance as well as verify the effect of several experimental factors, such as wideband SBS suppression, and mid-stage dispersion, on the 1P PS-FOPA already tested. The new setup had lower signal insertion loss, used PM amplification before the PSA, had counter-phased pumps to reduce idler broadening and had mid-stage dispersion compensation. Flat 1P amplification was obtained over 20 nm, with symmetric amplication/de-amplification of $\pm$6 dB. The 2P PS-FOPA had comparable gain. Recording higher levels of PS de-amplification once again proved problematic, which may have been due to the use of an OSA to perform the measurement.

A final experiment was devised to highlight the suitability of FOPAs for the amplification of optical combs.While certain attributes of FOPAs are undesirable in a telecoms environment, such as the high levels of nonlinearity in the amplifier, optical comb amplifiers would benefit from adding extra functionality, such as comb reshaping, wing enhancement and low noise amplification. A PI-FOPA was used to flatten a triangular -10 dB/THz input comb spectrum, and high gains of 33 dB were obtained at the FOPA gain peak. In PS mode, a clear 4 dB SNR improvement was shown, as compared to the PI-FOPA. It is worth noting that a more conclusive measurement would require proper phase locking, rather than the max/min hold technique used, although subsequent measurements with phase locking were in agreement.

Chapter 4

Regenerative Parametric Mixer Design Considerations

4.1 Introduction

The ability of a PSA to amplify one signal quadrature while de-amplifying the other inherently leads to a sub 3 dB noise figure for amplifiers in the high gain regime. Chapter 3 explains the origin of this property and details some experimental characterisation of wideband PS-FOPAs based on non-degenerate techniques. Within PHASORS however, delivery of a sub 3 dB NF amplifier was a role allocated to the University of Chalmers, with Southampton tasked with delivering a high performance DPSK regenerator based on the other property of the PSA, i.e. its ability to constrain signal phase to one quadrature. As such, there was a shift in emphasis from studying gain and noise properties of parametric amplifiers, to realisation of practical regeneration schemes. The low noise work did continue at Chalmers however, and a record low 1.1 dB NF was demonstrated by Tong, Lundström et. al. [67] using the cascaded FOPA concept (note that it is referred to as copier-PSA in their publications).

The concept behind the use of a degenerate PS parametric amplifier for the regeneration of binary phase encoded signals is well known, and has been previously assessed both theoretically [26] and experimentally [27, 79]. As mentioned in Chapter 3, while the PSA effect, and consequently phase regenerative capability, can be obtained in an interferometric PS-FOPA (indeed demonstrated by Croussore et. al. [79]), non-interferometric means were the method of choice for this study due to the prospects for more power efficient operation (see Section 3.3.3), a key issue for a telecommunications device.

This chapter details the preliminary groundwork carried out to enable a practical DPSK regenerator using FWM in HNLF. In particular, it looks into issues surrounding the design of PS-FOPAs for this application, including fibre selection and phase locked pump

requirements. This knowledge would later translate into development of regenerators for DPSK, and later on, QPSK.

4.2 Dual Pump PS-FOPA Transfer Function

4.2.1 Simplification of Analytical Gain Expression

An analytical expression for the gain in a FWM based parametric mixer has been previously shown, Eqn. 3.11 [13]. For the dual pump (degenerate) PS-FOPA, this can be re-written as

$$G_s(z) = \cosh(gz) + \frac{i}{g}\frac{\kappa}{2}\sinh(gz) + \frac{1}{g}r\exp\left(-i\left(\phi_{rel} - \frac{\pi}{2}\right)\right)\sinh(gz) \tag{4.1}$$

Where $r = 2\gamma\sqrt{P_1 P_2}$ and the parametric gain coefficient $g = \sqrt{r^2 - \frac{\kappa}{2}^2}$. In a well phase matched parametric amplifier, $\kappa \approx 0$, therefore Eqn. 4.1 reduces to:

$$G_s(z) \approx \cosh(gz) + \exp\left(-i\left(\phi_{rel} - \frac{\pi}{2}\right)\right)\sinh(gz) \tag{4.2}$$

By setting the sum of the pumps' phases as the phase reference, then

$$G_s(z) \approx \cosh(gz) + \exp\left(-i\left(2\phi_s - \frac{\pi}{2}\right)\right)\sinh(gz) \tag{4.3}$$

$$G_s(z) \approx \cosh(gz)\left[1 + \exp\left(-i\left(2\phi_s - \frac{\pi}{2}\right)\right)\tanh(gz)\right] \tag{4.4}$$

Assuming an input analytical signal $\exp(i\phi_s)$, then the output of the PSA can be obtained by multiplying the analytical input with the gain function, hence

$$\exp(i\phi_s)G_s(z) \approx \cosh(gz)\left[\exp(i\phi_s) + \exp\left(-i\left(\phi_s - \frac{\pi}{2}\right)\right)\tanh(gz)\right] \tag{4.5}$$

Observe that $\tanh(gz)$ is bounded within the range ± 1, and that $\cosh^2(gz)$ gives the peak power gain. Substituting $m = \tanh(gz)$ and $G = \cosh(gz)$ leads to the following simplified output function for the phase matched degenerate PSA,

$$G\left[\exp(i\phi_s) + m \cdot exp\left(-i\phi_s - \frac{\pi}{2}\right)\right], \text{ where } -1 \leq m \leq 1 \tag{4.6}$$

Eqn. 4.6 is evaluated in Fig. 4.1 for various values of m. It is clear that as m increases, the output power becomes more sensitive to the input phase, and simultaneously the output phase transfer function approaches a two level, π-step staircase. There is a direct correlation between the swing in power at the PSA output with the level of phase restoration achieved, and as a result the PS swing can act as a measurement of how well the PSA will perform as a phase regenerator. This is extremely useful in experimental terms, as the system can be optimised whilst monitoring the output power using a simple

photodiode, without having to have a coherent detection system to monitor the output signal phase.

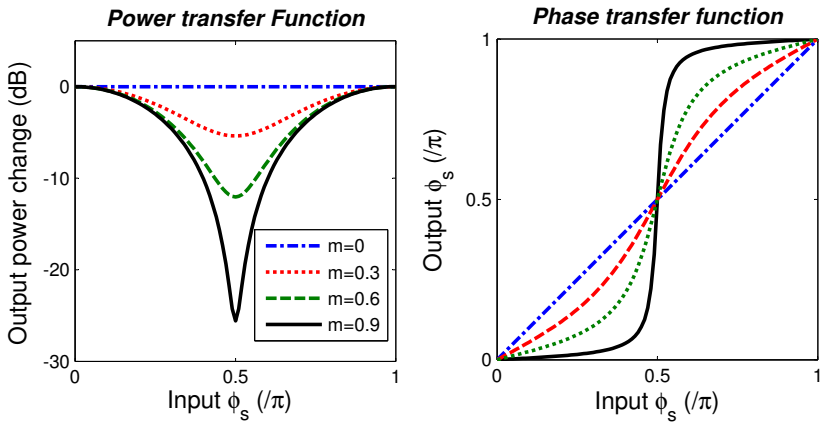

FIGURE 4.1: Evaluation of simplified degenerate PSA transfer function as written in eqn. 4.6, for various values of m.

4.2.2 Numerical Assessment of HNLF Samples

As discussed in Section 4.2.1, the dispersive and nonlinear characteristics of the HNLF used for the PS-FOPA dictate the ultimate performance of the phase regenerator. The product of the parametric gain coefficient $g = 2\gamma P$, and the fibre length, directly control how much PS swing is achieved, hence the flatness of the phase transfer function.

A series of numerical simulations were carried out using VPI Transmission Maker 8.0 to ascertain the phase regenerative capability of three different nonlinear fibres available at the time for experimental work. The fibre and pump parameters used were as follows (at 1550 nm) :

1. Bismuth oxide fibre [80]: Dispersion -260 ps/nm/km, slope 0.947 ps/nm^2/km, nonlinear coefficient 1350 /W/km, length 2 m, loss 0.9 dB/m, total pump power 1 W. This is a fibre with high dispersion but this is offset by the short length and high non-linearity suitable for degenerate narrowband PSA.

2. W-type soft glass fibre [81]: Dispersion -4 ps/nm/km, slope 0.947 ps/nm^2/km, nonlinear coefficient 850 /W/km, length 2 m, loss 2 dB/m, total pump power 1 W. This fibre has less dispersion than the bismuth oxide, potentially allowing higher parametric gain.

3. Germanium doped HNLF: Dispersion -0.18 ps/nm/km, slope 0.029 ps/nm^2/km, nonlinear coefficient 11/W/km, length 200 m, loss 0.83 dB/km, total pump power 0.4 W. This HNLF was provided by OFS Fitel. The low loss and dispersion allow long fibre lengths to be used, hence less pump power is required.

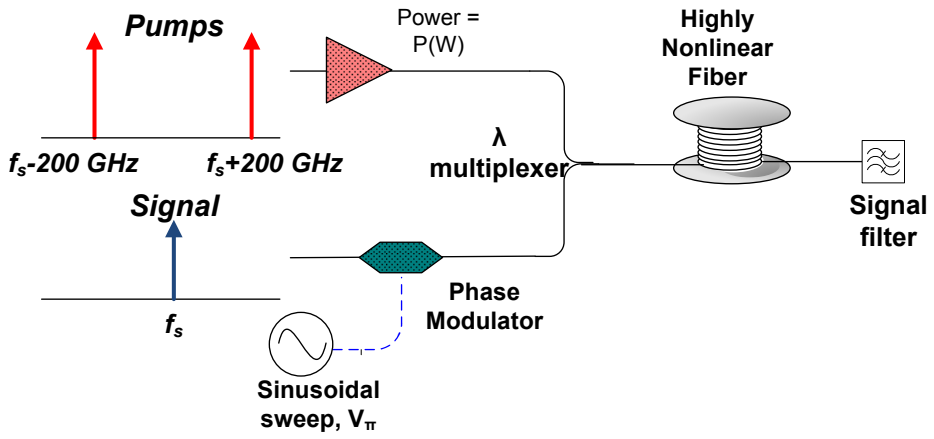

FIGURE 4.2: Test scenario for degenerate 2P PS-FOPA modelled to evaluate suitability of various in-house HNLF samples for BPSK regeneration.

The modelled scenario is shown in Fig. 4.2. A signal at frequency f_s was slowly phase modulated using a sinusoidal tone in a phase modulator driven up to V_π, hence ensuring that its phase varied by over a full π radians. Two pumps at $\pm$ 200 GHz from the signal were launched into the HNLF together with the modulated signal. The signal was weak compared to the pumps hence no saturation would be expected in the PSA. Also, the pumps and signals were assumed to be frequency and phase locked during the simulation. The physical bismuth oxide and W-type fibres available had insertion losses of 3 and 6 dB respectively. These losses were not considered in the simulations, hence during experiments the pump powers would ultimately need to be increased accordingly to offset them.

4.2.2.1 Bismuth Oxide Fibre

For the degenerate PSA based regenerator high fibre dispersions are tolerable because the signal and pumps are spectrally close, with 200 GHz detuning in this case. Fig. 4.3(a) shows the gain with two 0.5 W pumps (overall power of 1 W) coupled into the 2 m long bismuth fibre. Fig. 4.3(b) shows the phase sensitive gain. The PS swing was 17 dB.

4.2.2.2 W-type Fibre

Fig. 4.4 shows the gain with two 0.5 W pumps (total power of 1 W) coupled into the W-type soft glass fibre. There is a higher PS swing (close to 18 dB), as compared to the bismuth oxide fibre, due to the lower dispersion parameter.

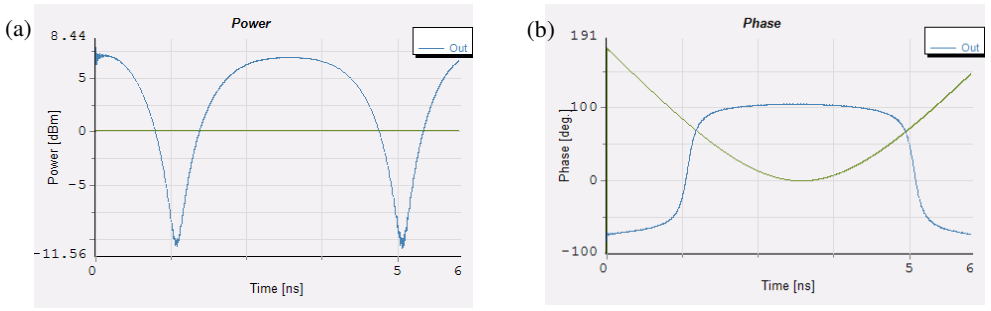

FIGURE 4.3: Gain (a) and output phase (b) characteristics as a function of the time for the bismuth oxide fibre (Green curves input, blue curves output).

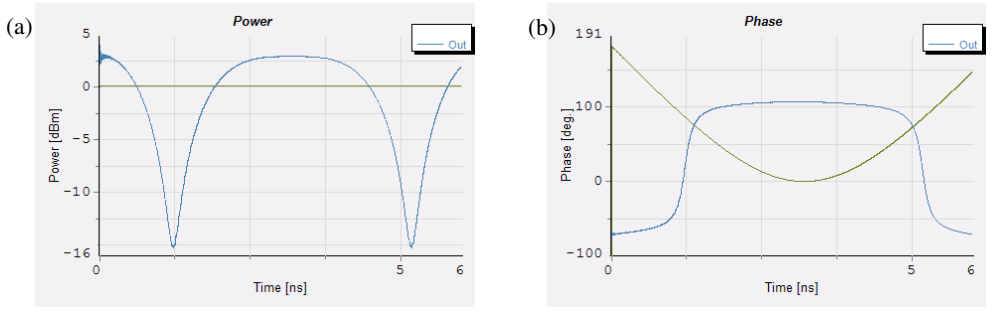

FIGURE 4.4: Gain (a) and output phase (b) characteristics as a function of the time for the W-type fibre (Green curves input, blue curves output).

4.2.2.3 Ge-doped Silica Fibre

The results shown in Fig. 4.5 utilise a 200 m germanium doped HNLF with operation close to the zero dispersion wavelength, i.e. dispersion under 0.2 ps/nm/km. The major point worth noting is that significant phase to amplitude conversion (over 15 dB) can be achieved for a total pump power of only 0.4 W (less than half of the power as compared to the previous experiments), which corresponds to 0.2 W per pump. This lower pump power is a key advantage, as it would translate both to lower component cost and better energy efficiency. The SBS threshold for this sample was under 20 dBm however, and therefore 0.2 W of CW pump power could not be directly coupled into the fibre without the use of active SBS suppression, such as pump phase dithering.

4.2.3 Experimental Validation of Phase Compression Behaviour

Following the theoretical simulation work an initial experiment was carried out to ascertain whether the PSA could perform comparably to the theoretical predictions. The bismuth oxide fibre was selected because of its relatively high SBS threshold (around 27 dBm per pump), as well as lower insertion losses than the W-type. For regeneration, the

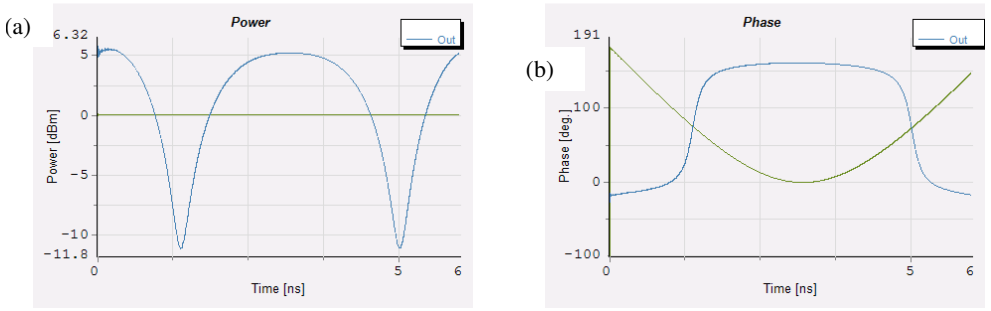

FIGURE 4.5: Gain (a) and output phase (b) characteristics as a function of the time for the Ge-doped silica fibre (Green curves input, blue curves output).

use of pump phase modulation for SBS suppression is not possible as the phase modulation would distort the signal phase during the parametric process. Work was taking place at OFS Denmark to deliver low loss SBS suppressed fibers using alumino-silicate doping, but in the interim the bismuth fiber that was already available in the lab proved to be a useful short term alternative. The experiment was performed with Dr. Radan Slavik, who had been working on injection locking of semiconductor lasers to optical combs, which is how the pumps for the following experiment were generated.

4.2.3.1 Experimental Setup

To generate phase locked pumps for the degenerate PSA, an injection locking technique was used. The corresponding set-up is shown in Fig. 4.6. A 1555.4 nm fibre Fabry-Perot laser (Rock by NPhotonics, with 3 dB linewidth below 10 kHz) was split into two paths; one portion was used as the signal for the PSA and the other was fed to a 10 GHz optical frequency comb generator (OFCG, OptoComb Inc.) The comb was then coupled into two discrete mode semiconductor lasers (manufactured by Eblana Photonics), operating at different wavelengths, via a circulator and a 100 GHz arrayed waveguide grating (AWG), so as to injection lock the two sources to the corresponding comb lines (forming two pumps for the PSA), and consequently phase-lock the three together. The narrow-bandwidth of the AWG channels was beneficial in improving the SNR of the two phase-locked beams to the >70 dB level, see Fig. 4.7 (left). The two combined phase-locked CW pumps were then amplified up to about 32 dBm, coupled with the CW signal and launched into the 2 m long bismuth oxide fibre.

The relative phase of the three combined lasers needed to be controlled dynamically, since it varies due to thermal changes and acoustic pick-up in the optical fibres. Fortunately, these induced drifts are relatively slow phase variations (mostly in the kHz range) and could be compensated electronically by driving a piezo-transformer (PZT) stretcher placed in the path of the master laser prior to combination with the two slaves (PSA pumps), Fig. 4.6. The feedback was derived from a second PSA, whose phase maximum

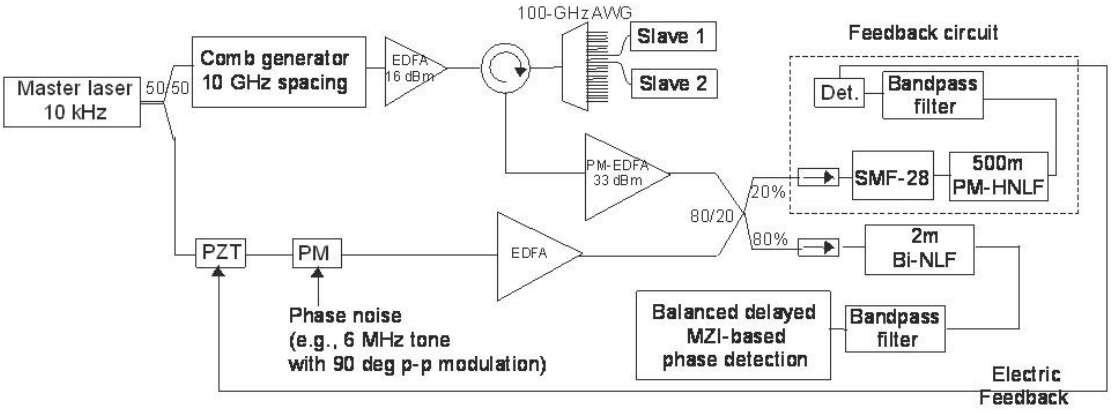

FIGURE 4.6: Experimental setup to observe phase squeezing in a 2P degenerate PS-FOPA. OSO - optical sampling oscilloscope.

was shifted by about 45° compared to the first one using a pre-calculated length of single mode fibre (SMF) [55].

4.2.3.2 Experimental Results

The spectra corresponding to the maximum and minimum PSA gain are shown in Fig. 4.7 (left), where a PS swing of about 10 dB was observed. The difference between the maximum signal gain and the signal power when the pumps were off was about 4 dB. To characterise the phase regeneration, a phase modulator was added to the signal arm (driven sinusoidally at 6 MHz) to induce about ±25 degrees of phase noise into the signal.

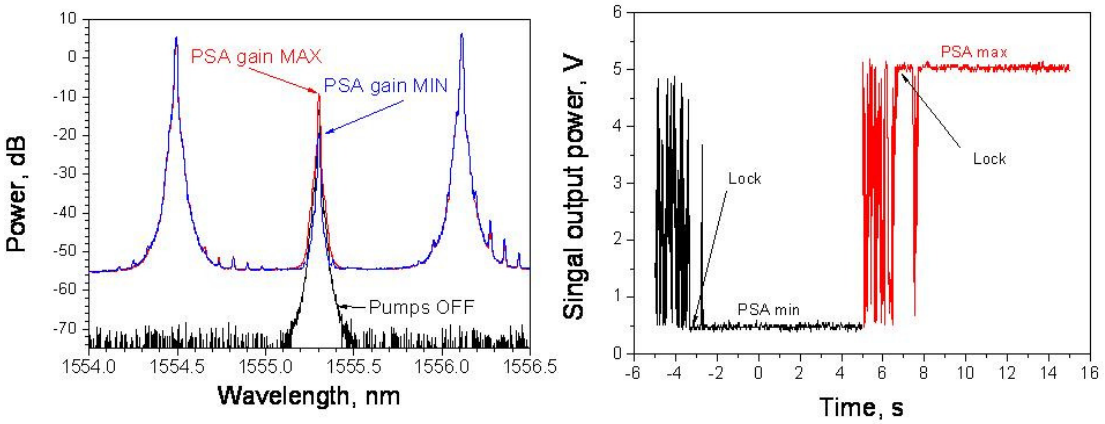

FIGURE 4.7: (Left) Optical spectra corresponding to maximum and minimum PSA gain. The signal spectrum corresponding to the case of pumps off is also shown as a reference. Right) Optical power as a function of time when the PZT was unlocked or locked to the PSA minimum gain (black) or PSA maximum gain (red).

At the output of the PSA, the two pumps were filtered out and the phase properties of the signal were studied. For this study, a delayed Mach-Zehnder interferometer was used together with balanced detection, Fig. 4.8. This device was constructed by Dr. Radan Slavik for purposes of laser characterization, but was ideal for characterising the signal quality before and after the regenerator. As such rather than a laser under test, the input was the filtered signal after the PSA. The interferometer served as a frequency-to-amplitude converter, and therefore frequency (phase change) information on the signal could be studied following direct optical-to-electrical conversion. The delay was optimised for the bandwidth of interest, and set to 6 m, corresponding to a free spectral range of 33 MHz (around 3 times the maximum frequency of interest for this experiment).

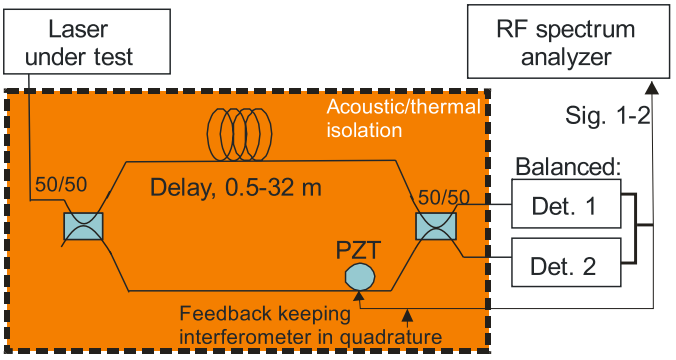

FIGURE 4.8: Set-up for frequency noise measurement using a delayed Mach-Zender interferometer [82]. Frequency fluctuations at the input are converted to amplitude fluctuations at the output, prior to electrical detection.

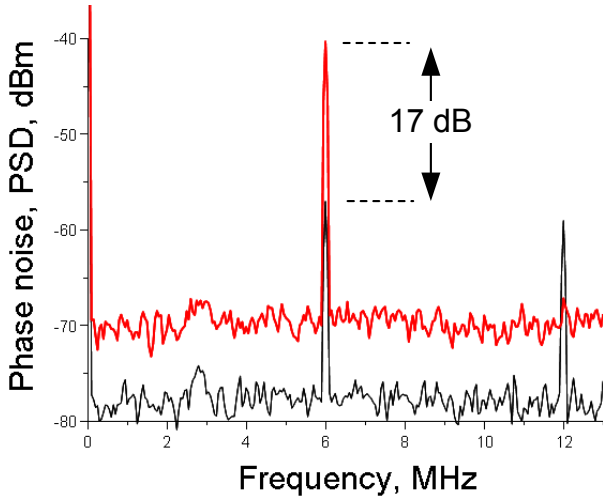

FIGURE 4.9: Balanced detection results illustrating suppression of 6 MHz phase noise tone; red line - before PSA, black line - after PSA.

Frequency noise power spectral density (PSD) results are shown in Fig. 4.9. The 6 MHz tone visible on the signal at the input with a measured improvement of 17 dB, which equates to about 8.5 dB improvement in terms of optical noise power suppression. The

12 MHz tone visible at the output was due to phase-to-amplitude conversion in the PSA (for every 2π phase change at the PSA input the output amplitude goes through two cycles); this amplitude noise is not cancelled out completely in the balanced detector because the Mach-Zender interferometer is not path length matched. This amplitude tone does not affect the conclusions drawn here however, as it is at a different (harmonic) frequency to the phase tone. It was already known that the input perturbations were $\pm 25°$ (estimated by measuring electrical drive signal to the phase modulator whose V_π was known). This information could then be used to calculate the peak-to-peak phase fluctuations on the output signal by reducing the input phase deviations by 8.5 dB ($\pm 25 * 10^{-\frac{8.5}{10}}$), with a result of approximately $\pm 3.5°$.

Fig. 4.10 shows a numerically evaluated phase transfer characteristic simulated using a total pump power of 27 dBm which approximately matches the experimental conditions. The simulation approach used was the same as in Section 4.2.2. The green line shows a time varying phase ramp on the signal at the PSA input, while the blue shows the phase compressed signal at the PSA output. The relative difference in slope between the PSA input (green line) and PSA output (blue line) indicates a phase compression by a factor of 8.4 in linear units, or 9.2 dB. This compares well with the experimental value of 8.5 dB. This level of phase compression suggested that the PSA would be a good choice for a BPSK phase regeneration experiment.

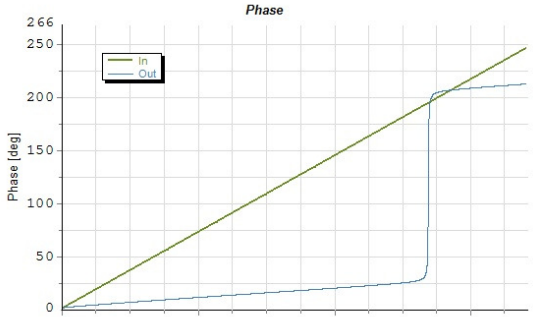

FIGURE 4.10: Theoretical phase transfer characteristic for bismuth oxide fibre with 27 dBm total pumping; relative slopes of the two lines indicate phase compression by a linear factor of 8.4 in the PSA. The horizontal axis corresponded to time in the simulation, but is irrelevant as information of interest is all in the vertical axis.

4.3 Saturation of PSA for Amplitude Noise Improvement

The phase regeneration function in degenerate PS-FOPAs is accompanied by phase-to-amplitude conversion, as shown in Fig. 4.1. As a result phase noise at the PSA input is transformed into amplitude noise at the output. In long-haul optical links, the dominant source of phase noise is nonlinear refraction (XPM and SPM) [14]. As a result, if such a PSA was used as a mid-span optical phase regenerator, the amplitude noise added within the regenerator would act to generate more phase noise in the next transmission span,

reducing the overall benefit of having a phase regenerator in the first place. In fact, it has been demonstrated that employing pure amplitude regenerators (limiters) in an optical link with DPSK signal modulation can significantly improve the BER at the receiver, by suppression of this amplitude-to-phase conversion process during transmission [24]. Saturation (also referred to as pump depletion) of PS-FOPAs, by boosting the input signal power, is a process known to reduce the impact of phase-to-amplitude conversion within a PS-FOPA phase regenerator [26]. The following experiment was carried out to study the saturation process in a degenerate 2P PS-FOPA.

4.3.1 Experimental Setup

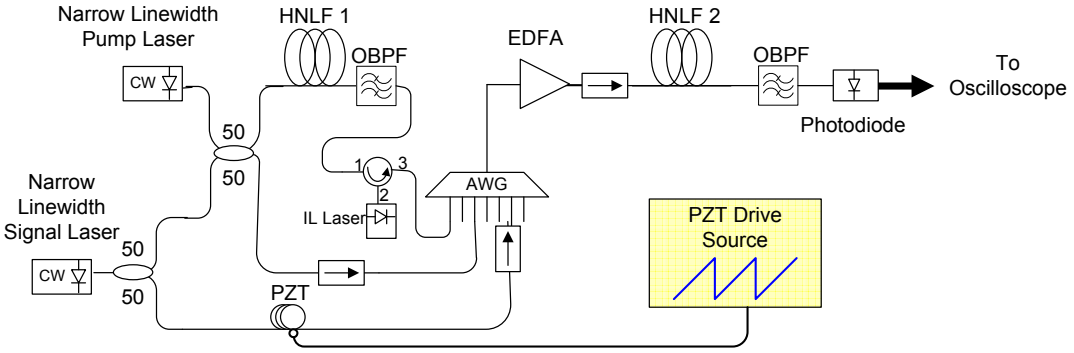

FIGURE 4.11: Experimental setup of dual pump degenerate PS-FOPA. OBPF: Optical Bandpass Filter

The experimental setup is shown in Fig. 4.11. Two narrow linewidth signals 200 GHz apart were mixed in a Ge-doped HNLF generating a weak idler. The HNLF length, dispersion, nonlinear coefficient and attenuation were 500 m, 0.09 ps/nm/km, 11.5 /W/km and 0.83 dB/km respectively. The idler wave was then injected into a (slave) semiconductor laser from Eblana Photonics to generate a third high SNR wave locked in frequency and phase to the PIA input signal. The three waves spaced 200 GHz apart could then be used as the two pumps and signal for the PS-FOPA. A variable attenuator (not shown in Fig. 4.11) allowed control of the signal power relative to the pumps.

The phase of the signal wave was modulated using a 50 kHz ramp function applied to a piezo-electric fibre stretcher. The choice of the ramp frequency was chosen to correspond to the resonant frequency of the piezo-electric stretcher used, allowing the phase to be swept by many multiples of 180° for a peak-to-peak drive voltage of under 100 V. The three waves were then combined, amplified to a fixed total power and launched into the degenerate PS-FOPA. This utilised a high SBS threshold strained alumino-silicate HNLF from OFS. The length, dispersion, polarization mode dispersion, nonlinear coefficient and attenuation of the fibre were 177 m, -0.13 ps/nm/km, 0.11 ps/km^2, 7.1 /W/km and 15 dB/km, respectively.

4.3.1.1 PIA Saturation

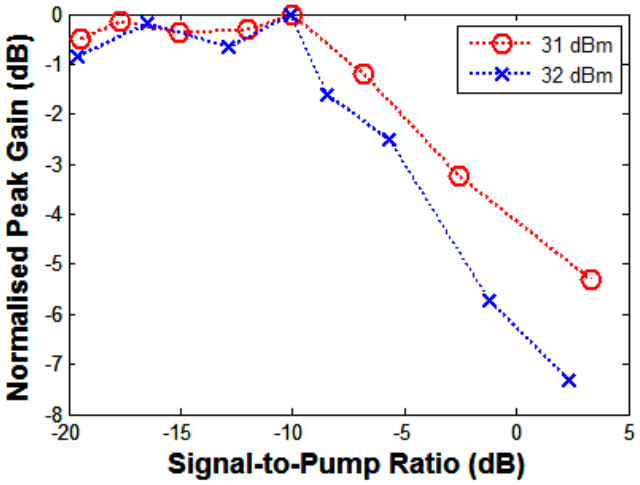

FIGURE 4.12: Phase insensitive saturation characteristics for total powers into 1P FOPA of 31 dBm (circles) and 32 dBm (crosses).

First, the PI saturation characteristics were measured by turning off one of the pump lasers. The signal power into the high power EDFA was then systematically incremented to increase the signal-to-pump ratio in the FOPA, for a fixed total power into the FOPA. The output signal power after the FOPA was monitored using an optical spectrum analyser and the normalised gain plotted on a logarithmic scale as a function of the input signal-to-pump power ratio. This was done for two total power levels out of the EDFA. The result is shown in Fig. 4.12.

Both gain curves measured show the expected PI saturation behaviour, with the gain dropping off as the signal-to-pump power ratio increases. The offset between the two curves arises from a combination of the increased absolute pump and signal power, leading to an earlier onset of saturation as a function of the signal-to-pump ratio. The trend is monotonic within the range of signal powers assessed, something that contrasts with PS saturation as discussed shortly.

4.3.1.2 PSA Saturation

The FOPA was then modified for PS operation by turning on the second pump laser. The signal at the PS-FOPA output was filtered, attenuated and coupled into a low power photodiode. The electrical signal from the photodiode was then observed using a high speed real-time digital sampling oscilloscope. Post-processing was carried out to eliminate high-frequency noise and normalise the gain curves.

The normalised signal gain curves for a total power of 29 dBm (pumps and signal combined) coupled into the fibre are shown in Fig. 4.13. At this moderate pump power,

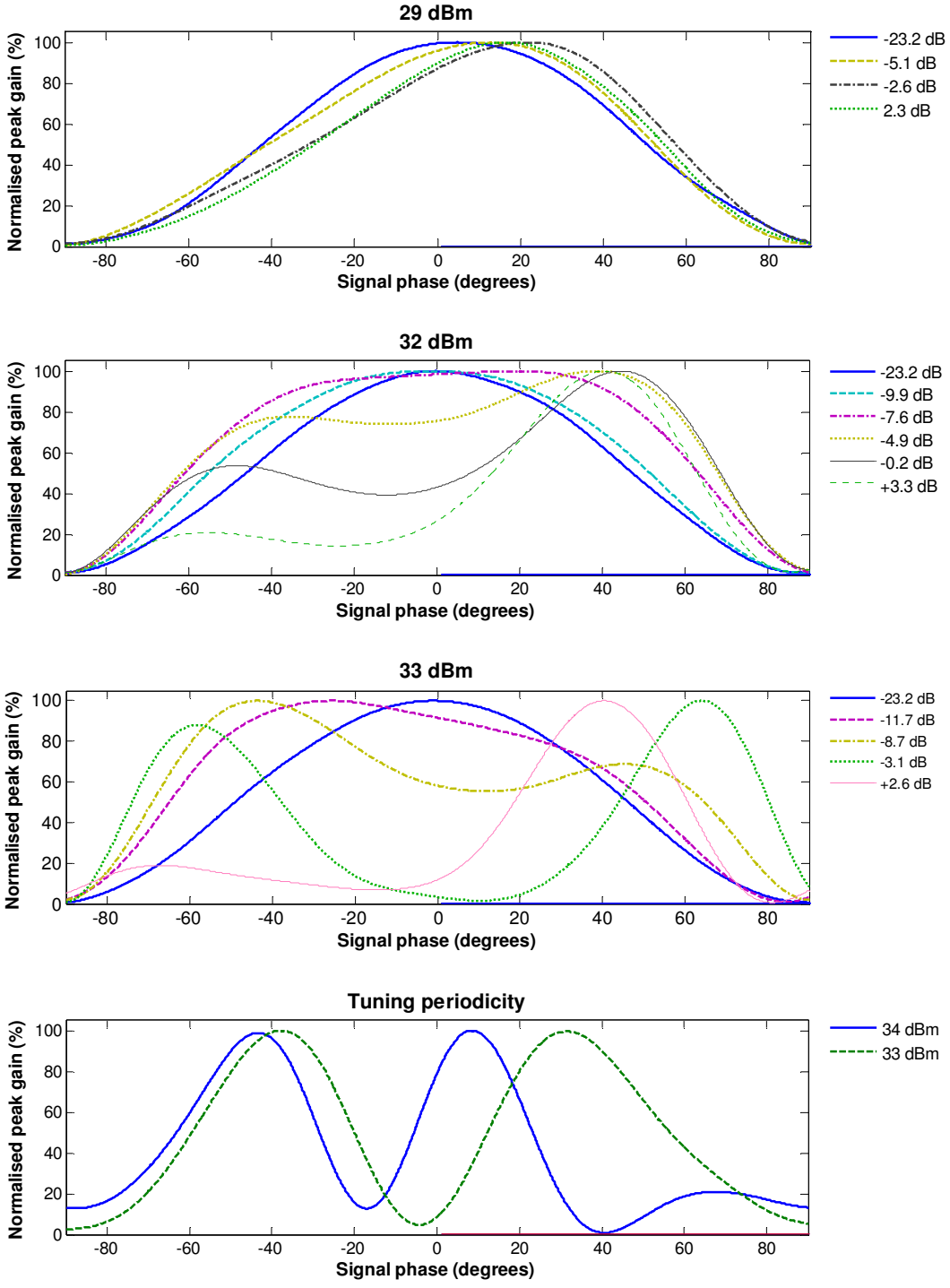

FIGURE 4.13: Phase-to-amplitude transfer characteristics for degenerate 2P PS-FOPA while pump-to-signal ratio is varied for various powers, as well as characteristics for two pump powers at a fixed 8 dB pump-to-signal ratio (bottom).

for low input signal levels, the gain versus relative phase curve is sinusoidal as expected from theory. As the signal power increases, the curves accumulate a skew, with the gain peak seemingly detuned in phase from the central phase position. Because each curve is captured for a fixed signal power at the PS-FOPA input, this differs from PI saturation (in which the gain varies with input signal power) because a nonlinear dependence on input signal phase exists. In this case, every point on the curve experiences a gain shift due to the alteration of the phase matching condition by the variation in the signal/pump power proportions during propagation. As the signal and pumps propagate down the fibre in which the PS interaction occurs, at every point a nonlinear contribution to the phase matching exists as a result of self- and cross-phase modulation (SPM and XPM respectively). Because the gain is dependent on the signal phase, the absolute powers and therefore the nonlinear phase matching varies with the input phase. For strong signal levels, this phase dependent behaviour leads to a modification of the gain characteristic, and ultimately to gain saturation.

For applications such as the regeneration of DPSK signals, a crucial requirement would be that the PS gain curves have a flat-top, minimising the transfer of phase to amplitude noise. To obtain such flattening, it was necessary to increase the total power coupled into the PS-FOPA to 32 dBm. A selection of the resulting gain curves are shown in Fig. 4.13. At the lowest signal level assessed a sinusoidal gain curve is obtained indicating the absence of significant gain saturation. As the signal power is increased, the gain curve is seen to acquire a flat-top. Increasing the signal power further reveals that the flattening is in fact due to the growth of a second peak in the gain curve that detunes in phase from the central position as the signal level is increased.

The total signal power was then increased further to 33 dBm and the gain measured. The gain curve goes from sinusoidal at low signal levels to skewed at moderate power levels. At high signal level (within 8 dB of pump power) it was possible to have two peaks in the gain curve for a 180° change in the input signal phase, contrasting with the single peak for an unsaturated PSA, with the separation between the peaks tuneable by varying the total pump power. This ability to tune the periodicity of the phase response of a PSA by saturation might open up several yet unknown applications.

4.4 Conclusion

Considerations regarding the application of the degenerate 2P PS-FOPA for D(or B)PSK signal regeneration have been presented. Substitutions have been made into the analytical gain functions of the PS-FOPA to enable the phase transfer characteristics in the linear high gain regime to be easily predicted. Numerical modelling was performed using the parameters of several in-house HNLFs, showing that good phase regenerative performance could be delivered in a PS-FOPA if PS swings over 15 dB are achieved. These

conclusions were verified using in an experiment based on a degenerate 2P PS-FOPA in a 2 m bismuth oxide fibre. In that proof of concept work, close to an order of magnitude reduction in small signal phase fluctuations at the PS-FOPA input were obtained. The experiment was also a validation of the use of injection locking to synthesis phase locked pumps for the FOPA.

The phase-to-amplitude conversion that accompanies the phase regeneration is undesirable in a telecom transmission environment, but fortunately this can be mitigated somewhat by increasing the signal power at the PS-FOPA input up to a PS gain saturation point. PI and PS saturation in an FOPA are experimentally contrasted, and dynamics of saturation in a PS-FOPA studied practically. The experiment revealed that saturation in a PS-FOPA is more complex than in a PI device - there exists an interplay between input phase and nonlinear phase matching along the FOPA fibre, which modifies the amplitude transfer characteristics quite markedly, particularly at high input signal levels. A regime for DPSK regeneration was identified for the available HNLF.

Chapter 5

PSA Based DPSK Regeneration

5.1 Introduction

The electromagnetic wave has the potential to carry vast amounts of encoded information over distances spanning the galaxies. However, the amount of information that can be carried down a real world transmission channel depends on the amount of noise added during transmission, noise that interferes with the devices performing detection at the receiver end. The limits to how much information can be carried by a wave in the presence of such noise was discussed in the seminal work of Shannon [60]. Currently, the trend in long haul optical systems is to use signals modulated in both amplitude and phase, both to increase spectral efficiency, as well as better mitigate transmission impairments. However, the use of phase in signalling gives rise to a new dominant limitation to system performance, namely nonlinear phase noise (NPN) [14].

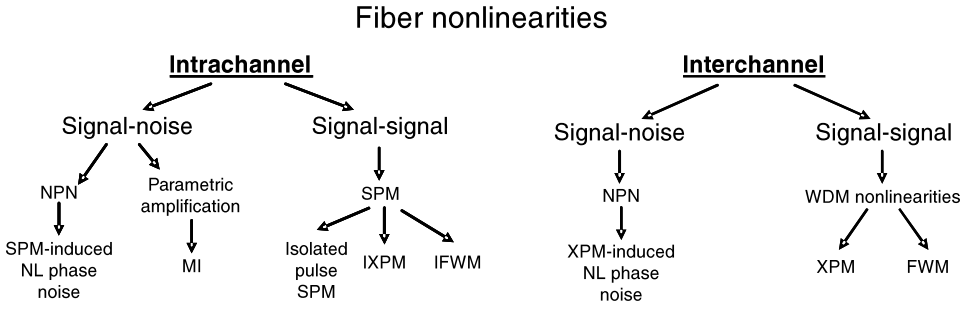

FIGURE 5.1: Classification of nonlinearities in optical fibres. Intrachannel and interchannel stand for nonlinearities occurring within or between WDM channels, respectively. SPM: self-phase modulation,(I)XPM: (intrachannel) cross-phase modulation, (I)FWM: (intrachannel) four-wave mixing,MI: modulation instability, NPN: nonlinear phase noise. Figure and caption taken from [37]

As shown in Fig. 5.1, there are several distinct nonlinear phase noise sources in a WDM system. The major contributor depends on the exact configuration of the link, e.g. amplifier span, power levels, dispersion management, WDM channel count, and signal channel bandwidth. However, interchannel XPM is often the main source of phase noise [83], and increases in a cubic fashion with propagation distance [23]. To ensure that the bit error rate at the receiver is within the limits for fidelity restoration using FEC, optical phase regenerators could be introduced periodically along the transmission span.

For links carrying DPSK signals, one approach to optical phase regeneration is to perform a phase-to-amplitude format conversion and then to apply amplitude regeneration before converting back to a phase encoded signal [84]. Besides being rather complex, the initial format conversion will more likely than not degrade the already-noisy signal. As a consequence, direct elimination of the phase noise is far more desirable. With this in mind, developing a practical DPSK regenerator was a key PHASORS objective. A significant amount of preliminary work was carried out, in terms of understanding PSA behaviour both theoretically and practically, and this is discussed in the earlier chapters of this thesis. The experiment described in Section 4.2.3 was in fact demonstration of a phase regenerator, although this was not black-box in the sense that the pumps were generated from the same laser as the signal.

As discussed in Chapter 3, the degenerate PSA requires two strong pumps located symmetrically in frequency around the signal to be amplified. In addition, for the PSA process to be useful, the average phase of the pumps should be locked to the phase of the signal carrier, even when the signal carrier is suppressed by an overlying modulation format such as DPSK. Proof of concept experiments on PSA based regeneration at a data rate of 10 Gbit/s were demonstrated [27] by Croussore et. al. Their demonstration relied on the use of high-frequency electro-optic modulation to generate multiple phase-coherent beams to be used as signal and pumps. This limits the pump spacing, and consequently the bandwidth of the signals that can be regenerated (as the signal should fit between the two pumps in spectrum) to a few tens of GHz. In addition, in a real transmission system, it is not desirable to transmit the pumps along with the signal as that would waste valuable spectrum. As such a key challenge in realizing a practical PSA based DPSK regenerator system lies in the synthesis of the phase locked pumps. This is described in the following section, following which the progress towards demonstrating a *black-box* phase regenerator will be detailed.

5.2 Pump Synthesis by Phase Erasure

5.2.1 Introduction

One approach to synthesize pumps for the PS-FOPA would be to directly recover the signal carrier from an input DPSK stream, and use the comb techniques shown in Section 4.2.3 to generate them. In fact, an experiment was performed proposing and demonstrating a novel technique to recover the carrier from PSK signals - this is described in Appendix B. However, for the dual pump PS-FOPA a simpler method to synthesize the phase locked pumps was proposed within the PHASORS consortium, and the first such demonstration using this new technique was by the PHASORS partners at University College Cork [85]. This scheme, also referred to as phase doubling, involves the use of a perfect binary phase modulated optical data train whose phase is $\phi_{signal}+0,\pi+\phi_{noise}$ to parametrically pump a narrow linewidth CW probe with phase ϕ_p in a nonlinear medium. An idler is generated with phase $2\cdot(\phi_{signal}+0,\pi+\phi_{noise})-\phi_p = 2\cdot(\phi_{signal}+\phi_{noise})-\phi_p$, thus stripped of the data phase modulation whilst maintaining whatever amplitude modulation was previously on the signal [86]. Any (high frequency) phase noise present on the signal beam, ϕ_{noise}, is transferred to the idler manifesting itself as spectral broadening of the otherwise narrow-linewidth CW idler. The noise can thus be eliminated by using a narrowband filtering mechanism, resulting in a phase locked pump for the PSA, free from the high frequency phase noise present on the signal.

It is important to specify the distinction between the carrier and the noise. Laser sources have finite linewidth, often in excess of 1 MHz, but these random phase fluctuations are inconsequential in DPSK systems if the baud rate is at least two orders of magnitude greater than the linewidth, because the demodulator compares the phase of consecutive bits, and at these time scales the laser is effectively noise free. As a result, any phase perturbations picked up during transmission that result in low frequency (<1 GHz for 40 Gbaud systems) fluctuations of less than π radians do not need to be regenerated. For coherent PSK systems, the phase tracking algorithms also perform some form of differential detection and therefore the same criterion applies.

5.2.2 Experimental observation of phase erasure

An experiment was carried out to assess the quality of the recovered carrier from a DPSK signal. A 40 Gbit/s $2^{31}-1$ pseudo random bit sequence (PRBS) was encoded onto a narrow linewidth CW at 1545.8 nm to generate a DPSK signal of power 16 dBm. The DPSK transmitter was based on a Mach-Zehnder modulator driven at $2V_\pi$, operating in non-return-to-zero (NRZ) mode. The signal was then combined with a 10 dBm CW probe at 1547.6 nm and launched into three different nonlinear devices. The first was a PPLN waveguide in which an idler is generated via a cascaded SHG/DFG

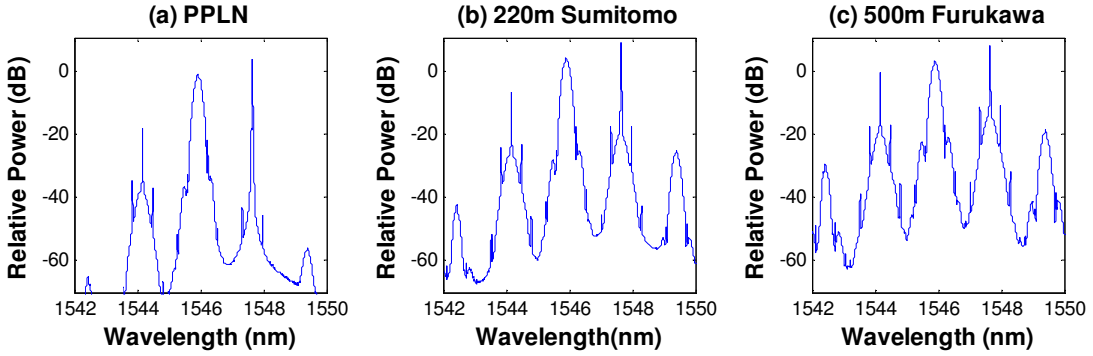

FIGURE 5.2: Phase erasure on 40Gbit/s DPSK signal carried out in three difference nonlinear devices. (a) PPLN waveguide, (b) 220 m Sumitomo HNLF, (c) 500 m Furukawa HNLF. DPSK signal is at 1545.8 nm, CW probe at 1547.6 nm and phase erased idler at 1544 nm.

process [87]. The others were 220 m and 500 m HNLFs, both with nonlinear coefficients approximately 20 /W/km, and 1550 nm dispersion < 0.1 ps/nm/km. The corresponding measured results are shown in Fig. 5.2. The phase erased idlers can be seen at 1544 nm. The fact that the idler is not a narrowband (sub-MHz) CW occurs mainly because the 0 to π transitions in the modulator are accompanied by amplitude fluctuations which are transferred to the 'phase erased' idler. This is not a problem in subsequent experiments as OIL is used to 'clean' the idler wave further. As can be seen in Fig. 5.2, the most efficient idler generation occurs in the 500 m fibre, a fact explained by the long length resulting in the highest nonlinear interaction.

5.3 First Generation Blackbox DPSK Regenerator

Following the delivery of a novel SBS suppressed alumino-silicate fiber from OFS [75], and lasers suitable for injection locking from Eblana photonics, a first full system demonstration was put together in Southampton targeting 40 Gbit/s DPSK regeneration. A feedback system to stabilise the PSA was initially provided by University College Cork, but this did not operate satisfactorily, and therefore the experiment used a feedback controller optimised by Dr. Radan Slavík. Carl Lundström from the University of Chalmers was present during the characterisation stage of this experiment and performed the coherent measurement of the signal before and after the regenerator - after this experiment the author developed a similar tool that was used in some of the QPSK regeneration work in Chapter 6. Other than these two specific tasks, the rest of the experiment was jointly carried out with Dr. Francesca Parmigiani and Dr. Radan Slavík.

5.3.1 Experimental Setup

The setup is shown in Fig. 5.3. The data signal was a 40 Gbit/s NRZ-DPSK, $2^{31} - 1$ pseudo random binary sequence (PRBS). In order to emulate the effects of phase noise, the signal phase was modulated in a deterministic fashion using an additional phase modulator, driven at a frequency close to half the baud rate and of a controllable modulation depth to emulate different levels of noise. The distorted signal was then launched into the black-box regenerator. A portion of the signal was initially tapped off to facilitate the frequency and phase locking of the two pumps, which occured in two steps.

First, the tapped signal was mixed in a germano-silicate HNLF with a narrow linewidth CW laser (Pump1) detuned from the signal by 200 GHz, to parametrically generate an idler wave that served as the seed for the second pump. The length, dispersion, nonlinear coefficient and attenuation of the HNLF were 500 m, -0.09 ps/nm/km at 1550 nm, 11.5 /W/km and 0.83 dB/km, respectively. Note that due to the phase erasure process, the binary data modulation was not transferred to the idler. Then, the weak idler wave was filtered and injected into a (slave) semiconductor laser (Pump2) by means of a wavelength division multiplexer. As the injection locking is a much slower process than FWM (typically having a (sub)-GHz bandwidth if the master power is < 30 dB that of slave [88]), any high frequency fluctuations (e.g., bit-to-bit phase variations) present on the original data signal were not transferred onto the output of the slave laser. The slave laser output was also free of any amplitude noise present on the idler.

At this stage Pump1 and Pump2 were phase locked to the signal and could serve as pumps in a degenerate PSA configuration. They were coupled together with the data signal and the three waves were amplified to a total power of 34 dBm and launched into an alumino-silicate strained HNLF for phase regeneration. The length, dispersion at 1550 nm, polarization mode dispersion, nonlinear coefficient and attenuation of the fibre were 177 m, -0.13 ps/nm/km, 0.11 ps/km$^{0.5}$, 7.1 /W/km and 15 dB/km, respectively. The relative powers of the pumps and signal were adjusted for optimal regeneration performance (by observing the demodulated eye diagram after the regenerator). Any slow (sub kHz) relative phase drifts between the interacting waves picked up due to acoustic and thermal effects present prior to the PSA fibre (e.g., in the HNLF that generates the seed of the second pump) were compensated for by an electrical phase-locked loop that controlled a piezoelectric-based fibre stretcher in the pump path. The feedback was implemented using a commercial analog PI controller.

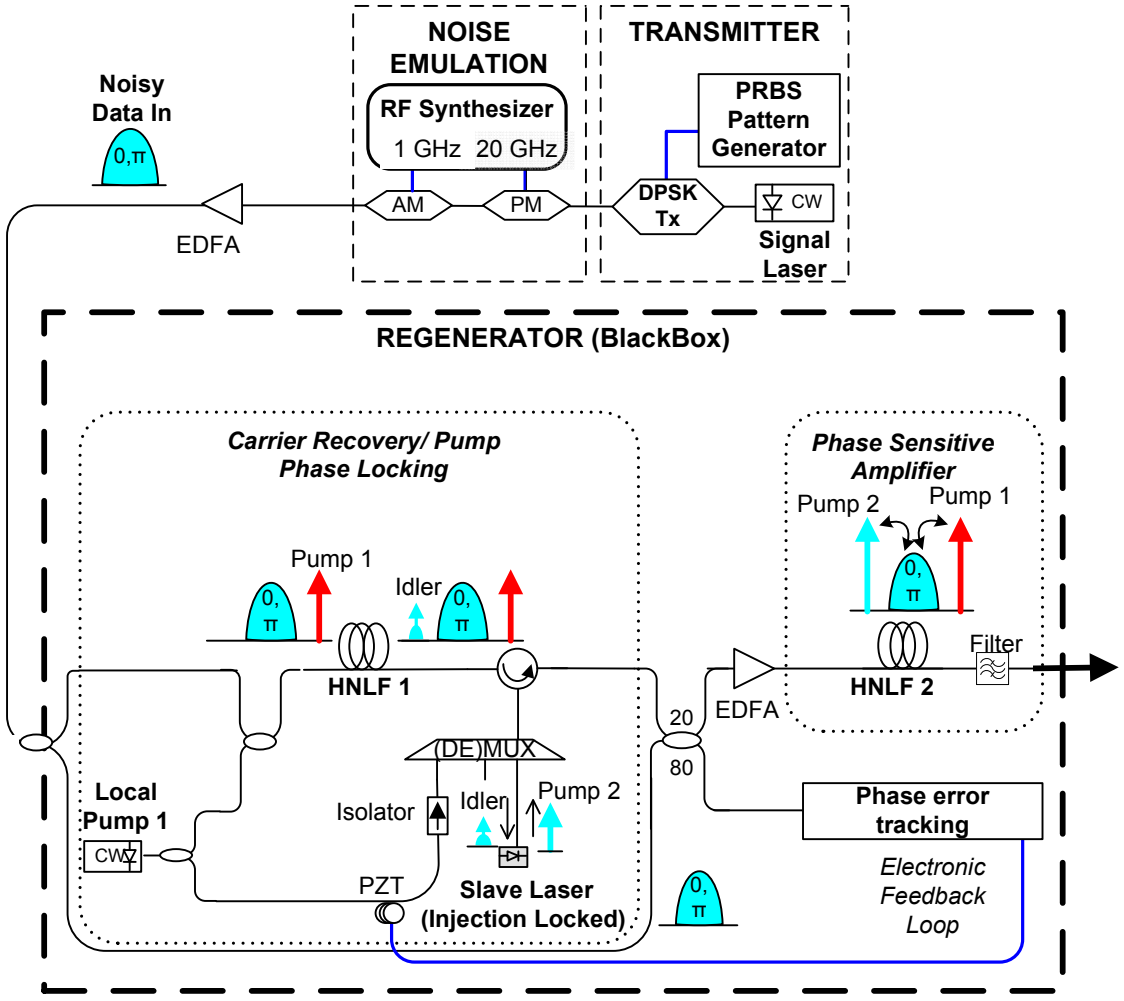

FIGURE 5.3: Experimental set-up for first generation blackbox DPSK regenerator. AM - Amplitude Modulator, PM - Phase Modulator.

5.3.2 Experimental Results

5.3.2.1 Static Characterization

The initial measurements were carried out at 10 Gbit/s due to the limited bandwidth of the constellation analysis setup available at the time. The spectrum at the output of HNLF1 is shown in Fig. 5.4. The power of the generated idler was approximately -17 dBm which provided a sufficient power margin to do the subsequent injection locking (the power used for injection locking was -25 to -30 dBm). Fig. 5.5 shows a tap of the input to HNLF2. Note that the pumps both have high OSNR (higher than is shown in the spectrum due to the 20 dB attenuation of tap). Fig. 5.6 shows the output of the locked PSA with the PSA set to minimum and maximum gain conditions. This shows

that 15 dB PS swing was achieved, which from the previous experiments (see Section 4.2.2) was potentially good enough for phase regeneration.

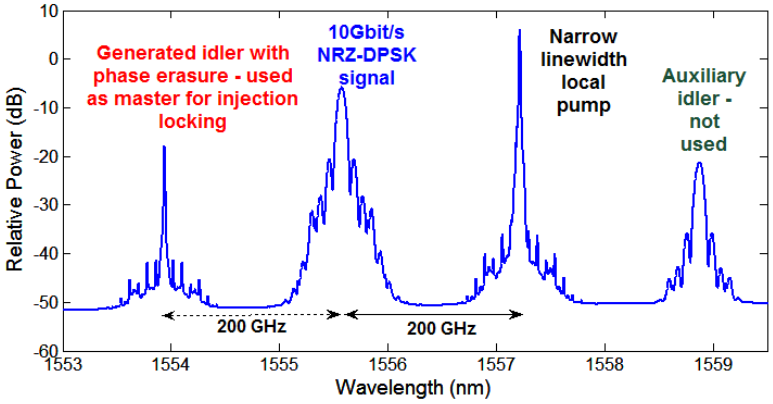

FIGURE 5.4: Spectrum at the output of HNLF1 showing the 10 Gbit/s DPSK signal, local pump and phase-erased idler.

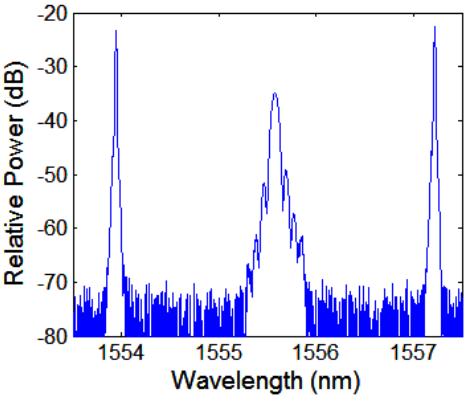

FIGURE 5.5: Spectrum at the input of HNLF2 showing the DPSK signal and two clean pumps.

5.3.2.2 10 Gbit/s Phase-Only Regeneration Results

The performance of the regenerator was first studied using a constellation analyzer based on a homodyne coherent receiver and offline digital signal processing (DSP) operating at 10 Gbit/s [89]. The homodyne approach was chosen over the intradyne one to avoid any artificial phase compression that might be performed during the digital carrier recovery process if an intradyne system were used. A local oscillator was combined with the signal using a 90 degree hybrid, and the hybrid's outputs detected using two balanced photodiodes and a 20 GHz real-time oscilloscope from Tektronix operating at 50 GS/s. The local oscillator used in the measurement was obtained by tapping off the signal laser before data encoding. The signal electrical field could then be reconstructed offline [89],

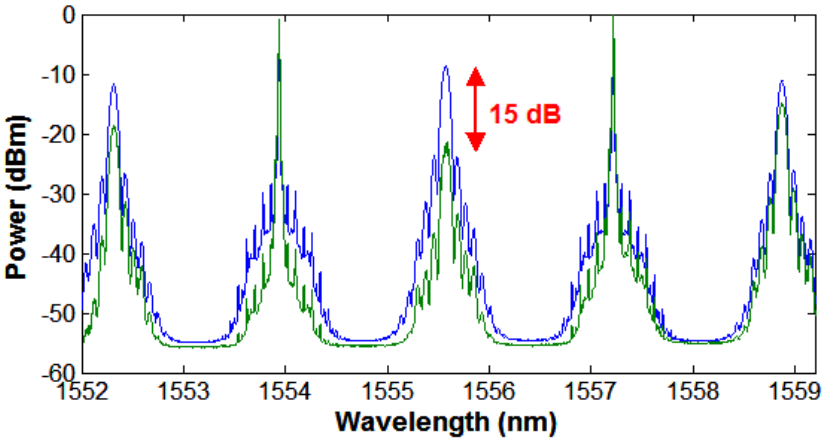

FIGURE 5.6: Spectrum at the output of HNLF2 showing the phase-regenerated DPSK signal as the feedback controller is varied to tune the PSA from maximum gain to minimum gain condition, showing a PS swing of 15 dB.

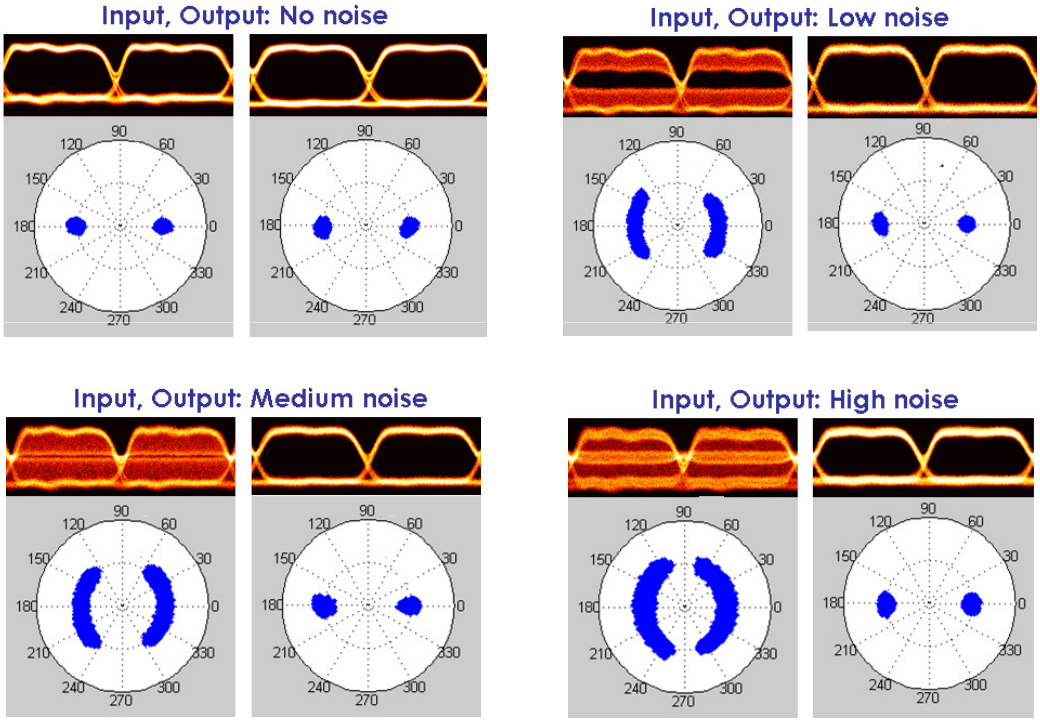

FIGURE 5.7: Signal quality at the input and output of the regenerator; eye diagrams measured using a high speed balanced photodiode and differential constellation diagrams (showing bit-to-bit phase changes) measured at 10 Gbit/s using a homodyne coherent constellation analyser.

and from these measurements, amplitude and bit-to-bit phase changes were determined and the corresponding DPSK constellation diagrams are shown in Fig. 5.7. Note that for these measurements, the data rate was adjusted to 10 Gbit/s and the phase modulator that distorted the signal was driven at approximately 5 GHz . The results showed that the phase noise could be squeezed by the regenerator to the back-to-back level and almost negligible amplitude noise was induced even for as extreme peak-to-peak values of phase distortion as $\pm 60^{\circ}$ (Fig. 5.7).

5.3.2.3 40 Gbit/s Regeneration Results

The regenerator was then fully assessed at 40 Gbit/s. First, the signal was degraded with sinusoidal phase noise. The RF power driving the phase modulator that imposed phase noise on the signal was calibrated to deliver two noise levels causing phase deviations of $\pm 30^{\circ}$ and $\pm 50^{\circ}$). The signal was then demodulated using a 1-bit delay line interferometer (DLI). BER measurements of the demodulated signals were performed using a high speed single-ended photoreceiver, while eye diagrams of the demodulated eye were recorded using an all-optical sampling oscilloscope. Eye diagrams measured at the input and output of the regenerator for no noise and for the highest level of the added phase noise are shown in the inset of Fig. 5.8a. Consistent with what was measured at 10 Gbit/s previously, the regenerator was able to improve a severely degraded eye with an output close to back-to-back level. BER measurements provide a more quantitative measure of the improvement, and these are shown in Fig. 5.8a. At the input of the regenerator, the added phase noise caused significant error levels. At the output of the regenerator an open eye diagram and error-free performance were achieved with a power penalty under 1 dB as compared to the back-to-back, for both added noise levels.

The signal was then degraded with sinudoidal amplitude noise at 1 GHz, to varying depths of 25% and 50%. Both BER and eye diagram data are shown in Fig. 5.8b (eye diagrams shown are for the higher noise level). Again, to allow a more quantitative analysis of the performance, BER curves are shown in Fig. 5.8b. At the input of the regenerator, the added amplitude noise caused the BER curves to reach levels ranging from 10^{-6} to 10^{-4} for the maximum input power available into the receiver (-22 dBm). At the output of the regenerator, BER of 10^{-9} was achieved for all noise levels investigated, albeit with up to 3 dB power penalties compared to the regenerator output in the absence of input signal degradation. For the highest level of noise, the regenerator output eye diagrams were quite open, although the corresponding BER curve starts to show a modest deviation from a straight line.

Finally, the regenerator performance was then assessed for various levels of simultaneous amplitude and phase perturbations when the lower levels of amplitude and phase perturbations were then simultaneously applied, i.e. $\pm 30^{\circ}$ of phase noise and $\pm 25\%$ of amplitude noise (Fig. 5.8c).The regenerator successfully eliminated both the amplitude

and phase noise, with error free BER (10^{-9}) achieved despite the input having an error floor at the 10^{-7} level.

It can be seen that in the absence of added noise, the signal at the regenerator output had better noise performance than that at the input, something that can be seen by the 0.5 - 1 dB power penalty improvement in Fig. 5.8. The reasons for this are unclear, although possibilities include the fact that perhaps the transmitter output was sub-optimal, or that the single-polarization components in the regenerator linearly filtered out noise from the orthogonal polarization.

5.4 Second Generation Blackbox DPSK Regenerator

One of the main challenges with the first generation regenerator was that the configuration (Fig. 5.3), in which the signal is split into two, with half the power being used for pump synthesis after which the pumps were combined with the other half, was very unstable. This was due to the pumps and signal being in separate fibres for over 500 m prior to the PS-FOPA. This made the device very susceptible to thermal and acoustic pickup, requiring kHz speed analog feedback. In addition, despite using a high voltage (100 V) driver for the fiber stretcher, the feedback needed a reset quite frequently (every 5-10 s) whenever the voltage amplifier had reached its maximum voltage. A new system was therefore designed that would be more stable, and hence more practical, by ensuring the interacting waves stayed in the same fibre whenever possible. Also, while the previous regenerator was only tested using sinusoidal phase and amplitude noise, measures were now taken to better emulate the white (wideband) noise present in real links. This natural progression of work was in line with the PHASORS project plan, that included demonstration of an improved regenerator using state of the art components. This experiment was jointly carried out with Dr. Radan Slavík and Dr. Francesca Parmigiani.

5.4.1 Experimental Setup

The set-up is shown in Fig. 5.9. A 40 Gbit/s (or 56 Gbit/s) non-return-to-zero (NRZ) DPSK $2^{31} - 1$ PRBS was modulated onto a narrow linewidth CW fibre laser (a Rock laser from NP Photonics, USA) with a $LiNbO_3$ Mach-Zehnder modulator symmetrically driven around its null transmission. To emulate nonlinear phase noise, the data signal was further modulated in a $LiNbO_3$ phase modulator driven by electrical white noise, generated by a fast photodiode fed by amplified spontaneous emission (ASE) noise of 0.4 nm 3 dB bandwidth. The 3 dB bandwidth of this electrical noise was measured using an RF spectrum analyzer to be 16 GHz. Further, it was characterized in the temporal domain using a fast electrical sampling oscilloscope (bandwidth of 60 GHz).

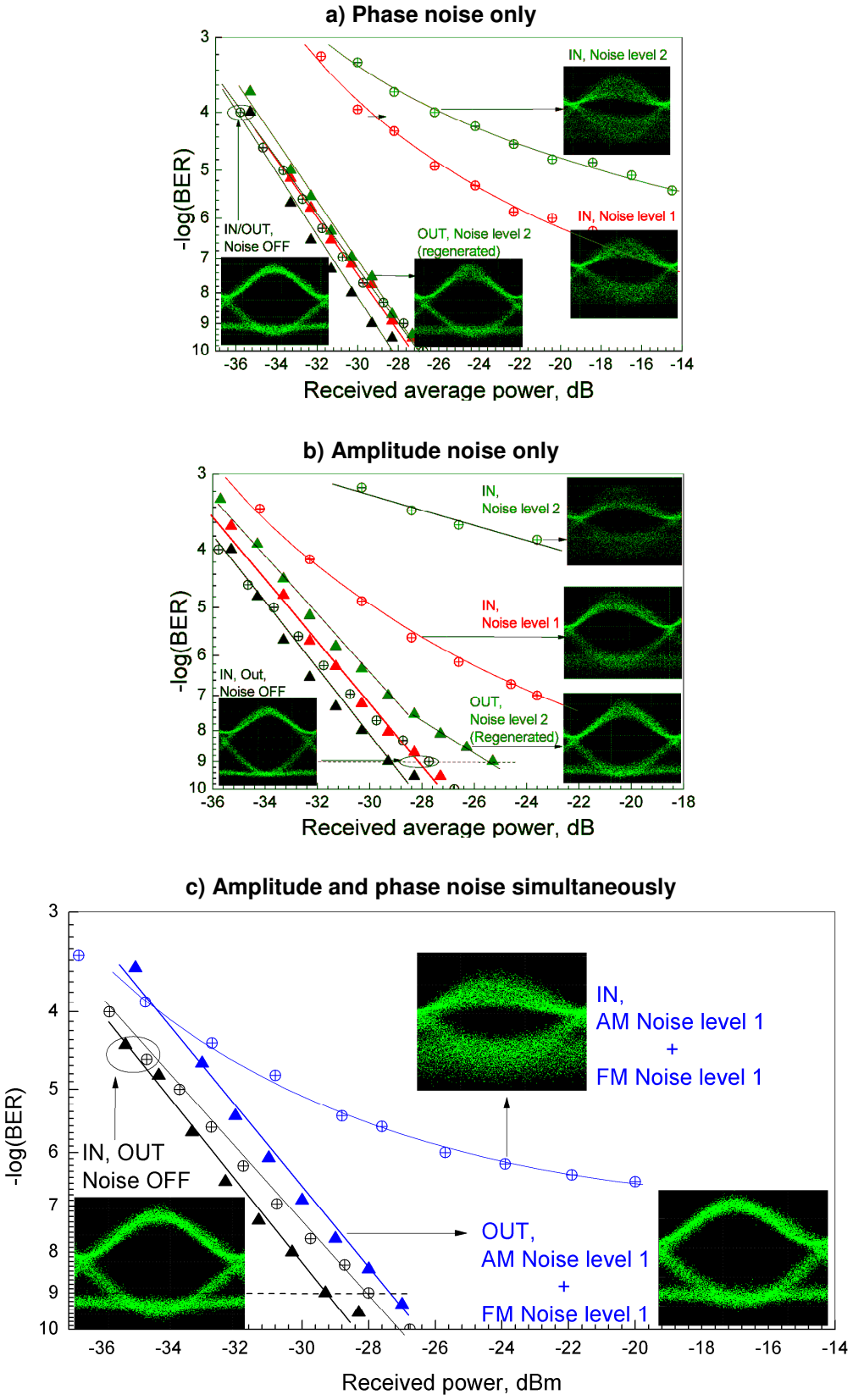

FIGURE 5.8: BER curves when phase-only (a), amplitude-only (b) and both amplitude and phase (c) noise is present at the input of the regenerator. The performance at the regenerator input and output is shown as circles and triangles, respectively (no noise: black; lower level of amplitude or phase noise: red; higher level of amplitude or phase noise: green; combined (lower level) amplitude and phase noise: blue).

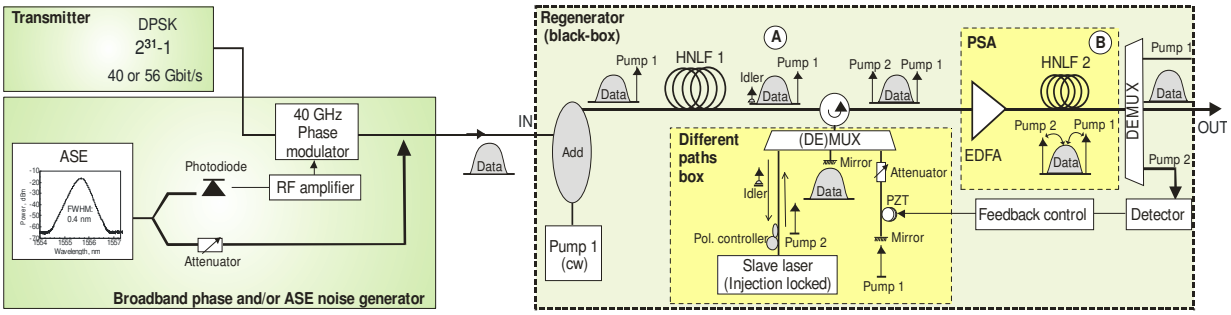

FIGURE 5.9: Experimental schematic for second generation blackbox DPSK regenerator.

For emulation of the linear amplitude and phase noise, a portion of the ASE, which was fed into the photodiode (inset in Fig. 5.9) was directly combined with the data signal. The magnitude of the amplitude and phase perturbations was controlled by varying the ASE power. In the PSA characterization, two levels of noise in phase and amplitude were used. Analyzing the electrical driving signal sent to the modulator with the fast sampling oscilloscope and using the estimated 5.5 V_π of the phase modulator, Levels 1 and 2 of the noise produced about 0.1% and 1%, respectively, of samples with added phase error of more than $\pm 45°$ (0.25 V_π). These drive noise statistics in the temporal domain are shown in Fig. 5.10. As for the ASE noise optically coupled to the signal, its optical power levels were -15 and -13 dB with respect to the signal.

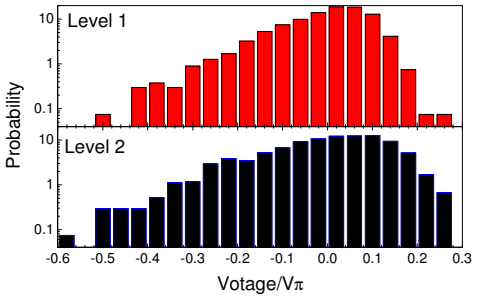

FIGURE 5.10: Statistics of the RF signal sent to the phase modulator to emulate non-linear phase noise for the two levels used.

The 13 dBm DPSK signal, now with added phase and amplitude noise, was launched into the regenerator. Care was taken to ensure that PM components were used, with the only exceptions being the section of the setup that operated in reflection, and the HNLF used for the PSA (HNLF 2). Rather than tapping off the data signal for the synchronization of the pumps as was the case in the previous implementation (Fig. 5.3), the data signal in its entirety was used in the phase synchronization process. First, the signal was combined with a CW local pump (Pump 1, its frequency was 200 GHz away from the data carrier frequency and its total output power was 17 dBm, Orbits

lasers Inc.) using an add-drop multiplexer (data insertion loss of 0.5 dB) and then sent to a PM HNLF (HNLF 1) to generate an idler used for subsequent injection locking, as explained earlier. The length, dispersion, nonlinear coefficient and insertion loss of HNLF 1 were 300 m, 1.3 ps/nm/km, 10.5 /W/km and 0.9 dB, respectively. The spectra at the output of this stage are shown in Fig. 5.11.

Following this stage, the three signals (Data, Pump 1, Idler) were separated in a 4-channel 200 GHz demux (insertion loss 1 dB) placed behind a circulator. A mirror provided retro-reflection in the data path as well in the path of Pump 1, which also included a PZT stretcher (60 mm total length, maximum phase change of 5π) and a variable attenuator. A semiconductor laser, which was injection locked to the idler, was used to generate Pump 2 in the idler path. Pump 2 was thus phase-locked to the idler (and thus also to the data and Pump 1). The operation of the demux in the double-pass (reflection) mode has several advantages: (i) it allows for direct injection locking of the semiconductor laser, and (ii) it provides filtering characteristics enhanced over those obtained if only used in single-pass operation, which proved essential in the following PSA stage. Note that all the optical waves involved in the regeneration process share a common path through most of the regenerator, except for the output side of the demux. This contrasted with the 500 m (in HNLF 1) in the previous setup (Fig. 5.3) where the signal was separate from Pump 1 and the idler. The lengths of fibre at the demux output ports can be kept short (<2 m in the set-up and could be reduced to a few tens of cm if needed) and all can be kept in even closer proximity during packaging to ensure that they experience similar acoustic/thermal pickup further reducing the environmental sensitivity of the system.

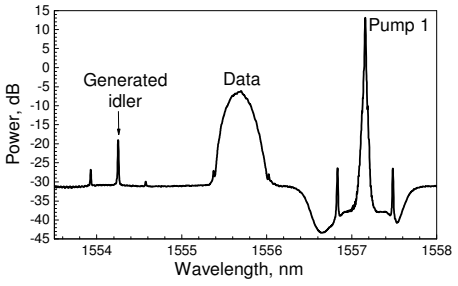

FIGURE 5.11: Spectrum at the output of the PIA stage

The data stream with the two phase locked pumps was then launched into the PSA which consisted of a high power EDFA (total power of 29 dBm) and a 180 m sample of a high SBS threshold HNLF (theshold over 26 dBm). This fibre had an alumino-silicate core and a linear strain gradient along its length (ranging from 400 to 20 g). The dispersion, polarization mode dispersion, nonlinear coefficient and attenuation of the fibre were -0.17 ps/nm/km, 0.35 ps/km$^{0.5}$, 7.5 /W/km and 15 dB/km, respectively. The relative powers of the pumps and signals were adjusted for optimal regeneration performance (using the

attenuator and the bias current of the slave laser in pump paths 1 and 2, respectively). For optimum performance the PSA was operated in deep saturation resulting in a strong variation of pump power at the PSA output as a function of the relative phase between the pump and signal beams, as shown in Fig. 5.12. This feature was used to control the PZT fibre stretcher (i.e. the minimum of the pump power corresponds to the maximum PSA gain of the data, which is the correct operation point of the regeneration). No sign of acoustic pick-up was observed in the output signal and only low bandwidth control (Hz range) was needed to compensate for thermal drift. Just 5π of continuous phase adjustment was required to keep the system locked, indicating in excess of an order of magnitude improvement over the previous embodiment.

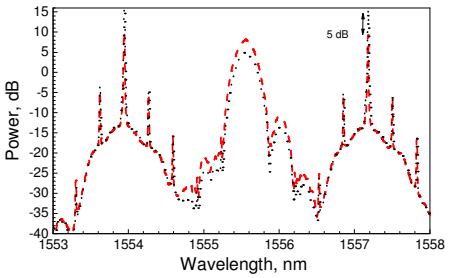

FIGURE 5.12: Spectra at the PSA output for maximum gain (red, dashed) and deamplification (black, dotted).

5.4.2 Experimental Results

The regenerator performance was assessed using an EXFO constellation analyzer (PSO-200) based on all-optical sampling and capable of operation up to 100 Gbaud, Fig. 5.13. Severe phase distortions were introduced using the phase modulator (these were larger than those subsequently used in the BER characterization) in order to verify that the regenerator can operate at extremely large levels of noise and in order to easily visualize the noise statistics by being able acquire data samples over a short time period. The results at 40 Gbit/s and 56 Gbit/s show that the phase noise can be significantly squeezed by the regenerator with negligible induced amplitude noise.

Subsequently, 40 Gbit/s BER measurements were taken at the input and output of the regenerator for various levels of the phase-only, ASE-only and combined noise, Fig. 5.14. The receiver consisted of a bandpass filter (0.5 nm bandwidth measured at -0.5 dB), attenuator (the received power was measured at its output), low noise EDFA, a bandpass filter, a 1-bit DLI, and a photodetector receiving an average power of 7 dBm. In Fig. 5.14a, it is observable that no power penalty with respect to the back-to-back is present when there is no noise at the PSA input. For all levels of phase-only (Fig. 5.14a), ASE-only (Fig. 5.14b) and combined noise (Fig. 5.14c), there is some error flooring for

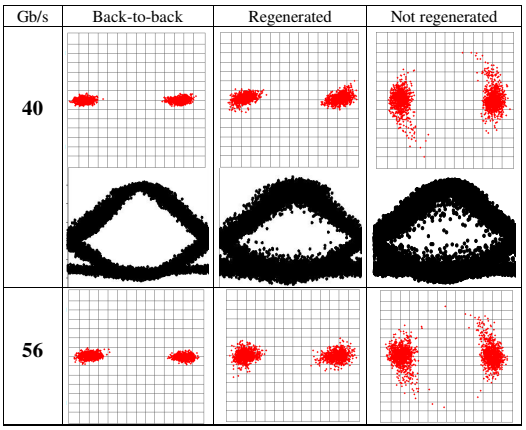

FIGURE 5.13: Constellation diagrams for back-to-back and for added phase noise for two data rates and the corresponding demodulated eyes for 40 Gbit/s.

the signal both with and without the regenerator. The floor levels are summarized in Fig. 5.14d. Included are simulation results using similar noise statistics [1]. Fig. 5.14d clearly shows the agreement between experiments and simulations and also highlights that the regenerative performance of the PSA is especially good in the case where the signal is impaired by nonlinear phase noise.

5.5 Field Trial of the PS DPSK Regenerator

5.5.1 Link and Regenerator Configuration

Having previously only tested the regenerator when placed just before the receiver with the input signal impaired using artificial phase and amplitude noise, a more realistic assessment was performed by installing it as an inline device in the middle of a dark fibre link. This experiment was performed jointly with Dr. Radan Slavík. The dark fibre link was part of the UK JANET Aurora Network and extended from Southampton to London and back again. Within the 400 km dispersion-compensated transmission distance were 6 in-line flat-gain EDFAs with maximum input/output powers of -5/15 dBm, operated in automatic gain control, each with nominal gain 20 dB. Configuring the link involved visiting the various access points, installing EDFAs and ensuring remote access to them via a telnet connection, installing dispersion compensation modules, and designing a power budget to ensure that the amplifiers were running at optimum power and gain levels, crucial for maximising the aggregate gain profile. It proved very useful exposure to real optical networks.

[1] The numerical simulations were carried out by A. Bogris, University of Athens, using noise statistics closely matching those used in the experiment. See [90] for further details.

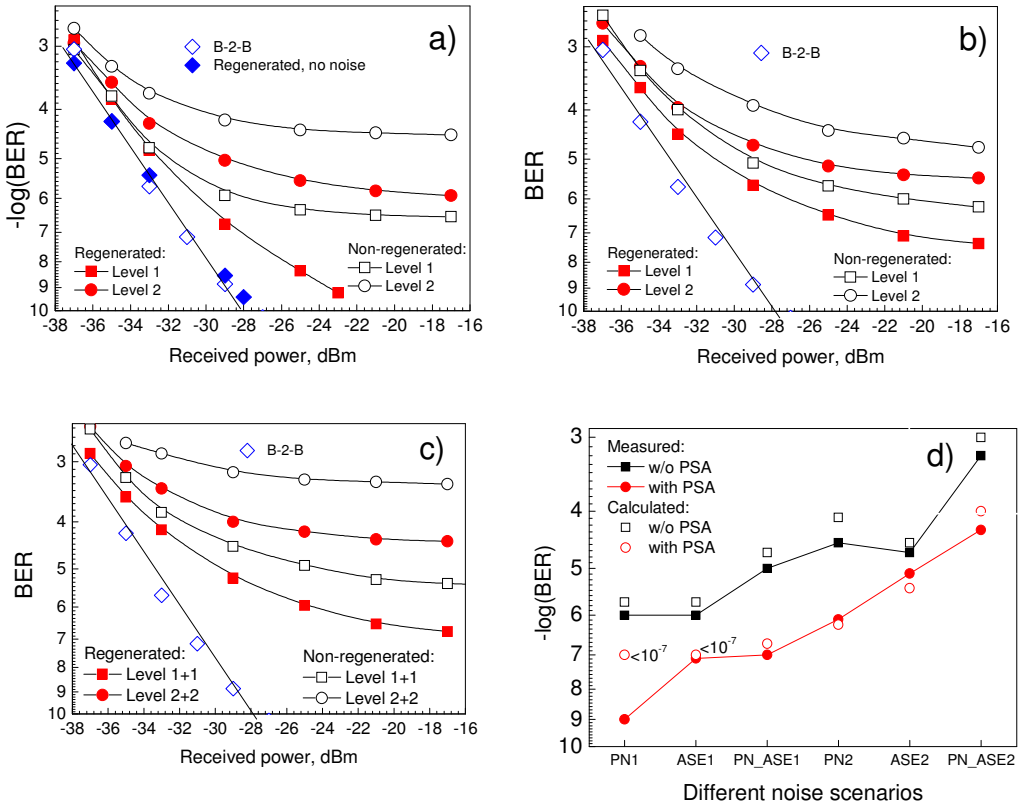

FIGURE 5.14: BER measurements for back-to-back and for added phase noise for two data rates and the corresponding demodulated eyes for 40 Gbit/s. (a) Phase noise only, (b) Added ASE only, and (c) Phase noise plus added ASE. (d) Minimum BER values for all the cases studied as measured during the experiments and calculated by extensive error counting simulations. In the simulations the BER calculation was limited to BER $> 10^{-7}$.

The link map is shown in Fig. 5.15. As all the access points along the network comprised single racks in large commercial datacentres, it would have been impractical to have installed the regenerator at an access point other than Southampton, as that would have needed space for the device and diagnostic equipment, as well as a continual human presence at these remote sites for the duration of the experiment. Instead, the solution was to send the data channel all the way through the loop-backed link (400 km), perform the regeneration in the lab in Southampton, and then send the data for a second pass through the link. This necessitated performing a wavelength conversion after the regenerator so that the pre- and post- regenerator channels could be present in the link simultaneously. This also meant that the effective link span was doubled to 800 km, a useful benefit. Obviously, conversion of the wavelength would not normally be required in most transmission applications, nevertheless, it serves to illustrate another useful potential application of these parametric devices.

A conceptual outline of the network and its practical implementation are shown in Fig. 5.15 and Fig. 5.16 respectively. At the transmitter, 37 CW semiconductor lasers

on a 100 GHz DWDM ITU grid were combined and modulated with a 40 GHz $2^{31} - 1$ PRBS. To de-correlate adjacent channels, the odd/even channels were split in an interleaver, and 55 ns of relative delay introduced between them before they were re-combined. 37 channels (excluding ITU Channel 23) were sent down the link. The maximum total power launched into the link was 7 dBm with maximum power along the link of 15 dBm. At the link output, ITU Channel 27 was routed to a separate path using an WDM demultiplexer and wavelength converted to ITU Channel 23 (either with or without regeneration) and sent through the link again with all other channels. This is schematically shown in Fig. 5.16. There were a total of 38 channels occupying the link at any point in time.

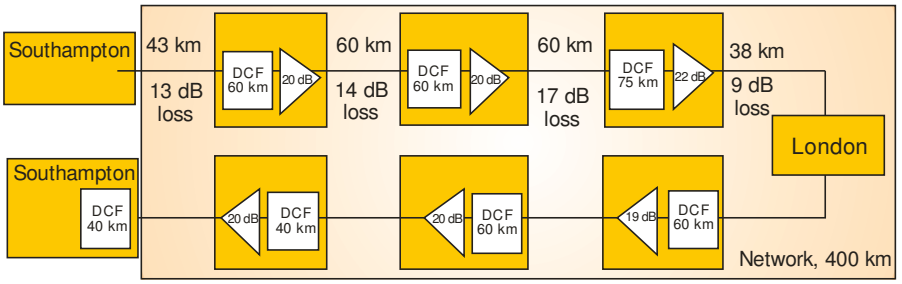

FIGURE 5.15: Dark fibre link configuration. DCF: dispersion compensating fibre.

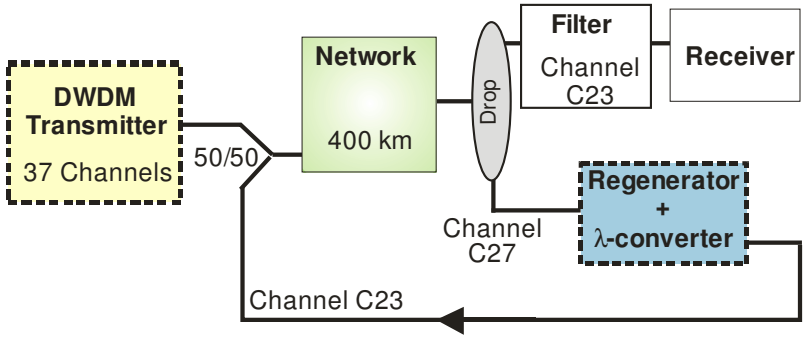

FIGURE 5.16: Schematic of link setup with regenerator as an in-line device

The regenerator setup was that shown in Fig. 5.9. A commercial endless polarisation tracker from General Photonics was installed at the regenerator input to ensure that any fast polarisation drifts emanating from the link were eliminated before the polarisation sensitive regenerator. It did turn out that the link was very stable, and it was possible to manually align the polarisation and it would remain stable for a period greater than the BER measurement time, i.e. many minutes. This agrees with with other measurements of installed fibre links [36]. As such the polarisation tracker was useful, but not essential.

5.5.2 Regeneration Results

The regenerator was configured to perform simultaneous regeneration and multicasting and was mounted into a standard telecommunication rack along with other network components and test gear. To enable comparative study with/without regeneration, conventional wavelength conversion could be carried out by switching off Pump 2, see Fig. 5.9, resulting in phase insensitive FWM based wavelength conversion. The receiver consisted of a 0.6-nm bandpass filter, an attenuator (the received power was measured at its output), a low-noise EDFA, a bandpass filter, a 1-bit DLI, and a balanced photodetector.

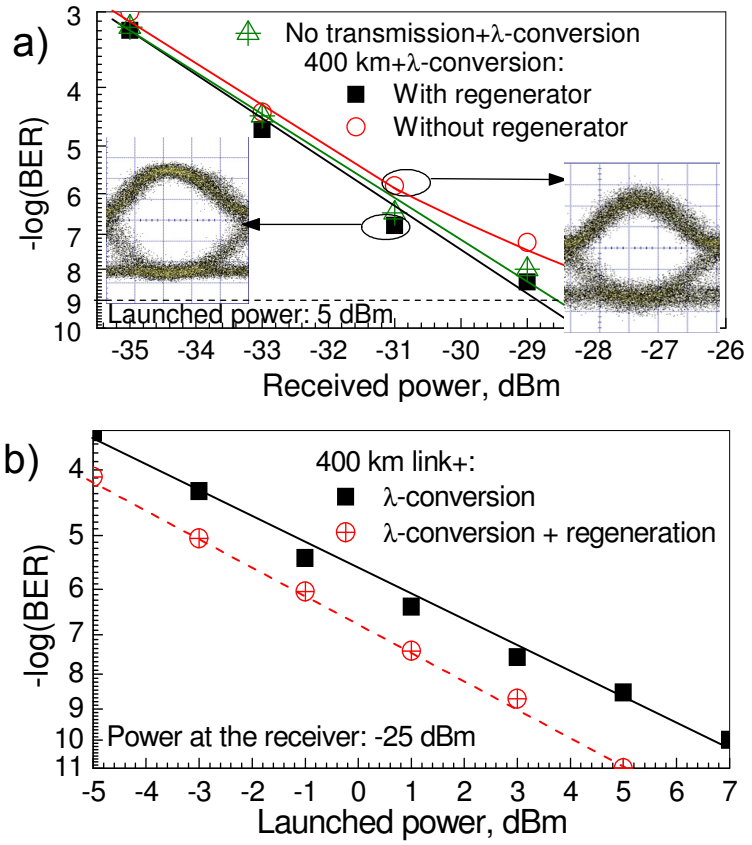

FIGURE 5.17: (a) BER curves at the output of the 1st round-trip (400 km) measured at the data Channel 23 measured for the maximum power into the link (7 dBm), For reference, a measurement of the λ-converted signal without transmission is also shown (green triangles). (b) BER measurement for various powers launched into the link and fixed receiver power of -25 dBm.

First, the transmitter/receiver and wavelength conversion stages were characterised without propagation through the network, Fig. 5.17a, triangles. Subsequently,the signal was sent through the network (400 km) and the regenerated + wavelength-converted signal was analyzed, Fig. 5.17. The regenerator fully restored data fidelity giving a received power improvement of 1.5 dB at a BER $> 10^{-9}$. Slight reshaping of the eye is also

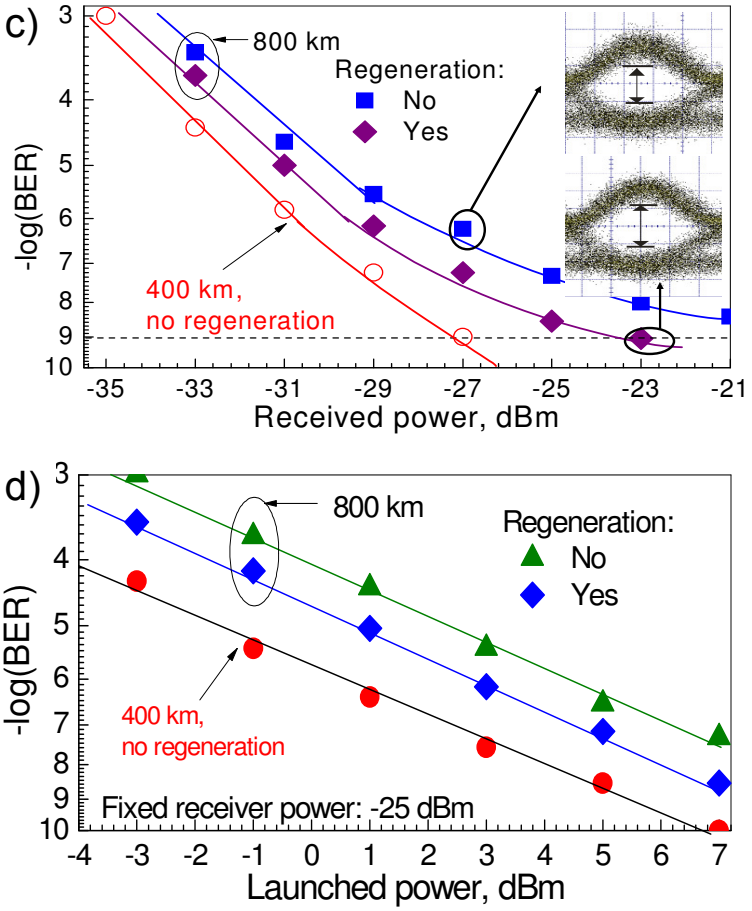

FIGURE 5.18: BER curves at the output of the 2nd round-trip (800 km) with and without mid-span regeneration: (a) for launched power of 5 dBm; (b) as a function of the launched power for fixed receiver power of -25 dBm. For reference, measurements of the signal at the mid-point (after wavelength conversion) are also shown.

observed, Fig. 5.18a, which may be responsible for the observed slight improvement of the BER curve as compared to that measured without transmission. Fig. 5.18b shows the improvement provided by the regenerator as the total power launched into the link (for a fixed power at the receiver) was varied. For identical performance, around 2 dB less total power can be sent through the link when the regenerator is used. As the BER improves monotonically with the launched power, it can be concluded that the noise generated in the link was dominated by the linear (ASE) rather than non-linear noise. This was a consequence of using many channels (low power per-channel) and propagation over a relatively modest distance.

Results obtained after two round-trips through the link (800 km, regenerator used in-line) are shown in Fig. 5.18. Use of a mid-point regenerator reduced the BER penalty by up to a factor of two (e.g., at BER 10^{-6}, it reduced the penalty from 2 dB to 1 dB and at BER 10^{-9}, from 5 dB to 2 dB). The error floor of the regenerated data was one order of magnitude less than without regeneration, meaning that the regenerator prevented

about 90% of errors in this regime. A closer study of the eye diagrams, Fig. 5.18a, shows about a 20% larger eye opening for the regenerated signal. Varying the input power into the link, Fig. 5.18b, showed almost 4 dB power penalty in the second round trip. This value was reduced to 2 dB when the regenerator was used.

5.6 Analog Error Correction in PS Regenerators

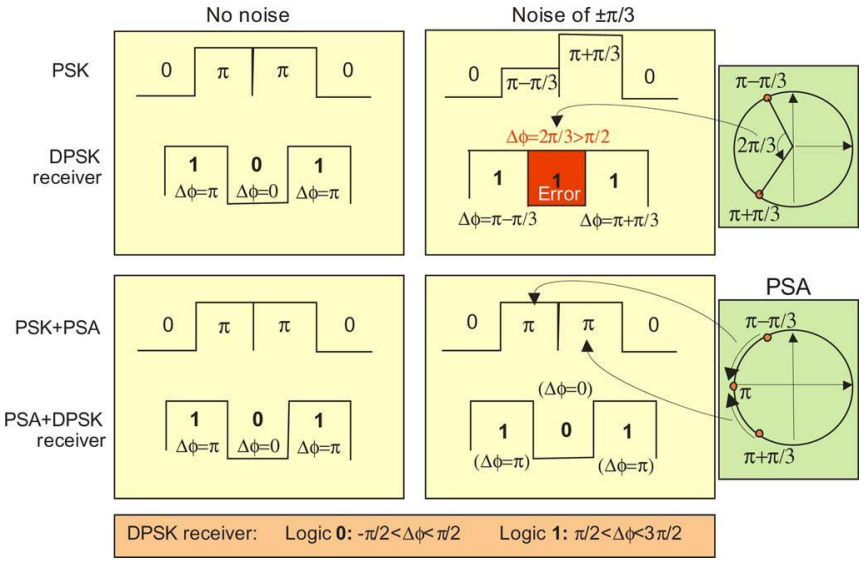

FIGURE 5.19: Schematic explanation of the PSA for BER improvement in differential coherent (DPSK) receivers. A data sequence of 0, π, π, 0 is considered

As suggested in Fig. 5.19, PS regenerators can correct errors when differential decoding of DPSK is performed, which is counter-intuitive, as regenerators typically do not improve BER when placed in front of a receiver. This phenomenon is due to a correctable class of errors specific to a 'differential' receiver. Consider an example - two consecutive bits with identical phases of π (Fig. 5.19) that during the transmission accumulate phase error of $\pi/3$ and $-\pi/3$, respectively. A DPSK receiver detects the difference in the phases of these consecutive bits of $2\pi/3$. The receivers decision point is at $\pi/2$ resulting in an erroneous detection of π rather than the correct value of 0. On the other hand, a PSA corrects the phase of each bit, before the evaluation of their difference in the differential receiver. Thus, a bit with phase $\pi + \pi/3$ is corrected to π, as signal of any phase within $\pi/2$ to $3\pi/2$ is pushed to the value of π by the PSA. The process is similar for the bit of phase $\pi - \pi/3$. Subsequently, the phase difference evaluated in the differential receiver results in the correct detection of 0.

This ability to correct for *differential* errors means that for signals degraded by nonlinear phase noise, after the PSA process the absolute and differential phase noise exhibit almost the same statistics [90]. This suggests that a DPSK receiver supported by a PSA

pre-amplifier could perform as well as an ideal homodyne PSK receiver. In principle this means that the homodyne coherent receiver, which is usually implemented with power greedy digital electronics, could be substituted by a simpler DPSK receiver which is assisted by a PSA regenerator.

5.7 Tolerance to Residual Dispersion

5.7.1 Experimental Measurement

The final test was a study of how the regenerator could cope with residual dispersion. A single channel at 40 Gbit/s was launched into the fully dispersion-compensated dark fibre link and propagated once (400 km). Various lengths of SMF-28 fibre were then added to the link output and the BER measured with and without the regenerator being placed in front of the differential receiver, Fig. 5.20. For a perfectly compensated link, the BER power penalty (at 10^{-9}) of the non-regenerated signal is 2 dB in respect to that regenerated. For 1 km SMF-28, there was negligible BER penalty both using the regenerator and without it. However, for 2.5 km of SMF-28, a BER penalty of 1 dB was measured when using the regenerator, while without the regenerator it rises to 4 dB. Thus, it could be concluded that the regenerator will give better improvements for small amounts of residual dispersion as compared to fully compensated link. When the SMF-28 length was increased to 8 km, the use of the regenerator resulted in poorer performance as compared to the non-regenerated case.

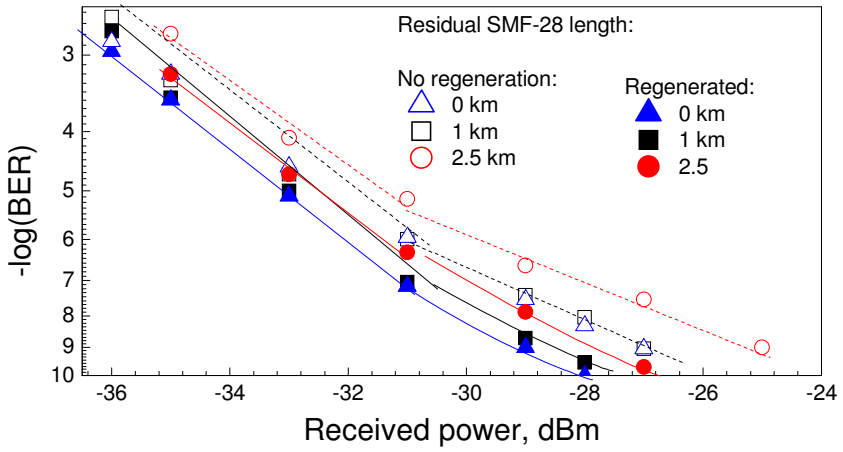

FIGURE 5.20: BER curves at the output of the 1st round-trip (400 km) using single-channel transmission when various length of dispersion-uncompensated SMF-28 fibre were added.

5.7.2 Analytical Explanation

The impact of uncompensated dispersion prior to the PSA can be understood by recalling that dispersion adds a quadratic frequency dependent relative phase shift to a dispersed signal. This phase shift can be calculated quite simply, using the relation [55]

$$\theta_{rel} = 2\pi c \cdot (\frac{\lambda_c - \lambda}{\lambda})^2 \cdot D \cdot L \tag{5.1}$$

where D is the fibre dispersion (17 ps/nm/km for SMF-28 at 1550 nm), L the length, λ_c the central, or carrier, wavelength and λ the wavelength at which the relative phase is being evaluated. It is then possible to estimate the phase-to-amplitude conversion as a result of this relative phase by using Eqn. 4.6. Fig. 5.21 shows this expression evaluated for a PSA of PS swing ≈ 20 dB. The effect on the signal power in many ways resembles a multi-lobe bandpass filter. One could define a 3 dB bandwidth for the main lobe of this hypothetical filter, and estimate how much residual dispersion is tolerable for a signal of a given bandwidth by ensuring the signal fits within the 3 dB bandwidth of this hypothetical filter. As can be seen from Fig. 5.21, 4 km of uncompensated dispersion would severely distort a 40 GHz signal.

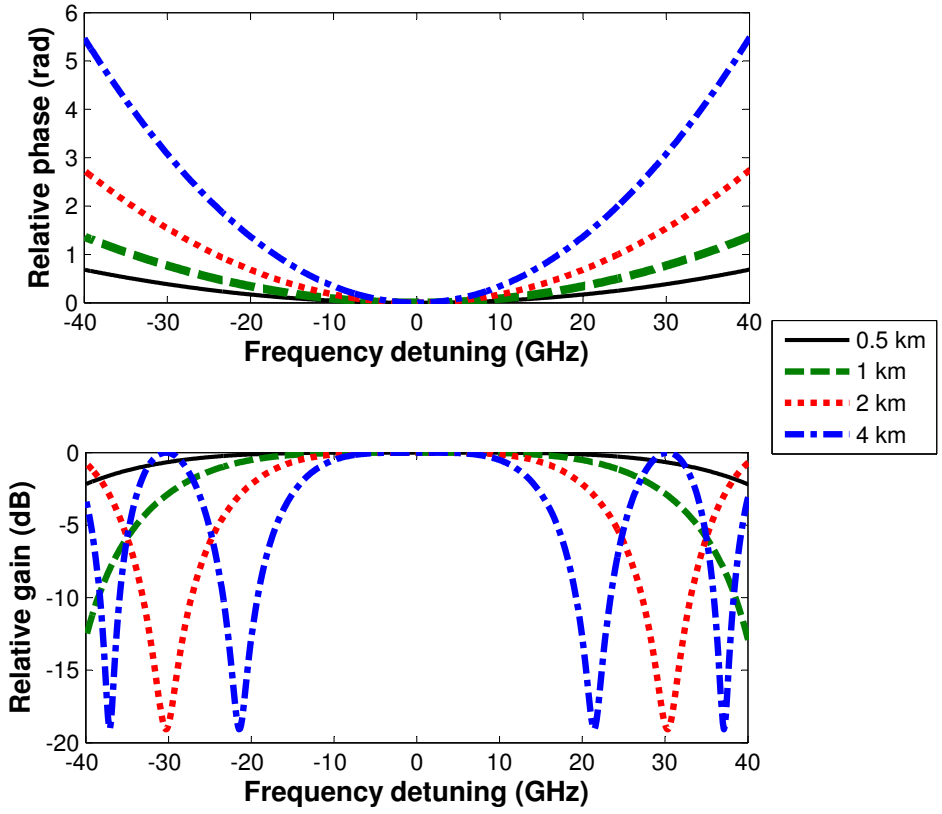

FIGURE 5.21: Analytical calculation of the frequency dependent relative phase added by propagation through varying lengths of SMF-28, as well as the resulting phase-to-amplitude conversion in a hypothetical PSA of 19 dB swing.

5.8 Conclusion

A DPSK regenerator based on a degenerate 2P-FOPA has been built and tested. The device advanced the state-of-the-art by incorporating a pump synthesis stage that allowed black-box operation. This involved the mixing of the incoming DPSK signal with a local pump, generating a modulation stripped idler that was then enhanced using injection locking, providing the second required pump. Because injection locking is a gain mechanism, the idler did not have to be very strong, hence modest powers could be used in the pump synthesis stage. The pumps and idler could then be combined and coupled into an SBS suppressed HNLF in which the phase was regenerated via the PS effect, while the amplitude was improved by power saturation. Detailed measurements using sinusoidal phase and amplitude noise confirmed the regenerative effects up to 40 Gbit/s.

The regenerator was then modified to make it less suceptible to thermal and acoustic perturbations and assessed with an input DPSK signal impaired by broadband non-deterministic noise, in both phase and amplitude. The device proved to be more stable. BER measurements showed signal improvement with the broadband input noise, although the improvement was not as large as was obtained with the sinusoidal noise. The regenerator was also tested mid-span on an installed 800 km link in a 38 channel system at 40 Gbit/s. While an order of magnitude BER enhancement was obtained, it is anticipated that better performance could be shown if the input signal had been deteriorated by nonlinear phase noise to a greater extent. The DPSK regenerator does have the ability to correct for a class of errors that occur in a differential receiver due to the fact that the bit-by-bit phase comparison that occurs in a DLI sums up analog phase deviations on successive bits, sometimes causing errors. Correcting for these phase deviations prior to the DLI can then prevent these errors from occuring. Finally, the impact of uncompensated dispersion prior to the regenerator was studied experimentally. It was concluded that dispersion should be compensated as would be done in a direct detection system, and a simple analytical theory supported that.

An objective analysis of the work involved in the DPSK regeneration work would conclude that it was a success. The final field demonstration was the culmination of 18 months of incremental work, both in terms of device fabrication from the partners, and system development in Southampton, and the body of results collected elicited a fair amount of positive feedback from the research community. This is perhaps best encapsulated in the acceptance of two post-deadline papers at the Optical Fiber Communications conference in 2010 and 2011, as well as a published paper in Nature Photonics.

Chapter 6

Multilevel Quantization of Optical Phase

6.1 Introduction

The exponentially increasing capacity demand in information systems will be met by carefully exploiting the complementary strengths of electronics and optics [91, 92]. Optical signal processing provides simple but powerful pipeline functions that offer high speed, low power, low latency and a route to densely parallel execution [93]. A number of functions such as modulation and sampling [94–97], complex filtering [98] and Fourier transformation [99] have already been demonstrated. However, the key functionality of all-optical quantization still required addressing.

All-optical quantization could be applied to regeneration, in which noise on digital optical signals is suppressed, crucial for fiber communications as well as photonic computing and regenerative photonic buffers. Also, it is key for all-optical analog-to-digital conversion (ADC), with benefits over the electronic equivalent including orders of magnitude higher bandwidth and quantum limited timing jitter [100]. Phase quantization could also find a role in processing the analog phase modulated optical signals being increasingly used for radio-over-fiber and antenna remoting applications, e.g. in radar and radio-astronomy [101].

All-optical quantizers have mainly been reported with reference to binary optical regeneration for legacy telecommunications applications requiring just a two step response. The Mamyshev regenerator [102] utilises Kerr nonlinearity to shift the carrier frequency of binary OOK signals, whilst not transferring the lower intensity analog noise. The nonlinear optical loop mirror (NOLM) performs a similar function, except that the signal and noise are separated into different ports of an optical coupler [103]. BPSK signals can be regenerated using NOLMs if in addition to the noisy signal, a pump beam at the

same wavelength is coupled into it [79]. Alternatively, degenerate parametric amplifiers can be used as is discussed in Chapter 5.

The above mentioned binary schemes are incapable of directly supporting advanced formats such as quadrature phase shift keying (QPSK), whose four phase states allow two bits per transmitted symbol. To achieve regeneration of signals with more than two levels, a number of indirect approaches have been suggested. One of these is the use of parallel BPSK regenerators, each regenerating one of the I and Q quadratures in a QPSK signal [104]. Another solution is to perform BPSK to OOK conversion using linear interferometers, amplitude regenerate the OOK streams in parallel, and perform all-optical format conversion to synthesize a clean (regenerated) QPSK signal [105, 106] . The parallelistic approach of both these schemes, often favoured in electronics, is complicated in optics due to the requirement to equalize and stabilise multiple optical paths (often over 100 m long with silica fiber implementations) in phase, polarization and propagation delay, which is both complicated and costly. In addition, linear scaling of component count and power utilisation would offset much of the benefit of adapting higher order modulation formats.

In addition to regeneration, for more sophisticated processes such as ADC, quantization to more than two levels is a must. Research into photonic quantizers for ADCs has been ongoing for four decades. Whilst numerous architectures have been proposed [100], a niche for an ultrafast all-optical quantizer still exists. Photonic quantizers providing bandwidths $>$ 100 GHz, effective number of bits (ENOB) of at least 4 and power consumption under 5 W would offer real competitive advantage as compared to the current electronics alternative [100, 107]. With this in mind, effort was made to realise a scheme to quantize phase encoded signals to multiple levels. Multilevel phase regeneration was listed as one of the stretch objectives of the PHASORS project, and following the initial system demonstrations of DPSK regeneration this piece of work commenced, and run parallel to the DPSK regeneration work. Dr. Adonis Bogris from the University of Athens is acknowledged for providing support in terms of numerical simulations that validated some of the hypotheses behind this concept.

6.2 Concept

In electronics, the use of digital systems relying on the flow of electrical currents, as well as the fortuitous availability of the *pn* junction with its intrinsic switching capability means that quantizers are built acting on input amplitude. Phase on the other hand is inherently a 2π bounded variable, raising the question as to whether phase quantization would be easier to achieve than doing the same with amplitude.

Consider the cosine function as an example. For an input ϕ ranging from 0 to 2π, $cos(\phi)$ resembles a 2 level phase quantization operation as its result is a variable of phase $\phi_s = 0$

for $\pi/2 \leq \phi < 3\pi/2$, and $\phi_s = \pi$ everywhere else. We can rewrite $cos(\phi)$ as the sum of complex exponentials obtaining:

$$A_s(\phi) \cdot \exp(i\phi_s) = \cos(\phi) = \frac{1}{2}(\exp(i\phi) + \exp(-i\phi)) = \begin{cases} 0 & \text{if } \pi/2 \leq \phi < 3\pi/2 \\ \pi & \text{otherwise} \end{cases} \tag{6.1}$$

where ϕ_s is the 2 level quantized phase output, and $A_s(\phi)$ is the accompanying π-periodic amplitude response.

Equation 6.1 suggests that an arbitrarily phase encoded signal $exp(i\phi(t))$ can be quantized in phase to 2 levels phase quantizer by coherently adding to it a phase conjugated version of the input signal, $exp(-i\phi(t))$. This is in fact what happens in a degenerate PS-FOPA, as can be seen in the simplified transfer function, Equation 4.6. The real leap forwards enabling multi-level phase quantization is the realization that Equation 6.1 can be generalised by rewriting it as

$$A_s(\phi) \cdot \exp(i\phi_s) = \exp(i\phi) + \frac{1}{M-1}\exp(-i\phi(M-1)) \tag{6.2}$$

where M refers to the number of phase levels. Fig. 6.1 shows the result of evaluating Equation 6.2 for 3 values of M. For M=2, the phase transfer function is very sharp, with a perfect π step. This is accompanied by a strong phase-to-amplitude conversion. As the value of M increases, the periodicity of the phase TF matches M as expected, but the step becomes less defined, and the depth of the phase-to-amplitude conversion is also seen to reduce. The phase transfer functions as derived in Equation 6.2 are all monotonic with M turning points. While this provides maximum local flatness at 0, $2/M\pi$, $3/M\pi$ etc., it is not necessarily ideal for a quantizer in which the target is to minimise the global phase error variance. One solution is to rewite Equation 6.2 by substituting the coefficient of the conjugate term with a variable m.

$$A_s(\phi) \cdot \exp(i\phi_s) = \exp(i\phi) + m \cdot \exp(-i\phi(M-1)) \tag{6.3}$$

Fig. 6.2 shows the result of varying m in Equation 6.3 for M=4. Three values are used, including 0.33, which is the coefficient as calculated from Equation 6.2. To optimise for m, a misfit factor was designed such that an ideal value can be numerically identified. The misfit factor, as shown in Equation 6.4, integrates the difference between a given phase transfer function, and an ideal step.

$$\text{Misfit Factor} = \log(\frac{2}{\pi}\int_{-\pi/M}^{\pi/M} |\phi_s(m,\phi)| \quad d\phi) \tag{6.4}$$

The impact of varying m on the misfit factor are shown in Fig. 6.3, for M values of 2 to 5. A misfit factor of 0 is obtained for $m = 0$ for all values of M, indicating that no phase quantization is achieved, and that the output phase is identical to that at the input. The smaller the misfit factor, the closer the phase transfer function approaches

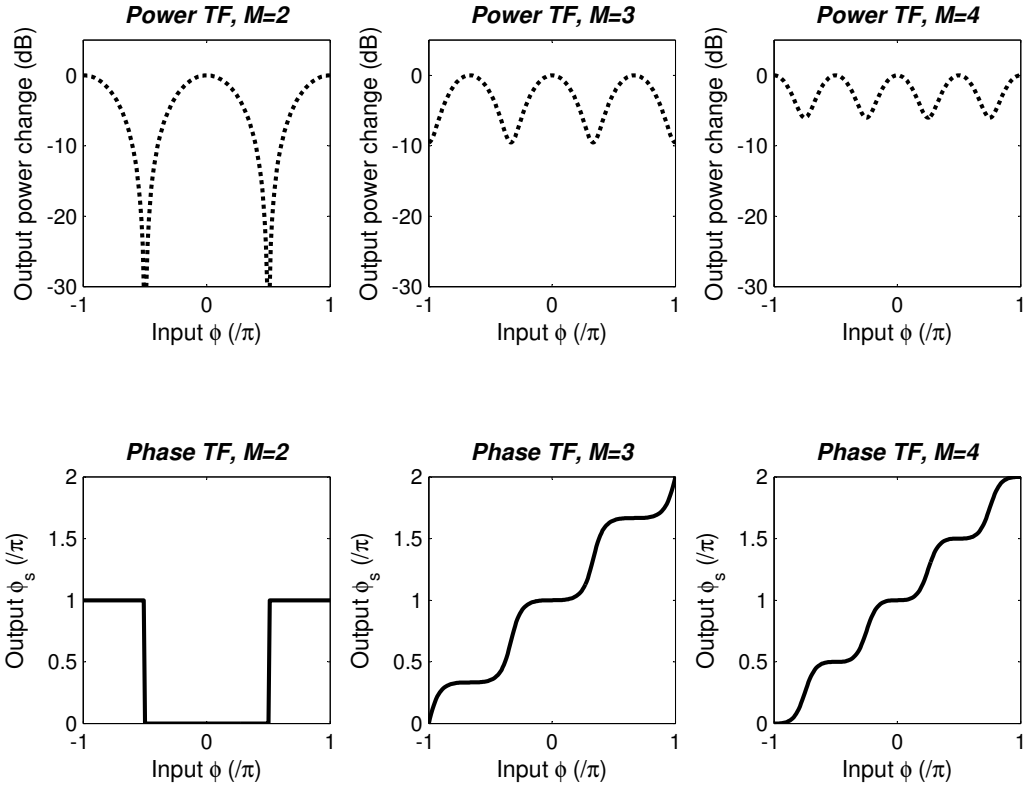

FIGURE 6.1: Evaluation of Eqn 6.2 showing how multilevel phase transfer functions are achieved as M is varied.

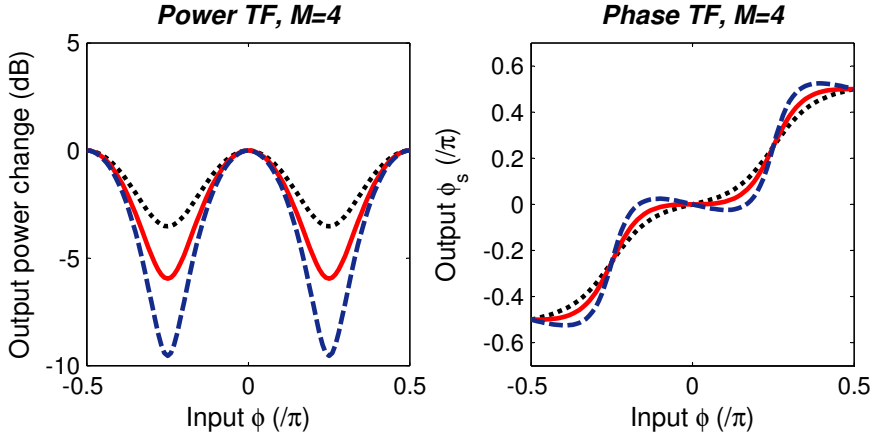

FIGURE 6.2: Evaluation of Eqn 6.2 for M=4, showing the transfer functions for various values of ms. Dotted line is for $m = 0.25$, solid line $m = 0.33$, and dashed line $m = 0.5$.

an ideal step. Clearly, phase quantization is easily achieved for M=2, at $m = 1$. The optimal values of m for higher values of M depart somewhat from 1/(M-1). Also, as M increases, the degree of quantization achievable is compromised, as evidenced by the decreasing misfit factor. Note also that the minima are fairly broad, meaning that m does not have to be set very precisely.

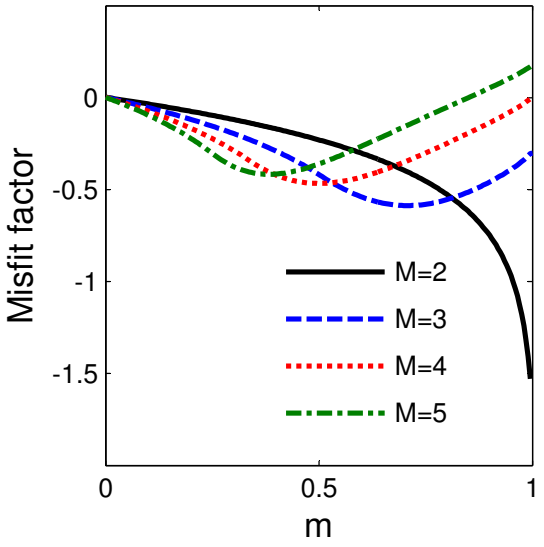

FIGURE 6.3: Evaluation of Eqn 6.3 showing how the misfit factor (as calculated in Equation 6.4) as a function of m for various values of M. Optimum values for M = 2, 3, 4 and 5 are $m = 1$, 0.71, 0.50 and 0.38 respectively.

6.2.1 Realisation

The advantage of the exponential notation in Equation 6.3 is that it can be immediately deduced how to phase quantize to M levels an arbitrary analytical phase encoded signal, $exp(i\phi(t))$. This can be done by coherently adding to the signal a conjugated phase harmonic bearing a temporal phase modulation M-1 times that on the input. Provided that the conjugation mechanism used is much faster than the data modulation (this criterion is met by utilising the ultrafast Kerr effect), ϕ in Equation 6.3 can be replaced by time-varying phase modulation, $\phi(t)$. The question is then how to synthesize, from an input phase modulated signal, the M-1$^{\text{th}}$ phase harmonic, conjugate it, scale it to m, and coherently add it to the input.

The functions of phase multiplication, conjugation and coherent addition are performed using FWM as shown in Fig. 6.4. First, the phase harmonic is generated from the signal using a cascaded FWM process (Fig. 6.4a). This is done by combining the signal with a strong pump beam at a frequency detuning Δf in a nonlinear medium. By optimising the phase matching and the strength of the nonlinear interaction, a spectral cascade of FWM products are generated (Fig. 6.4a). Because FWM is momentum

conserving, the comb of products possesses an overlying phase modulation that is a perfect integer multiple of the modulation present on the signal at the mixer input. Next, a second FWM process is carried out using two pumps located symmetrically around the signal and phase harmonic (Fig. 6.4b) to coherently conjugate and add the M-1th phase harmonic to the signal.

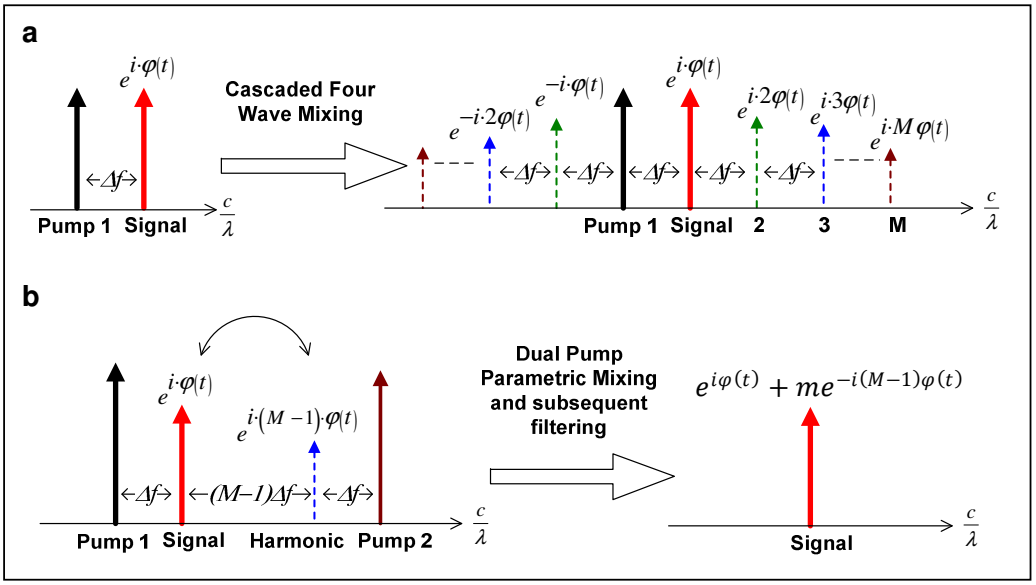

FIGURE 6.4: Illustration of how the M-level staircase transfer function necessary for phase quantization is achieved. a, By mixing a pump beam with a phase modulated signal in a nonlinear medium higher order phase harmonics of the signal can be generated. b, The signal is then coherently combined with the M-1th harmonic using a two pump parametric process.

6.3 Dual-Stage Blackbox QPSK Regenerator

An experiment was setup to demonstrate the concept in Fig. 6.4. The dual-stage quantizer can be operated in blackbox fashion, similar to the DPSK regenerator in Chapter 5, due to the fact that the FWM process used to generate the phase-multiplied harmonic also generates a modulation stripped wave that is locked in relative phase to the signal carrier, and is therefore ideal, once improved by injection locking, to be used as the second pump in the second stage mixer. The experiment was carried out with a 10 Gbaud QPSK signal.

6.3.1 Experimental Setup

The experimental setup is shown in Fig. 6.5. A CW wave at 1555.7 nm was modulated in a single MZM with a 2^{31}-1 PRBS pattern to generate a 10 Gbaud BPSK signal.

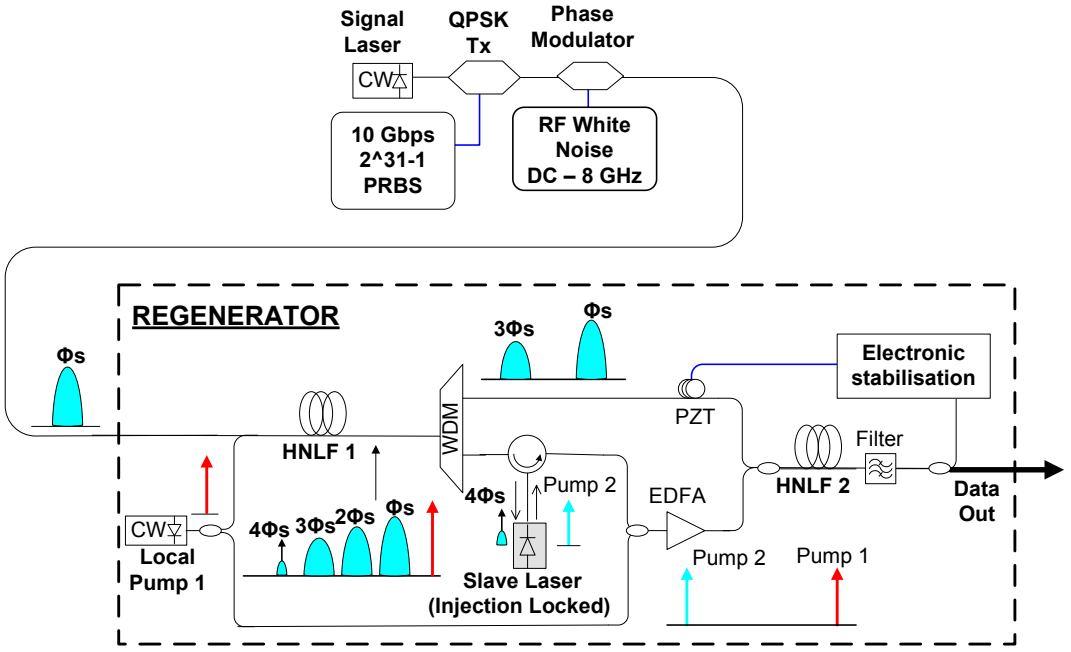

FIGURE 6.5: Experimental setup, PZT - piezo fiber stretcher, HNLF - highly nonlinear fiber, CW - continuous wave, QPSK Tx - QPSK transmitter.

A QPSK signal was then synthesized by passing the BPSK signal through a 400 ps DLI setup up to have a 90° phase shift between the two arms. To emulate the effects of nonlinear phase noise, the signal was coupled through a $LiNbO_3$ phase modulator driven by variable power levels of electrical white noise spanning up to 8 GHz, again repeating the technique used in Chapter 5 during the initial characterization of the DPSK regenerator.

The signal was amplified to 22 dBm and combined in HNLF 1 (OFS) with a 14 dBm portion of pump 1 at 1557.5 nm to generate the FWM comb as shown in Fig. 6.6. HNLF1 was 500 m long with nonlinear coefficient 10.7 /W/km, ZDW 1544 nm and dispersion slope 0.029 ps/nm^2/km. The modulation free harmonic at 1551.2 nm was de-multiplexed from the comb and injected into a semiconductor laser, providing pump 2. The rest of the comb was passively filtered out leaving the signal and harmonic at 1552.7 nm. These were combined with the pumps in HNLF 2 (OFS), with a total pump power of 24 dBm. This fiber had a length of 300 m, nonlinear coefficient 11.6 /W/km, ZDW 1553 nm and DS 0.018 ps/nm^2/km. It also had a strain gradient to increase its SBS threshold. Any slow relative phase drifts at the PSA input were eliminated by monitoring the signal power at the PSA output and controlling a PZT. The signal was then assessed using a self-homodyne constellation analyser. The 20 GHz bandwidth of the constellation analyser was the limiting factor in the choice of signal baud rate for the experiment.

The simple study carried out in Section 6.2 predicts that for optimum regeneration the harmonic to signal ratio should be 0.5 in field, i.e 6 dB in power. This should only be used as a rough starting point - the exact value will depend on the specific pump and fiber parameters used. Generally speaking, if high gains are not possible in the parametric mixer, the power of the harmonic would need to be increased somewhat to ensure that sufficient energy is transferred from harmonic to signal.

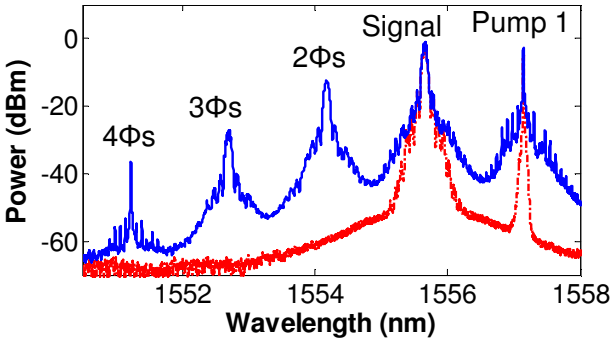

FIGURE 6.6: FWM comb generation stage input (dotted) and output(solid).

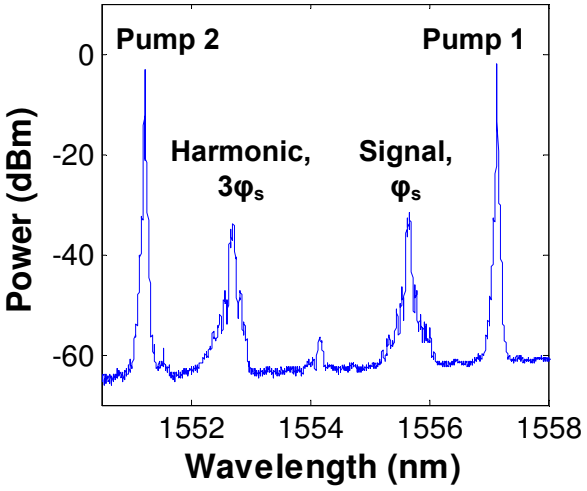

FIGURE 6.7: Spectrum at HNLF 2 input.

6.3.2 Experimental Results

The PSA input is shown in Fig. 6.7. The phase sensitive swing was measured at around 7 dB as shown in Fig. 6.8. The constellation diagrams in Fig. 6.9 show the regeneration for three added phase noise levels. In the absence of any added noise, there was a slight degradation; see Fig. 6.9(a), (b). This stems primarily from the amplification and filtering of the signal within the regenerator, as well as ASE added by the EDFA amplified pumps. Future system iterations would be expected to remedy this

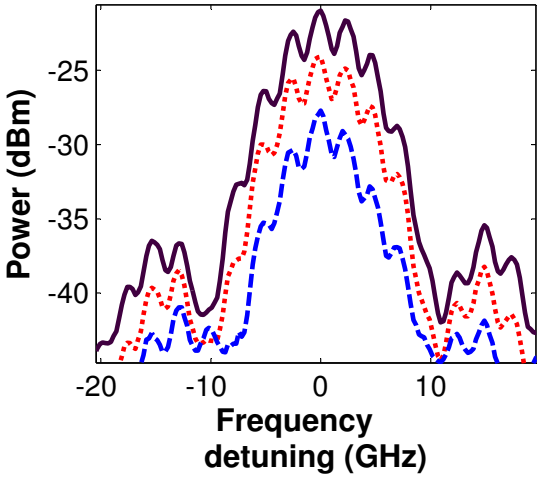

FIGURE 6.8: Signal spectrum at HNLF2 output, solid line (top) is PS maximum, dotted line (middle) is PI, and dashed line (bottom) is PS minimum.

degradation. Absolute phase deviations of up to 60° per symbol (peak-to-peak) were squeezed down to about 30°; see Fig. 6.7(c), (d).

The regenerator was able to squeeze even larger phase fluctuations (6(e), (f)) but this was accompanied by phase-to-intensity conversion. It is possible to suppress this by saturating the PS-FOPA. However, for phase-only formats such as QPSK, amplitude fluctuations impose little penalty, and therefore this is not absolutely crucial. The level of squeezing illustrates one of the key benefits of PSA regenerators: assuming they are placed before a differential optical receiver, they have the potential to significantly reduce the BER for severely degraded signals. This is because phase deviations are magnified by up to a factor of 2 during differential detection and therefore peak-to-absolute deviations over 22.5° for DQPSK can cause errors when differentially decoded, but these can be eliminated by this regenerator.

6.3.3 Further Analysis

It might be interesting to observe the signal and harmonic idler waves at various points in the regenerator, as shown in Fig. 6.10. These earlier measurements were recorded with an 18 GHz Agilent N4391 constellation analyser, and were performed at 10 Gbaud. The comb signal and idler refer to the signal and harmonic waves as measured at the output of HNLF1. PIA output is the signal after HNLF2 with the idler attenuated heavily prior to the PSA, while PSA output is the regenerated output.

The comb idler can be seen to be have greater phase fluctuations that the signal, which agrees with the fact that it is trebled in phase relative to the signal. This is more noticeable for the constellations recorded with noisy PSA inputs. Also, note that the PIA output is always noisier than the PSA input,which would be expected given the

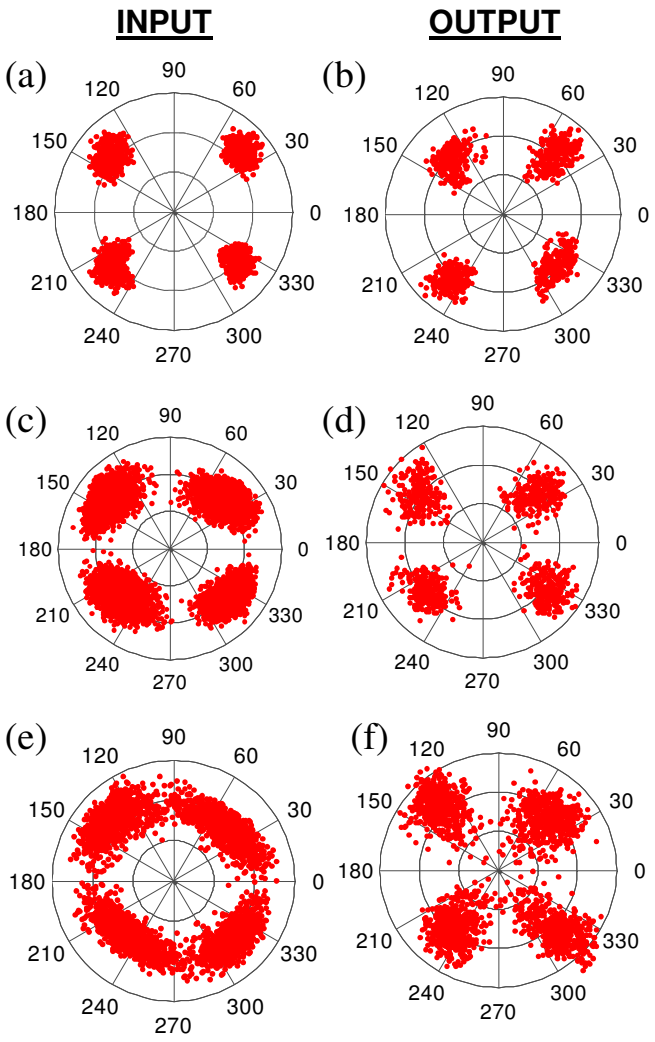

FIGURE 6.9: Signal constellations, (a),(c) and (e) regenerator input, (b), (d) and (f) regenerator output respectively.

lossy passive components as well as noisy amplifiers between these two points. The regenerative capability can be observed from the output constellations. Worth noting also is that the transitions between the data points are transformed by the PSA, with a phase-to-amplitude conversion taking place that compresses the outermost transitions from straight to curved.

6.4 Single-Stage QPSK Regenerator

As described in the preceding section, the dual-stage regenerator clearly differentiates between the first HNLF in which the phase multiplication and pump recovery occurs, and the second HNLF in which the conjugated idler is coherently added to the signal, hereby regenerating the phase. A remarkable variant of that scheme was discovered, in

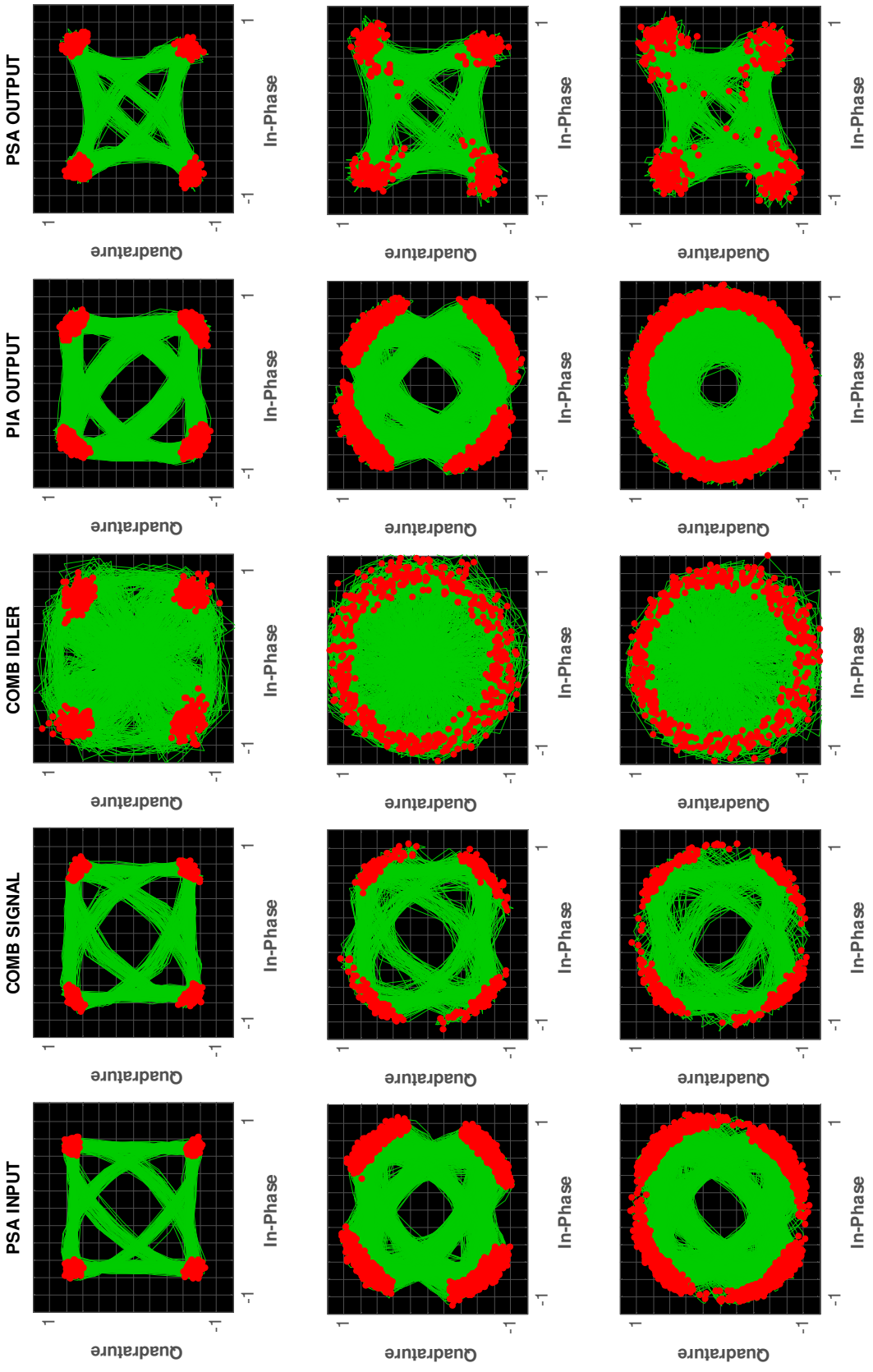

FIGURE 6.10: Constellations showing the signal and idler waves at various points in the regenerator, for various levels of added noise. The output constellations are shown for both PSA mode, and PIA mode with the harmonic idler turned off.

which phase sensitive gain is obtained directly from a 2P non-degenerate parametric amplifier without an idler at the amplifier input, in apparent contradiction to the expected characteristics of a non-degenerate PSA. This device configuration, in addition to allowing QPSK phase regeneration in a simpler configuration relying on just one nonlinear element, provides significantly enhanced amplitude noise improvement.

The concept is in effect a fusion of the two separate parametric effects into one distributed action. Provided that both pumps 1 and 2 as well as the signal are present at the mixer input, the coherent mixing process can then be distributed along the fiber length; initially the cascaded mixing process dominates, and then as the harmonic idler starts to grow in power the coherent conjugated addition takes place. Unlike the dual-stage regenerator, this setup is not black-box in that phase locked pumps have to be provided prior to the PSA, but given advances in electronic phase locking it is increasingly possible that this will not be a significant disadvantage in the near future. An experiment was carried out to validate this assumption.

6.4.1 Experimental Setup

The output of a CW laser at 1555.7 nm was split into two, with one portion coupled into a 10 GHz comb generator, see Fig. 6.11. Comb lines at -190 and +570 GHz detuning were injected into semiconductor lasers, providing two pump beams phase locked to the signal carrier. The rest of the signal light was modulated with a pseudo-random binary sequence to generate single polarization QPSK. This was sent through a noise additive module to emulate the effects of linear (related to quantum noise and ASE) and nonlinear phase noise (related to nonlinear amplitude to phase conversion). This module (shown as an inset in Fig. 6.11) comprised an ASE source whose output was split into two, one portion being detected and the resulting electrical white noise being used to drive a LiNbO3 phase modulator through which the signal was passed, and the other portion being optically combined with the signal in a coupler.

The signal was then combined with the pumps and all the waves were amplified in an EDFA, leading to 50 mW of signal power and 250 mW power per pump. They were then sent into an HNLF (OFS, Denmark). The HNLF parameters were length 300 m, nonlinear coefficient 11.6 /W/km, ZDW 1553 nm and 1550 nm DS 0.018 ps/nm^2/km. It also had a strain gradient to increase its SBS threshold, allowing the use of continuous wave pumps. Slow thermo-acoustic relative phase drifts were suppressed by monitoring the signal power at the PSA output and controlling the PZT. The signal was then assessed using an EXFO constellation analyzer (PSO-200) based on all-optical sampling capable of operation up to 100 Gbaud.

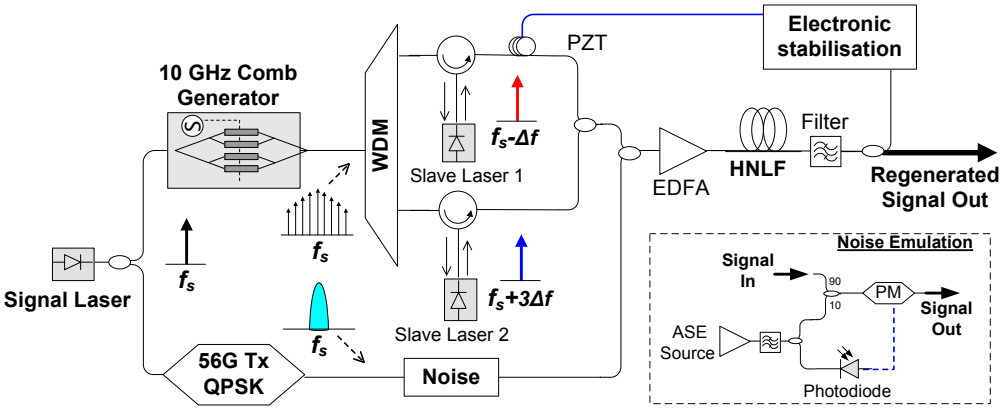

FIGURE 6.11: Regenerator setup, Tx - transmitter, WDM - wavelength division demultiplexer, PZT - piezo-electric fiber stretcher, PM - phase modulator,

6.4.2 Experimental Result

The input and output spectra to the PSA are shown in Fig. 6.12 and Fig. 6.13 respectively. At the input to the PSA, there is a very weak component at the idler frequency (+380 GHz detuning) emanating from weak FWM in the high power EDFA, but at -40 dB relative to the signal this does not affect the subsequent parametric interaction as verified by numerical simulations. 7 dB phase sensitive gain variation was obtained at the PSA output as measured with the feedback to PZT turned off (Fig. 6.15). The spectrum at the output to the PSA (Fig. 6.13) suggests two separate interactions occur simultaneously first, the presence of the strong component at +190 GHz detuning indicates coherent phase multiplication via mixing of the signal with the pump at -190 GHz, and the strong idler at +380 GHz indicates conventional 2P phase insensitive amplification. There are many other parametric interactions that occur due to the strength of the signal and pumps, as shown in the wideband output spectrum, Fig. 6.14. These extra mixing products can be used to enhance the functionality of the device, such as being used as a wavelength multicaster by accessing the wavelength-translated copies of the input signal. It could however be viewed as being energetically inefficient, but this transfer of energy to unwanted frequencies can be minimised by careful selection of the fiber parameters.

To characterise the regenerator, colorgrade signal constellations including data on the phase error variance and normalised variance of amplitude noise are shown in Fig. 6.16. While this statistical information would be more robust if obtained from a homodyne receiver without digital phase compensation for the intradyne local oscillator, as measured in Section 6.3.1, it is still useful for quantifying relative signal improvements derived from the regenerator.

The regenerator was first assessed at 10 Gbaud with added phase noise only, emulating the nonlinear regime. Pseudo-Gaussian phase fluctuations would be expected at the

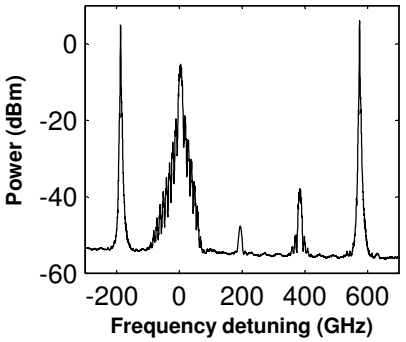

FIGURE 6.12: PSA input spectrum, signal located at 0 GHz detuning.

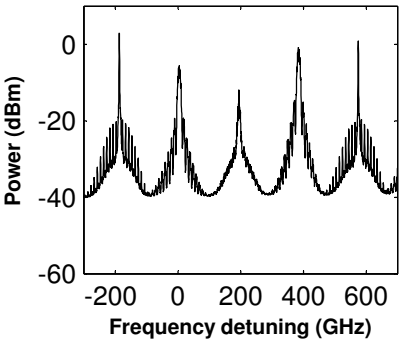

FIGURE 6.13: PSA output spectrum, signal located at 0 GHz detuning, output idler at +380 GHz.

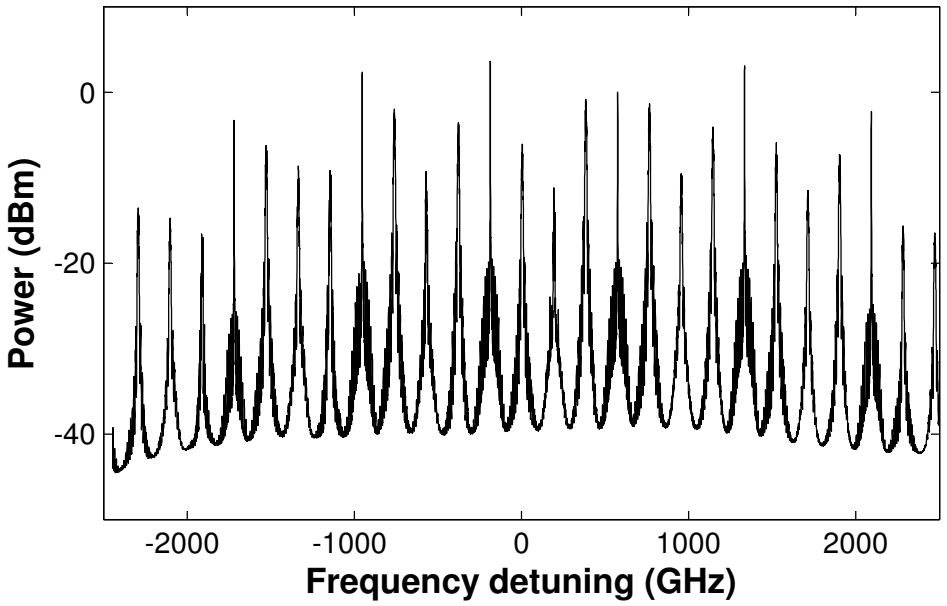

FIGURE 6.14: PSA output spectrum showing wideband mixing products

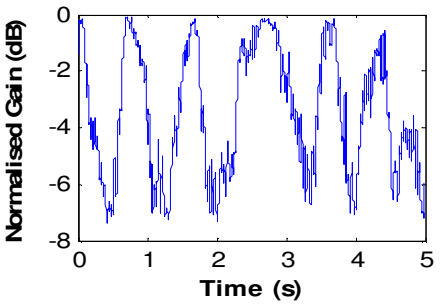

FIGURE 6.15: Normalised PSA gain fluctuations with electronic stabilisation turned off.

input, with an artificial roll-off at the tails of the distribution due to saturation of the photodiode for high ASE levels. The regenerator desirably reduced the phase error variance by a factor of 6, while the amplitude noise variance only increased by 2.6 (Fig. 6.16, Cell A), suggesting an overall benefit as the input BER is dominated by the phase noise. This phase noise reduction is comparable to the numerically predicted factor of 5.5 for the parallel BPSK regenerator scheme [104], denoting that the inline compactness of the approach does not come with an associated performance penalty. For QPSK, a comparison with studies on the impact of phase estimation errors on BER suggests that the output phase error variance of 0.0042 rad^2 (Fig. 6.16, Cell A) approximately corresponds to an SNR penalty under 0.5 dB for a BER of 10^{-4}, while the input variance corresponds to a penalty $\gg$ 4 dB [108]. This nonlinear phase noise reduction implies that i) the reach of the transmission span can be increased ii) the tolerance to nonlinearity is significantly enhanced; hence higher receiver OSNRs can be envisaged.

In the presence of linear noise emulated by ASE loading (hence degraded OSNR with both phase and amplitude fluctuations), the phase error variance and normalised amplitude variance are simultaneously reduced by approximately 3.2, indicating even better net regenerator performance (Fig. 6.16, Cell B). This ability to concurrently reduce both absolute phase and amplitude variance prior to the receiver suggests that the regenerator should provide significant signal quality improvement if deployed before a differential receiver, which normally requires a trade off between reduced complexity and lower noise tolerance compared to a fully coherent one.

The symbol rate was increased to 56 Gbaud and the measurements repeated. Without added noise, the regenerator preserves the phase quality at the expense of some amplitude noise (Fig. 6.16, Cell C). It is believed that this is a result of the wideband parametric interactions occurring in the PSA, as shown in Fig. 6.14, that transfer some amplitude noise to the signal. In the presence of phase noise, the phase error variance is reduced by a factor of 3.2, with increased amplitude noise at the output Fig. 6.16, Cell D). For QPSK however, in which the information is solely contained in the phase, this

increased nonlinear phase noise tolerance would translate to increased reach or higher signal launch powers to improve OSNR at the receiver.

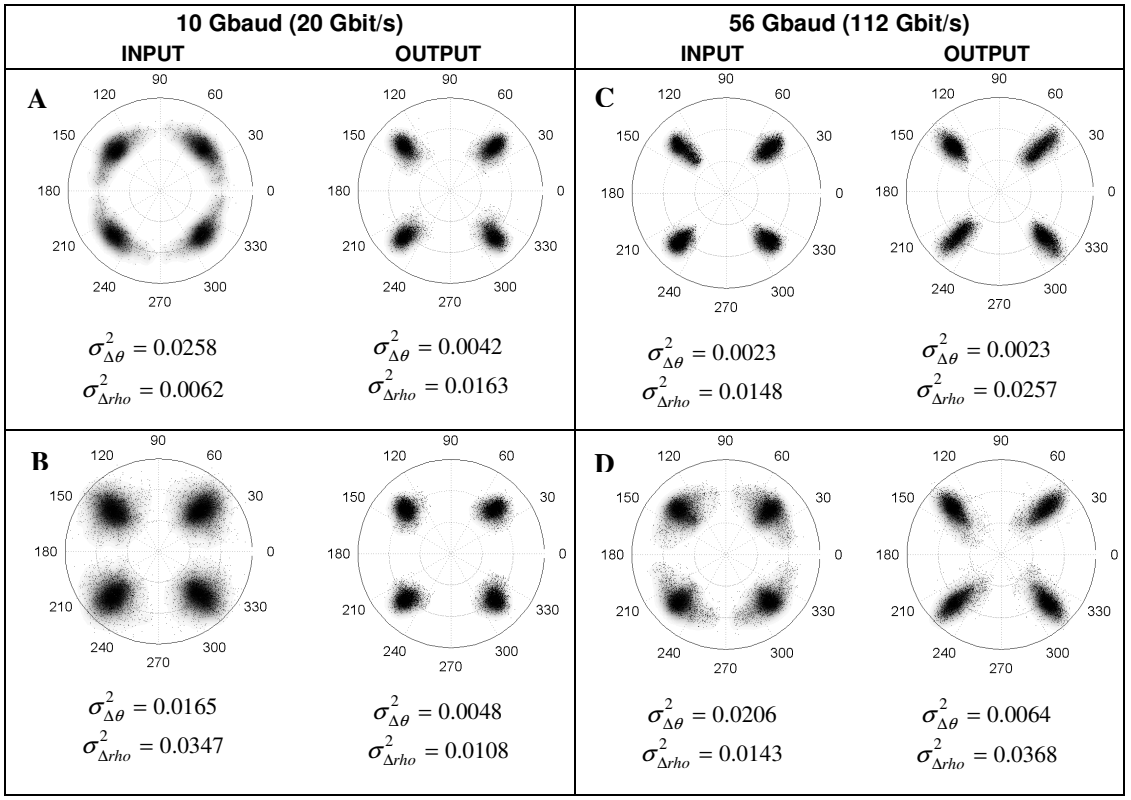

FIGURE 6.16: Regenerator performance. A - Input phase noise only; B- Phase and amplitude noise; C- No noise; D- Phase noise only. $\sigma^2_{\Delta\theta}$ is the phase error variance, $\sigma^2_{\Delta rho}$ is the normalised amplitude noise variance;

6.5 Reconfigurable M-PSK Phase Quantizer

The initial experimental demonstrations all focussed on QPSK regeneration, due to the importance of that modulation format given its selection for longhaul 100 Gbit/s optical links. However, having predicted that the device could readily be reconfigured to handle other PSK modulation formats, an experiment was designed to demonstrate this.

6.5.1 Experimental Setup

A narrow linewidth CW fibre laser (Rock laser, NP Photonics) at 1555.7 nm was split into two, with one portion coupled into a 10 GHz comb generator (Optical Pulse Generator LP-5011, Optocomb). Two semiconductor lasers were injection locked to comb lines, one (Eblana Photonics DM laser, output power 10 mW and natural linewidth below 300 kHz) representing pump 1 at approximately -200 GHz detuning from the signal

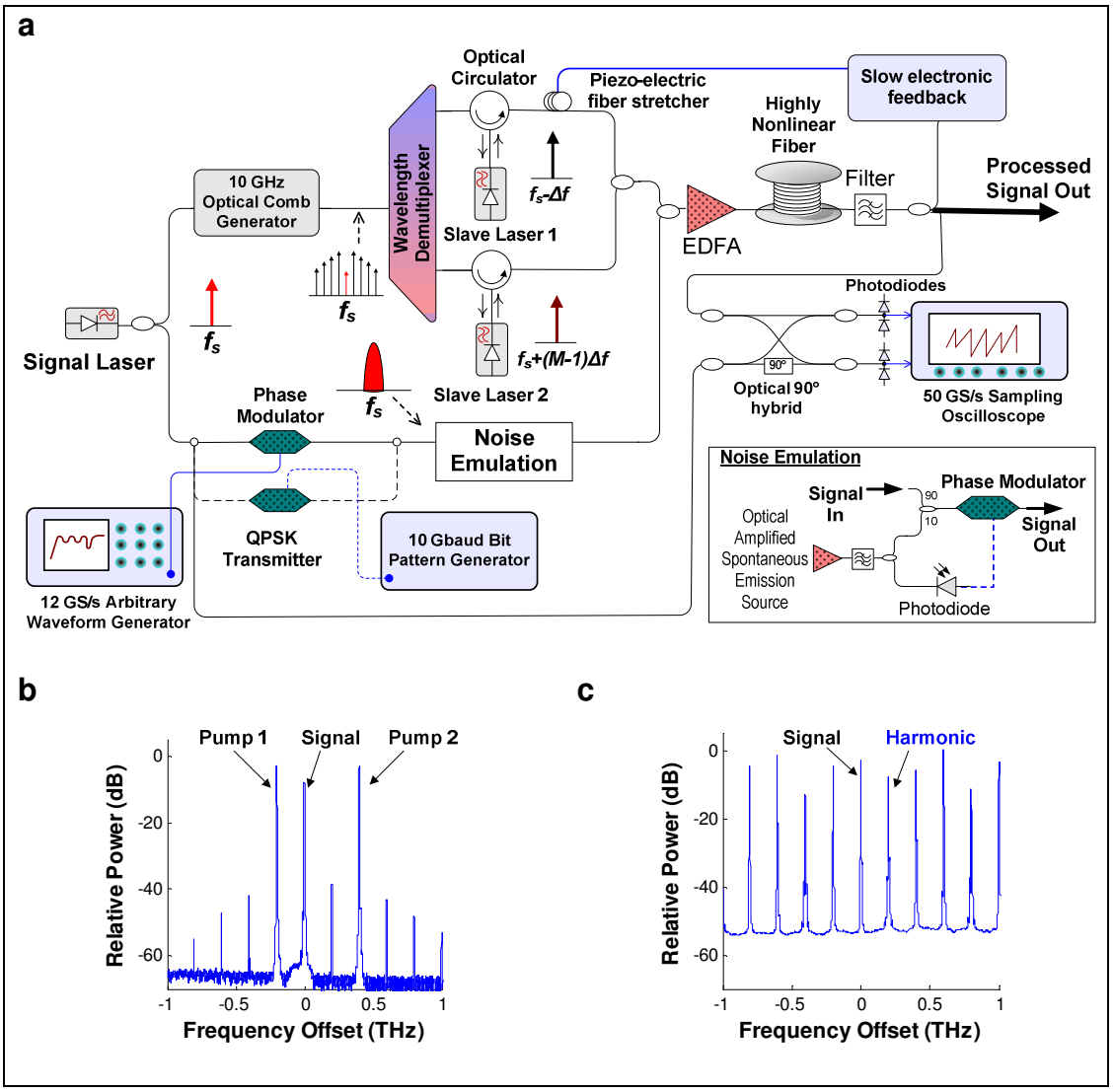

FIGURE 6.17: a, Schematic of the quantizer. EDFA, erbium doped fiber amplifier. b, Optical spectrum at the input and c, output of the highly nonlinear fiber. The weak tones (over 35 dB less than pumps) in b result from FWM in the EDFA and can be ignored.

frequency and the other (EM4 Inc, output power 100 mW and natural linewidth below 1 MHz) at a frequency (M-1)*200 GHz away with the value of M depending on the modulation format being assessed. For both lasers the injected power was close to -30 dBm. The rest of the signal light was modulated, either in a Lithium Niobate phase modulator with information generated in a 12 GS/s Tektronix arbitrary waveform generator, or in the case of QPSK, in a Lithium Niobate MZM driven by an electrical PRBS pattern, the optical output of which was coherently multiplexed from BPSK to QPSK in a DLI.

The modulated signal was sent through a noise additive module to emulate the effects of linear (related to quantum noise and ASE) and nonlinear phase noise (related to

nonlinear amplitude to phase conversion). The signal (50 mW) was then combined with the pumps (total power 500 mW) and all the waves were amplified in a PM EDFA. Use of a PM EDFA ensured that the signal and pumps were co-polarised in the subsequent HNLF.

They were then sent into an HNLF (OFS, Denmark) HNLF parameters are length 300 m, nonlinear coefficient 11.6 /W/km, zero dispersion wavelength 1552 nm and 1550 nm slope 0.018 ps/nm^2/km. This had a strain gradient to increase its SBS threshold, allowing the use of CW pumps. Optical spectra at the input and output of the HNLF are shown in Fig. 6.17b and 6.17c respectively. Slow thermo-acoustic relative phase drifts were suppressed by monitoring the signal power at the PSA output and controlling the PZT. The processed signal was then combined with a local oscillator (tapped off the signal laser prior to data modulation) in a 90° hybrid followed by real-time 50 GS/s (Tektronix 72004) sampling of the two hybrid outputs detected in single ended fashion using Agilent 83440D 32 GHz lightwave detectors, and off-line post processing to retrieve the phase and amplitude of the signal.

6.5.2 Experimental Result

To verify the operating principle, the signal phase was first varied over 2π at a rate of 150 MHz. To switch to M-level quantization, the only requirement is to tune the frequency of laser 2 to $f_s+(M-1)\Delta f$, and optimise the pump and signal powers into the HNLF. This means that from a practical point of view, changing the modulation format or supported signal bandwidth (given by Δf) can be achieved in milliseconds or less without any hardware changes, relying on the rapid tuning capability of semiconductor lasers. The choice of signal and pump powers depends on the fiber parameters, M-level, and application, but as an example, 50 mW and 250 mW respectively proved ideal for QPSK regeneration.

The signal can be represented in constellation diagrams, as shown in Fig. 6.18. Quantization to 3, 5 and 6 levels in Figs. 6.18b, 6.18c and 6.18d respectively was demonstrated. As expected, the quantization is accompanied by a sinusoidal amplitude response, whose depth decreases as M increases. If stronger phase squeezing was required, as might be for the higher levels of M, multiple nonlinear elements can be cascaded in series. The quantization is accompanied by phase-to-amplitude conversion which would be undesirable for some applications; this however can be eliminated by subsequently regenerating the signal amplitude in a high dynamic range limiting optical amplifier, such as an injection-locked semiconductor laser [109]. Fig. 6.19 shows the intermediate stages for 3- and 5-PSK, between the condition of zero pump power hence no nonlinearity, and the optimum pump power for ideal phase regeneration.

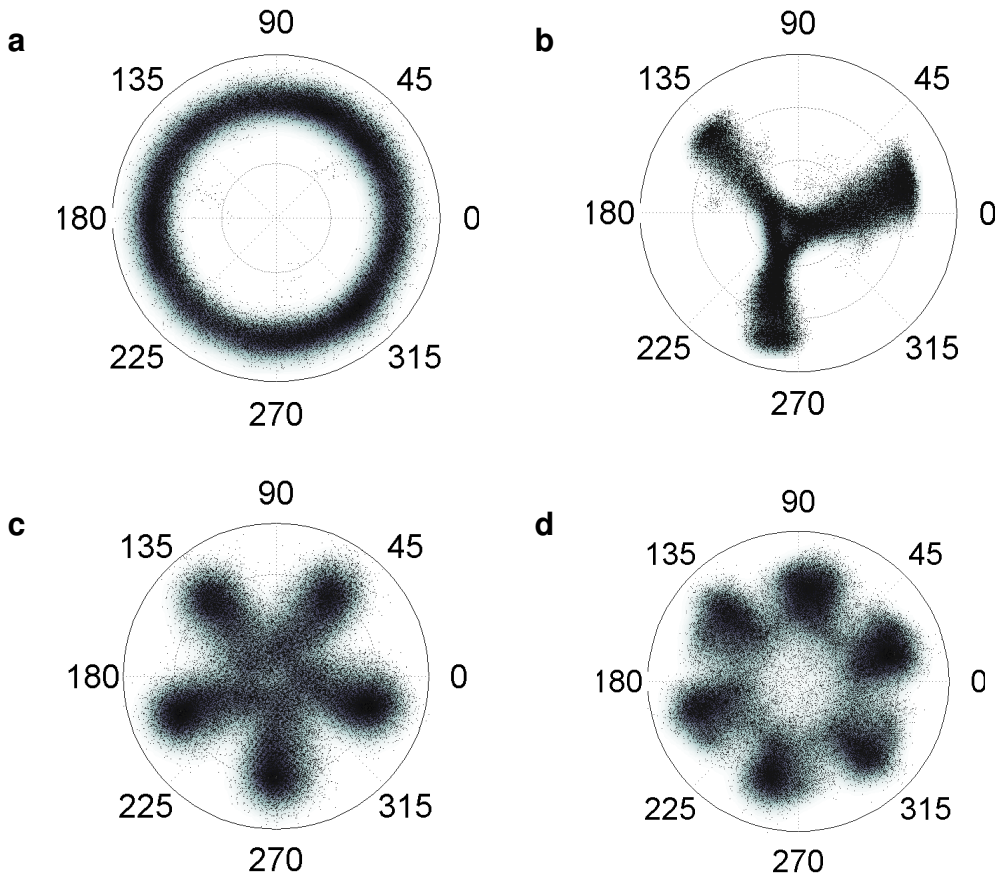

FIGURE 6.18: Signal constellation diagrams. a, Before the quantizer, signal occupies every phase state. b, After phase quantizer with pump 2 at $f_s + 2\Delta f$, giving 3 levels. c, After phase quantizer with pump 2 at $f_s + 4\Delta f$, giving 5 levels. d, After phase quantizer with pump 2 at $f_s + 5\Delta f$, giving 6 levels.

The quantizer was then assessed for its phase regenerative properties, as would be required in an optical telecommunications link. This was done for 3-PSK and QPSK. Whilst 3-PSK is not a conventional modulation format due to its fractional (1.5) number of bits per symbol leading to coding complexity, one could envisage a more complex format being derived based on 3-PSK. It is also a useful demonstration of the ability of the scheme to deal with odd values of M, which can not be done with other techniques such as the parallel approach.

The constellation data at the output of the phase regenerator are shown in Fig. 6.20. First, a pseudo-random 3-PSK signal was generated at 6 Gbaud and noise added to it by optically adding ASE. This led to a constellation with a broad phase and amplitude distribution. Following the regenerator, the phase and amplitude excursions weresignificantly reduced. Also plotted are the differential phase error distribution (symbol-to-symbol phase difference). As can be seen, the probability of differential decoded

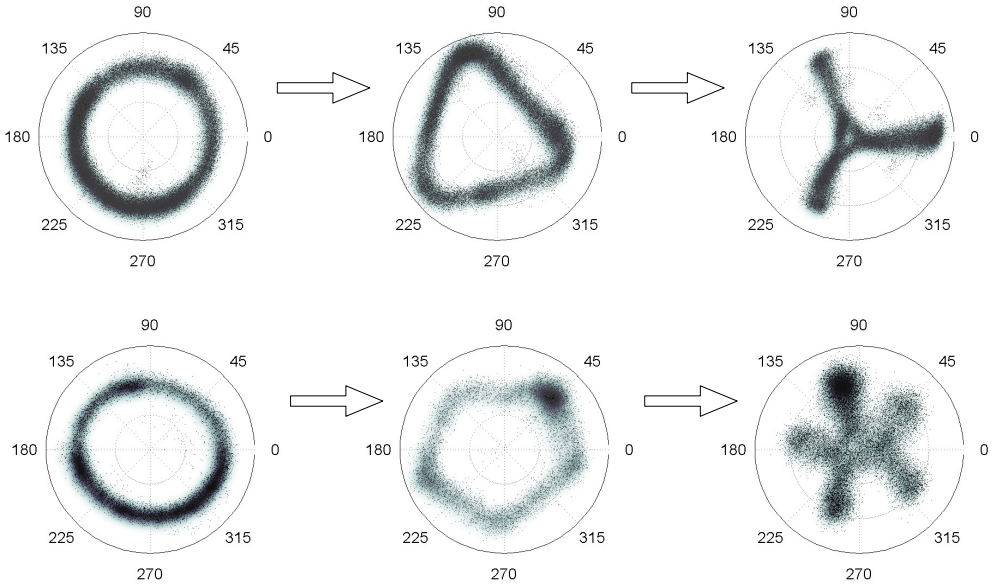

FIGURE 6.19: Output constellations with quantizer configured for 3- and 5-PSK, showing transformation as pump power is increased from zero to an optimum value.

digital errors (when the analog error is over 60° for 3-PSK) is reduced by two orders of magnitude.

The regenerator was tested with a 10 Gbaud QPSK signal. Phase and amplitude noise were artificially imposed onto the signal leading to a constellation with a broadband phase and amplitude distribution. Following the regenerator, the phase excursions are significantly reduced. The device is also capable of simultaneously reducing amplitude noise at the input, achieved by slight saturation of the amplifier induced by having relatively high input signal powers. The differential phase error distribution (symbol-to-symbol phase difference) are also plotted showing that the probability of differential decoded digital errors (when the analog phase error is over 45° for QPSK) is reduced by at least an order of magnitude. This phase squeezing ability could therefore be applied within a communications link, extending its reach and/or improving the signal quality prior to the receiver, adding to the system margin.

6.5.3 Conclusion

For the first time, a practical concept for performing QPSK regeneration, that can be scaled to higher density PSK constellations has been proposed and demonstrated. This scheme relies on the coherent addition of an M-level PSK signal with a conjugated (M-1)th phase harmonic, scaled by a coefficient m. A simple analytical theory can be used to predict the optimal value of m, located using a numerical misfit factor minimization process. The concept was demonstrated with QPSK signals, relying on a two stage

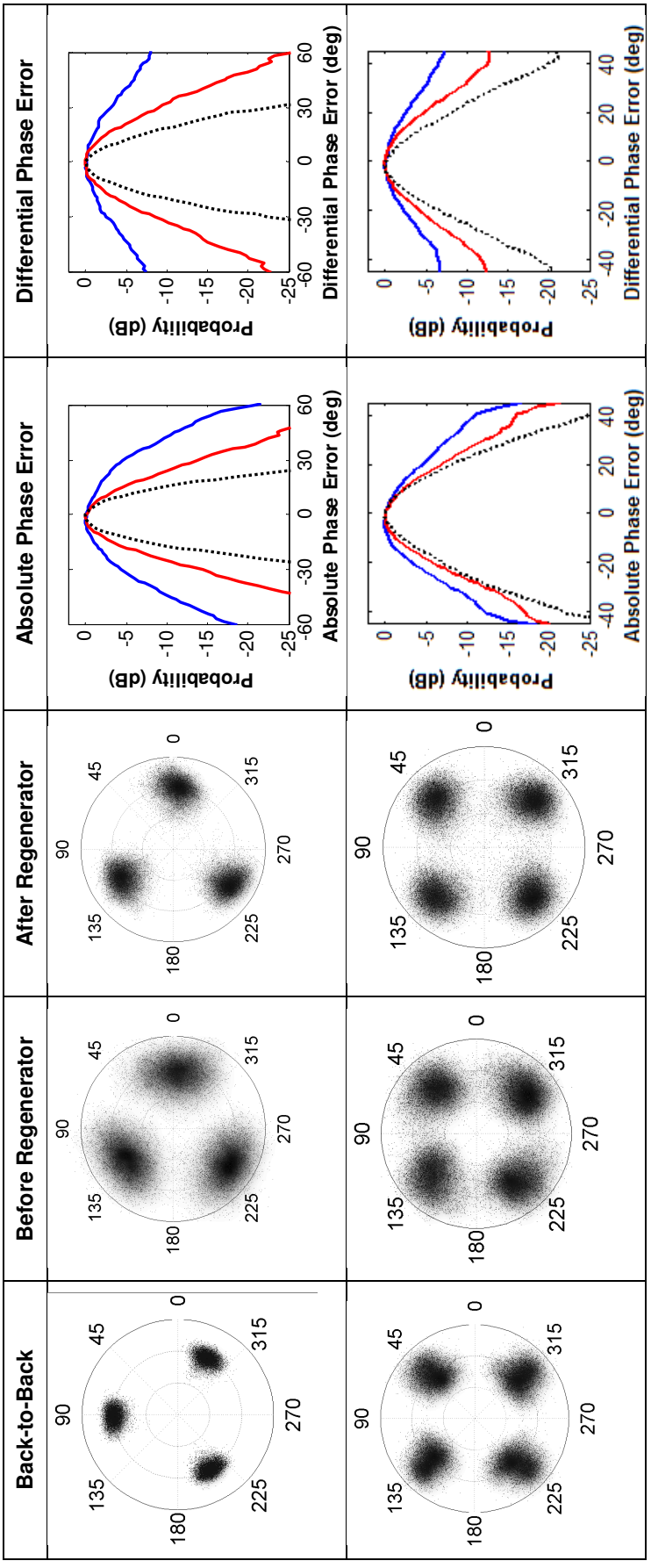

FIGURE 6.20: Constellation data when quantizer is operated as a multilevel phase regenerator for 3-PSK and QPSK formats. For the phase error distribution, blue lines (top) are at quantizer input, red lines (middle) at quantizer output and black dotted line is signal without any added noise.

parametric process - in the first stage a third order phase harmonic is generated, and in the second this is mixed with the original signal. Homodyne optical constellation diagrams showed that the concept works. A further modification is to combine the two processes in a single fibre, by mixing a QPSK signal with two pumps in an HNLF. Constellation measurements taken up to 56 Gbaud (112 Gbit/s) showed up to a four-fold reduction in the phase error variance. The device is capable of reducing noise in both phase and amplitude via a saturation mechanism, similar to the DPSK regenerator. The generalised concept was further demonstrated up to 6-PSK.

These results were well received, with a postdeadline paper at the European Conference on Optical Communications in 2010, as well as published in Nature Photonics in 2011. In addition, this work generated two patents on the key enabling technologies behind it.

Chapter 7

Conclusions

The body of research presented in this thesis was closely aligned with the goals of the EU FP7 project PHASORS. Launched in 2008, PHASORS targeted "*...the development and applications of fibre based phase sensitive amplifier (PSA) technology in 40 Gbit/s broadband core networks*". PSA specifically, and all-optical signal processing in general, were felt to be technologies able to help deliver the 1.5 dB/year increase in fibre capacity needed to cope with demand [1]; the concensus at the time was that electronics on its own provided neither the speed nor the power efficiency required to meet this growth curve.

PSA based on Kerr nonlinearity in optical fibres required several key enabling technologies. The demonstrations of optical regeneration shown here would not have been possible without access to SBS suppressed HNLF, allowing the use of the high power narrow linewidth pumps required for the phase sensitive parametric process. While progress has been made on this front, a few issues remain, particularly with the strained $AlSiO_3$ fibres - non-negligible insertion losses, large ZDW fluctuations along the fibre length, and PMD. These factors mean that the parametric process is not as efficient as it can be.

The strained Ge-doped silica HNLF which was used for the multilevel phase quantization work allowed the use of pump powers (out of the EDFA) of 27 - 28 dBm. Getting to the level of only 20 dBm per pump would represent a significant milestone, as such power levels could be delivered directly by semiconductor lasers without the need for optical booster amplifiers, making parametric devices cheaper and more compact. As stated before, ensuring uniform dispersion characteristics along the device length significantly improves efficiency and bandwidth characteristics, but this is very difficult to do over long (hundreds of metres) fibre spans, although a dispersion optimisation technique relying on applying variable strain along the fibre length offers some promise [46]. A personal recommendation, based on a survey of the literature, would be to further investigate the

[1] Cisco Visual Networking Index: Forecast and Methodology, 2010 - 2015

use of resonator structures [13] based on short lengths of HNLF with pump reflective elements on both ends, allowing the peak pump within the nonlinear medium to increase by orders of magnitude. Cost savings would arise from the use of low power pump diode lasers, as well as being able to use short HNLF lengths. Devices based on this technology should also be much more compact. This architecture does present several challenges however, including stabilising the optical pump to what would effectively be a high finesse nonlinear Fabry-Perot cavity, as well as managing temperature dissipation.

The demonstrations of blackbox DPSK regeneration herein relied on optical injection locking to provide a pair of pumps locked in phase to the signal carrier. OIL is a very handy technique for this purpose - it only requires the addition of an optical circulator to the setup, and allows large phase locking bandwidths (more than hundreds of MHz). Electronically assisted phase locking technologies currently offer < 1 MHz bandwidth, and this should not increase significantly in future. However, the use of narrow linewidth lasers in telecom systems, driven by the adoption of coherent communications in which optical phase carries information, means that electronically assisted locking could replace OIL in these parametric sub-systems, as loop bandwidth requirements would be reduced. This is of vital importance - electronic locking would allow the DPSK regenerator to be compressed to a single nonlinear device, and not two as demonstated in Chapter 5. Also, the QPSK regenerator in Chapter 6 utilises a single nonlinear stage, and while a blackbox demonstration is shown using a first stage in which a modulation stripped pump is first generated, this comes at the expense of optical power.

At this stage it is worth assessing the merits of the system demonstrations shown herein, starting with the DPSK regenerator. An all-optical DPSK regenerator should ideally have a number of features.

1. High speed operation (> 1 THz): Semiconductor technology has advanced greatly over the last 3 decades, and the current semiconductor industry roadmap (as of 2008) has targets of transistor bandwidths of 1 THz by 2021, [2] implying digital signal processing speeds in excess of 100 GHz. It is crucial that all-optical processing techniques allow scalable operating bandwidths at least an order of magnitude greater than this figure, to make their deployment economically viable and future proof.

2. Power efficiency: All-optical signal processing techniques have for a long time been touted for their superiority in terms of low power per processed bit in comparison to electronics. While there is no clear concensus regarding whether this superiority can be maintained indefinitely [93], optical techniques will have to out-perform electronics in terms of power efficiency, in order to stand a chance of in-field deployment.

[2] http://www.itrs.net/Links/2008ITRS/Home2008.htm. International technology roadmap for semiconductors, Table RFAMS1. Targets 1 THz F_{max} CMOS NFET transistors by 2021

3. Amplitude noise suppression capability: Because amplitude noise within the signal channel is a major seed of intra-channel nonlinearities, it is important that the regenerator not only suppresses amplitude noise at its input, but also minimises the phase-to-amplitude conversion that is a characteristic of linear phase sensitive amplifiers.

4. Multi-channel (WDM) operation: It goes without saying that multi-channel regeneration remains the holy grail of all-optical signal processing, and this remains a goal of research groups in this field. However, provided the single-channel all-optical regenerator has a small component count and reasonable low power requirement, future advances in photonic integration and in the design of nonlinear optical materials will certainly make it possible to economically manufacture and package many such devices together, delivering a multichannel system.

The DPSK regenerator went a long way towards meeting most of these requirements. It provided significant compression in both amplitude and phase noise. Operation up to 56 GHz was demonstrated, but the setup was capable of achieving up to 200 GHz, limited by the spacing between the pumps. If a much wider pump spacing was utilised, 1 THz should be feasible. Achieving these speeds would ultimately be limited by dispersion, not the nonlinearity. Flat parametric gain over the entire signal bandwith would be required, but phase sensitive parametric gain bandwidths in excess of 2 THz were demonstrated in the early stages of this work. The device was also operated with less than 1 W of optical power, a breakthrough in itself. However, to get below the level of pJ per bit, even lower pump powers are required. The degenerate PS-FOPA is inherently a single channel device, and while multi-channel PSA amplification can be achieved in a non-degenerate PS-FOPA, data information must be duplicated over transmitted signal-idler pairs, and these must all be coherent relative to a master pump, something that would require full dispersion and delay compensation prior to the PS-FOPA. Even if this were practical, cross-talk in the parametric device would be difficult to mitigate, especially since amplitude noise suppression often requires high signal powers for pump depletion. An alternative approach has recently been presented [110], this requires a separate high power pump for each regenerated channel. As would be expected, this scheme suffers from considerable unwanted FWM between the pumps, ultimately limiting channel count. It therefore appears best to focus future development efforts on compact, low power, low component count single channel regenerators.

Ironically, the same relentless match in technology that has enabled the PS-FOPA DPSK regenerator to be feasible appears to have made it redundant, at least for long-haul applications. The need for greater system capacities, mean that QPSK has superceded DPSK, at least for the time being, as the modulation format to which mid-term R&D efforts should be targeted. This is not to say that no other applications for DPSK regeneration exist, or will emerge, but what these applications are, or will be, is still unclear.

It was therefore a significant development to demonstrate for the first time QPSK regeneration in a PS-FOPA. Previously, it had been suggested that QPSK regeneraion could be achieved by taking a QPSK signal, splitting it into two, and using two parallel BPSK regenerators to process each of the two phase quadratures separately [104, 105]. This concept should work, although several disadvantages spring to mind. Firstly, the two BPSK regenerators would have to be matched in length quite accurately, at 56 GHz this would need to be to precisions better than 1 mm. Matching in phase, gain and polarization would also need to be done. Even when possible using integrated photonic technologies [106], as discussed in the introduction, having to use one optical sub-system per processed bit means that any economic advantage all-optical processing has over electronics would rapidly shrink.

The multilevel phase quantization concept, of combining an MPSK signal with a selected phase harmonic, is extremely powerful due to the fact that a single device is used per input symbol, not per input bit. The device is capable of performing QPSK regeneration, which is demonstrated here at up to 112 Gbit/s with up to a four-fold reduction in the phase error variance observed. It is also capable of processing higher order modulation formats, due to the general nature of the concept, experimentally demonstrated up to 6-PSK. One main attraction is the fact that the device is reconfigurable, meaning that switching between modulation formats could be done without any hardware changes, a flexibility up to now only accessible using electronic devices.

It is only fair to provide an objective assessment of the weaknesses, and not just the strengths, of the current approach. There are several. To begin with, achieving high levels of M, such as 16, is a task complicated by two effects. Firstly, this requires the generation of high order phase harmonics (the 15th in this case). Note that the highest generated experimentally during this research project was the 7th. Also, the phase transfer function is not a perfect staircase, but is smooth, meaning that the device copes best with signals that are not very noisy, and the smoothness increases the higher the value of M. At this point it appears that coping with M levels higher than 10 is probably unfeasible, at least not in a single nonlinear device.

The solution to the first of these problems is to not to use the signal and (M-1)th harmonic for regeneration, but to use a different pair. For 8-PSK for example, rather than trying to sum $\exp(i\phi)$ and $\exp(-i7\phi)$, combining $\exp(i3\phi)$ and $\exp(-i5\phi)$ delivers a similar 8 level quantization function, except that the phase points get re-ordered, albeit in a predictable way. The benefit of this is that one only needs to generate harmonics up to the 5th, and not the 7th. For higher modulation formats, such as 16-PSK, this becomes even more beneficial - only harmonics up to the 9th, and not the 15th, would be required. As for obtaining better phase quantization properties, cascading multiple devices, or somehow synthesizing mixers that allow the combination of the signal with not just one, but multiple phase harmonics, might be a solution.

Finally, it is worth discussing the future of PSA technology from a low noise amplification perspective. Record low noise figure of 1.1 dB has already been demonstrated [67], and it is estimated that Raman coupled noise will limit PS-FOPAs to 0.5 dB at best [111]. While 2.5 dB advantage over DFAs is noteworthy, it is on its own arguably not sufficient from a telecom system perspective to justify replacing DFAs with PS-FOPAs. In ultimate capacity terms, PS-FOPAs render one quadrature redundant for information carrying. In addition, what long haul links require currently is a breakthrough technology, one that is capable of delivering orders of magnitude increase in capacity, and not just an extra 1 bit/s/Hz as upgrading to PSAs would deliver. PI-FOPAs on the hand are still attractive given their simplicity, and might prove to be a the solution of choice if systems are built operating outside of the C-band. As for the PS-FOPA itself, discounting it from fibre telecoms does not mean that applications do not exist - there are single channel systems that would suit it, such as those where noise performance matters more than capacity (such as interplanetary communications).

Appendix A

Spectral pump counter phasing in dual pump FOPAs

Small core Ge-doped silica HNLFs are often the medium of choice for parametric amplifiers, due the long nonlinear interaction lengths, and maturity of dispersion tailoring techniques. From a practical perspective, they are also easy to splice to with low insertion loss, can be designed with various amounts of birefringence, can cope with high power levels without device damage, and by leveraging advances in fibre draw technology may be feasible to manufacture in volume [1]. One main drawback with these fibres, however, is that their SBS thresholds are lower than the pump powers required for modest parametric gains, i.e. < 20 dBm.

One method to get around the SBS issue is to apply phase modulation to broaden the pump(s) linewidth [112]. In the case of 1P PI-FOPAs, the pump modulation is transferred to the idler wave, an undesirable phenomenon. One way to prevent to this idler broadening is to use a 2P FOPA and apply complementary phase modulation on the two pumps [113]. This technique, which is sometimes referred to as 'counter phasing', relies on the fact that the idler phase, in the event that the signal was modulation free, is the sum of the pump phases. By ensuring the pump phases are exactly opposite, no phase information from the pumps is transferred to the idler.

One method of counter phasing is to individually modulate the pumps using two phase modulators driven by complementary (inverted) electrical signals.A sample schematic using discrete components is shown in Fig. A.1. This approach is complicated by the need to match the propagation lengths between the two phase modulators and the 50/50 coupler in which the pumps are combined. In addition, the frequency response of the

[1] Compound glass microstructured fibres have started to show some potential in this regard, particularly in terms of achieving low enough dispersion, but this technology was still in its infancy at the start of this research project.

phase modulators and RF amplifiers need to be matched across the bandwidth of the electrical dither signal.

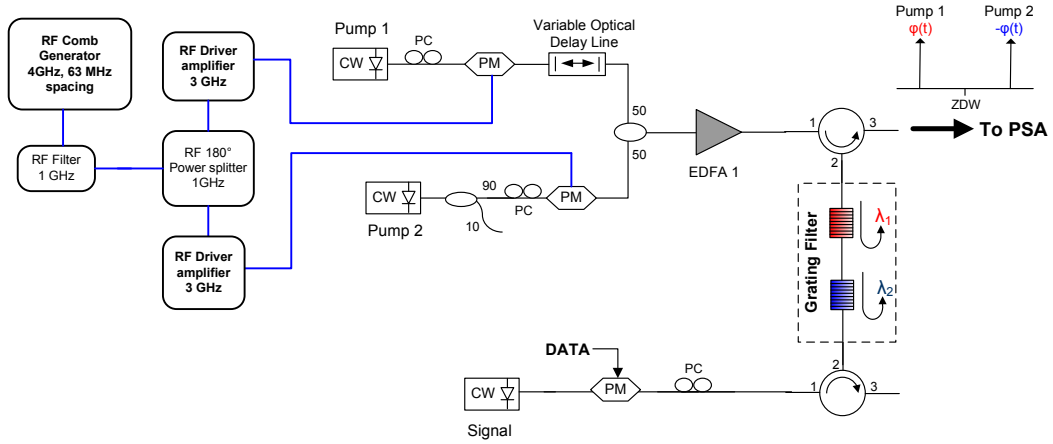

FIGURE A.1: Electrical counter phasing using two phase modulators driven by complementary electrical signals

An alternative to the electrical solution was pursued relying on a nonlinear process to generate the counter phased pumps.

This experiment was carried out to try and achieve counter phased pumps by using a periodically poled Lithium Niobate (PPLN) waveguide. with a gain mechanism utilising a cascaded second order nonlinear process. The first of the two pumps required in the 2P FOPA was spectrally broadened using a phase modulator driven by an electrical signal. This wideband pump was then mixed with a frequency detuned probe beam, generating an idler wave that is the phase conjugate of the wideband pump relative to the probe. The parametric process in the PPLN involved second harmonic generation (SHG) followed by difference frequency generation (DFG) [87, 114]. This cascaded process has properties similar to FWM as it involves three photons mixing. Two waves: a wideband pump, and a probe, with frequencies of ω_{wp} and ω_p respectively, are injected into the waveguide. The probe generates a wave at the second harmonic frequency ($2\omega_p$) via SHG, which interacts with the wideband pumpl to generate an idler wave at frequency ω_i via the DFG process ($\omega_i = 2\omega_p - \omega_{wp}$). If ϕ_{wp}, ϕ_i and ϕ_p are the absolute phases of the wideband pumpl, idler and probe respectively, then $\phi_i = 2\phi_p - \phi_{wp}$.

This implies that the idler wave was opposite in phase with respect to the wideband pump, with a small phase error originating from the $2\phi_p$ term. By carefully filtering out the signal-idler pair, they could be used as the spectrally counter phased pumps for parametric processing in an HNLF based FOPA. The benefit of this approach is that very large dither bandwidths can be employed while maintaining the counter phasing. Note that the cascaded SHG/DFG effectiveness in the PPLN sample available was sufficient to generate a counter phased pump, but not enough to operate as a high gain FOPA on its own.

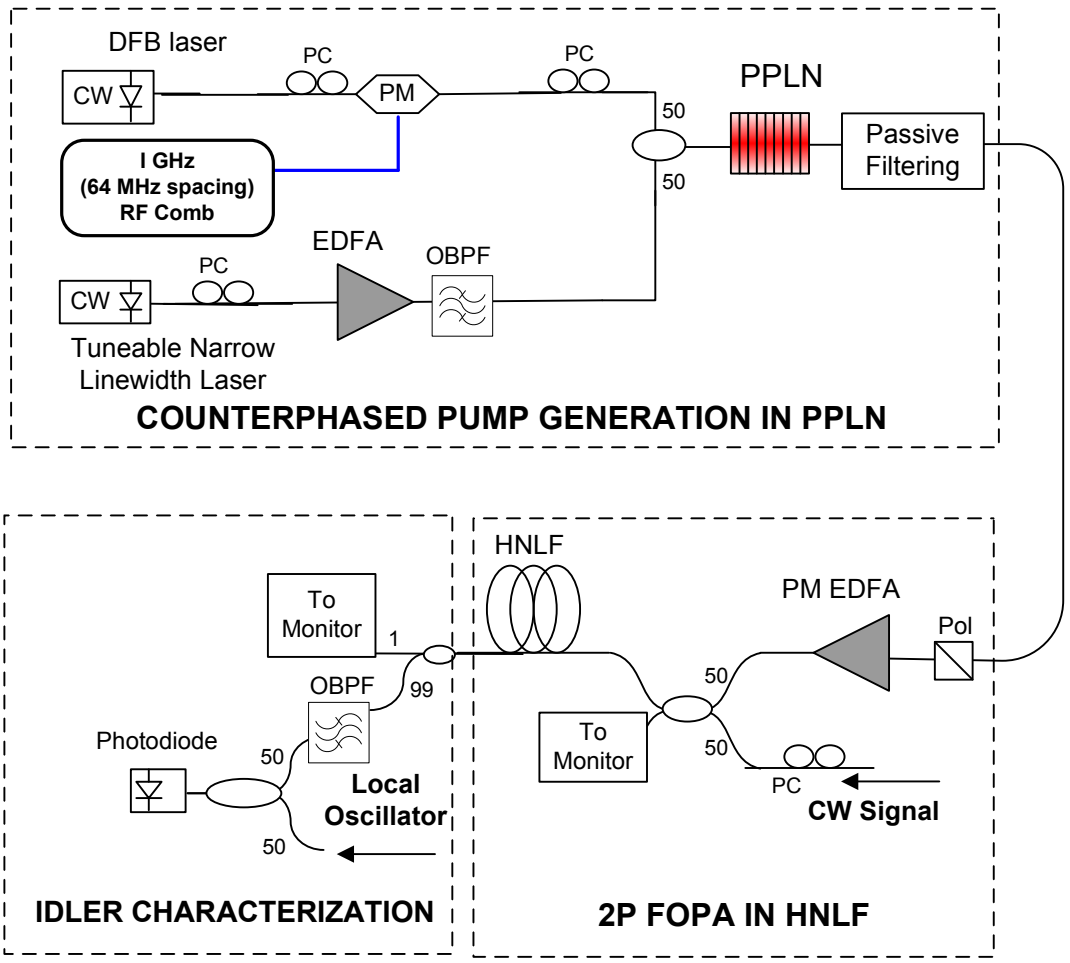

FIGURE A.2: Optically assisted counter phasing using cascaded SHG/DFG in a PPLN waveguide.

The corresponding experimental setup is shown in Fig. A.2. The goal was to realise two counter phased pumps around 1539 and 1552 nm. The first wideband pump, at 1539 nm, was generated from a standard distributed feedback (DFB) laser with a linewidth of 15 MHz, and was subsequently electro-optically phase modulated using a 64 MHz spacing electrical radio frequency (RF) comb to broaden its linewidth to 1 GHz. This was then combined with the probe at 1545.5 nm. The probe was derived from a tunable narrow linewidth laser (Agilent 8168C), with a linewidth under 100 kHz. These two waves were then mixed in a PPLN waveguidel generating an idler at 1552 nm which served as the second counter-phased pump. The PPLN waveguide had coupling loss 1.4 dB , propagation loss 0.3 dB/cm, nonlinear SHG coefficient 25 pm/V at 1064 nm. The total input power was 21 dBm (limited by the device damage threshold), split equally between the pump and probe.The phase matching wavelength of the PPLN device was 1545.5 nm at 44°C, hence the choice of probe wavelength.

The generated idler was 17 dB lower than the signal, see Fig. A.3(a), and therefore an intermediate stage, comprising EDFAs and band-reflect grating filters was used to equalise the signal-idler pair in power,as well as suppress the probe once the mixing process is complete. The two remaining waves, the corresponding spectrum of which is shown in Fig. A.3(b), were then amplified in a PM EDFA providing two co-polarized counter phased pumps.

To evaluate the phase correlation of the counter-phased pumps and to show its usability in an FOPA, the following characterization was carried out. A 2P FOPA was setup to generate an idler from a CW signal and the counter phased pumps. The two pumps were coupled into a 500 m HNLF (ZDW 1550 nm, dispersion slope 0.03 ps/nm^2/km, nonlinear coefficient 20/W/km and loss 0.53 dB/km) and combined with a 15 MHz linewidth CW signal at1548 nm, generating an idler at 1542 nm via FWM. A spectral plot at the HNLF output is shown in Fig. A.3(c). The idler OSNR was better than 20 dB.

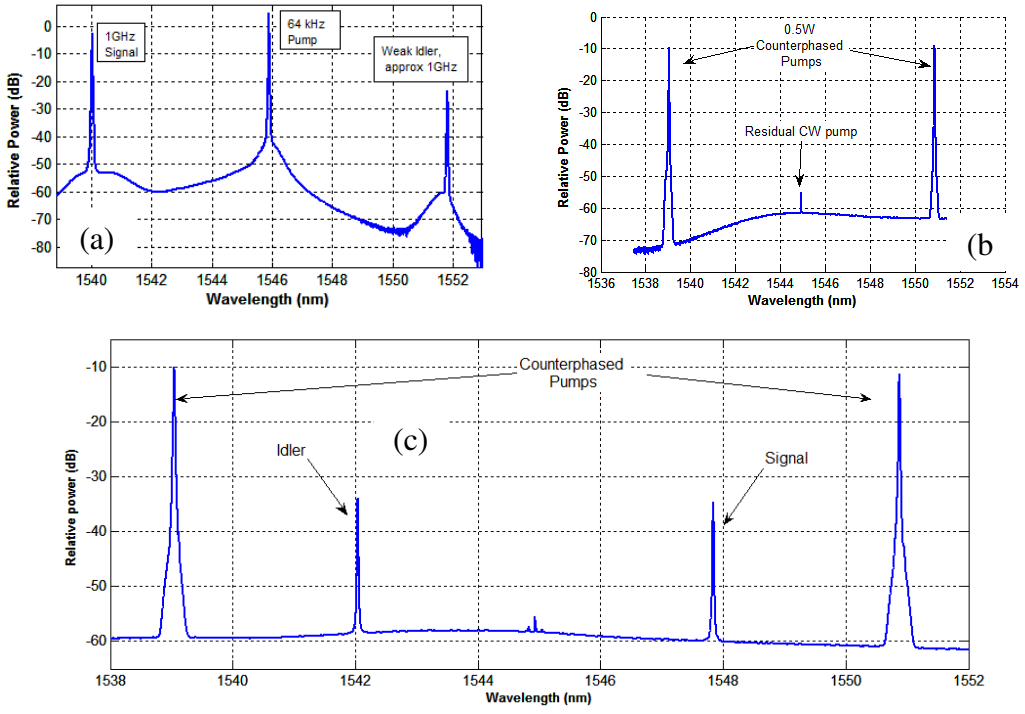

FIGURE A.3: a) Spectral trace at the very output of the PPLN. b) Spectral trace after the equalizing stage. c) Spectral trace at the very output of the system, before optical filtering.

The idler was then filtered out at the output of the HNLF using a 2 nm bandpass filter. Subsequently, it was combined with another CW beam with slightly different carrier frequency (about 520 MHz apart) and electrically detected for further characterization.

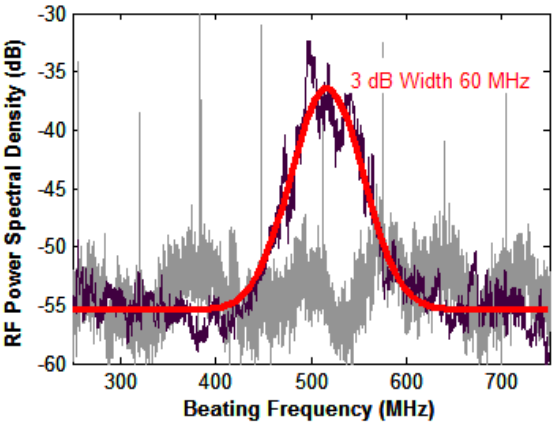

FIGURE A.4: Heterodyne signal generated by mixing idler and a local oscillator, thick solid line is 60 MHz fit, dashed grey line shows mixing result with both pumps co-phased.

The signal at the photodetector consisted of the heterodyne beat signal (which gives information on the linewidth of the idler) and broadband low power noise (with a bandwidth roughly given by the bandwidth of the output bandpass filter), mainly due to ASE from the EDFA being amplified via FWM in the HNLF. To distinguish between the noise contribution and the heterodyne signal, the beat signal generated by the filtered idler was measured first by switching off the mixing CW signal. Subsequently, the mixing CW signal was switched on, and a second electrical beat signal detected, from which the noise contribution could be subtracted. The resulting signal showing heterodyne beating of 60 MHz full width at half maximum (FWHM) - is shown in Fig. A.4. Although the beat signal is about two times broader than would be expected by beating two 15 MHz linewidth signals, the value is well below the linewidth expected in the absence of counter phasing between the two pumps.As a comparison, the dashed grey line in Fig. 2(c) shows the mixing result when two co-phased pumps are used in the same 2P FOPA, revealing the transfer of the pump dither(including the strong 64 MHz spaced tones) to the idler and a linewidth exceeding the 750 MHz measurement bandwidth. In addition, pump powers in excess of 30 dBm were coupled into the 2P FOPA without exceeding the SBS threshold, indicating a threshold increase of at least 13 dB.

Appendix B

PSK Carrier Recovery

To access or manipulate the phase information on complex signals, a phase reference is required. In differential systems, each symbol utilises the previously received symbol as the phase reference, allowing for easy modulation and demodulation. Differential schemes such as these are more susceptible to noise than those using an independent phase reference due to the fact that not only do they allow phase noise on one bit to affect the demodulation of another. In DSP- based coherent systems, the signal is detected using a free-running local oscillator, and the reference carrier synthesized in the digital domain, typically by averaging the modulation stripped signal phase over many bits. Performing carrier recovery in the optical domain however opens up several possibilities, such as coherent all-optical regeneration and homodyne signal detection.

A number of all-optical methods to recover the carrier from PSK signals have been previously been proposed. One utilises injection locking to amplify a residual carrier left within the signal spectrum [115]. This scheme is modulation format independent, although it sacrifices some bandwidth due to the need to deploy special line codes minimises the amount of low frequency information in the signal. Another utilises a NOLM in which a BPSK signal serves as a pump in a degenerate PSA, causing the NOLM to lase at the signal carrier frequency [116]. Here, a new method is proposed (conceived and experimentally demonstrated jointly with Dr. Radan Slavik) that allows high precision recovery of the signal carrier from a BPSK signal using FWM in a parametric device. While demonstrated with BPSK, it is possible to extend the technique to higher order PSK formats. The concept is described in Fig. B.1.

The concept was experimentally evaluated using BPSK signals up to 56 Gbaud and the setup shown in Fig. B.2. Rather than performing the two mixing processes simultaneously, the setup was designed so that in one direction in an HNLF, the pump was mixed with probe, while in another direction, the pump was mixed with the BPSK signal. The signal was at 1555.5 nm, the pump at 1557.3 nm and the probe at 1555.6 nm. The mixing was performed in 493 m PM HNLF, with all waves aligned to the fast axis whose

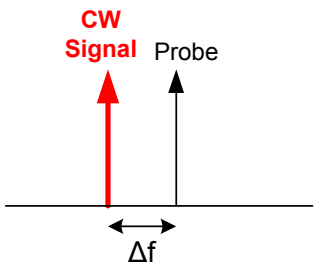	In the absence of data modulation, the conventional way to force a probe to track the frequency of a signal is to mix the two waves together at a photodetector, giving an electrical beat at Δf, where Δf is identical to the optical frequency difference between pump and probe. Frequency shifting the probe by Δf locks it to the signal's frequency.
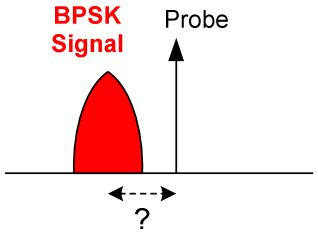	When the signal has phase modulation, the electrical beat is not narrowband, but is corrupted by the phase information present on the signal. As a result, the frequency difference between the signal carrier and the probe cannot be determined in a straightforward manner.
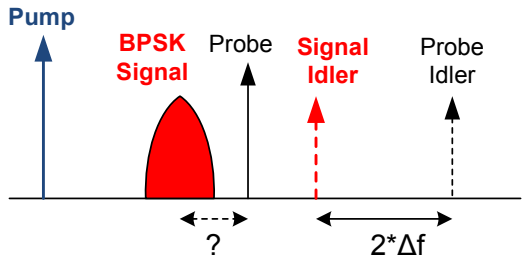	To get around this, first the signal and probe are mixed (using FWM) with a local pump. This generates two idlers. As the phase of the signal idler is twice that on the signal, provided that the signal modulation was BPSK, the signal idler is a CW. The frequency difference between the two idlers can now be detected, and dividing this by 2 gives Δf. The probe can now be shifted by Δf, thereby forcing the probe to track the signal carrier frequency.

FIGURE B.1: Concept behind FWM-based carrier recovery for BPSK signal.

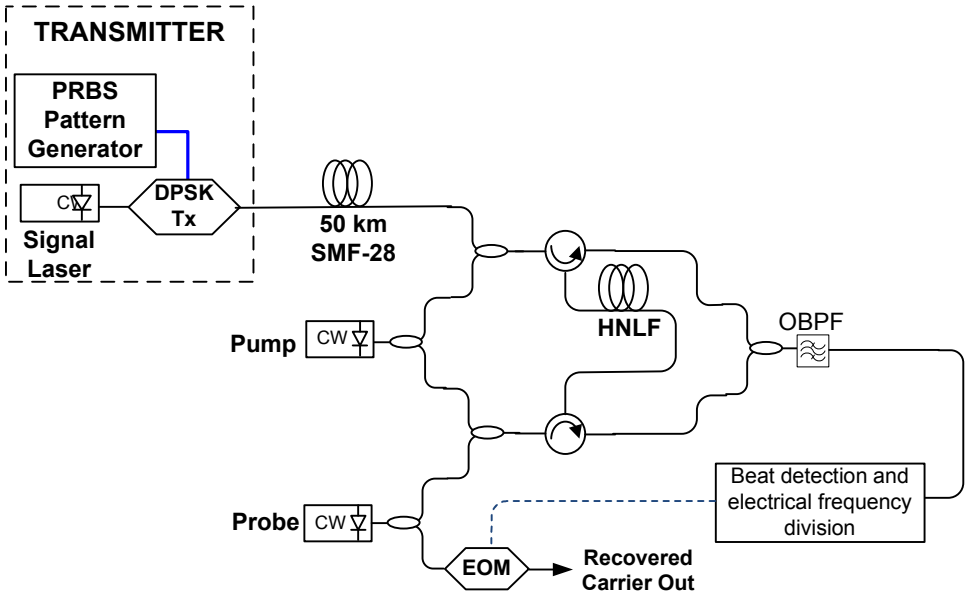

FIGURE B.2: Carrier recovery experimental setup.

properties were ZDW 1544 nm, dispersion slope 0.029 ps/nm^2/km and nonlinear coefficient 10.7 /W/Km (OFS Fitel, Denmark).The SBS threshold of the fiber was around 18 dBm. Two optical injection locking stages were used (although not shown in schematic). The first of these was used to amplify the signal's idler, thereby eliminating amplitude noise originating from the BPSK signal itself, noise that would have compromised the frequency division process. The second one was used to amplify the frequency shifted probe after the EOM. The signal and probe wavelengths were chosen to be roughly 5 GHz apart, therefore a 10 GHz frequency divider was used.

First, the DPSK modulator was switched off so as to characterise the how well the system could synchronise a CW probe to a CW signal (200 kHz linewidth laser, Eblana Photonics, Ireland). For this characterization,the interference pattern between the original input signal and the recovered carrier was observed, Fig. B.3a. It could be clearly seen that the two signals were interfering together with a phase difference only varying slowly (at a time scale of seconds) due to thermal drift in the fibers through which the signal and probe idler travel separately prior to being combined. This experiment was further complemented by analyzing the RF spectrum of this interference (to shift it from zero frequency, a 140-kHz phase dither was introduced at input of the original signal), Fig. B.3b. Here, was observed that the beating between the two signal and recovered carrier was narrower than 1 Hz (resolution limited by the RF spectrum analyzer), confirming the carrier had been recovered to better than 1 Hz precision (more than five orders of magnitudes below the natural linewidth of the signal laser).

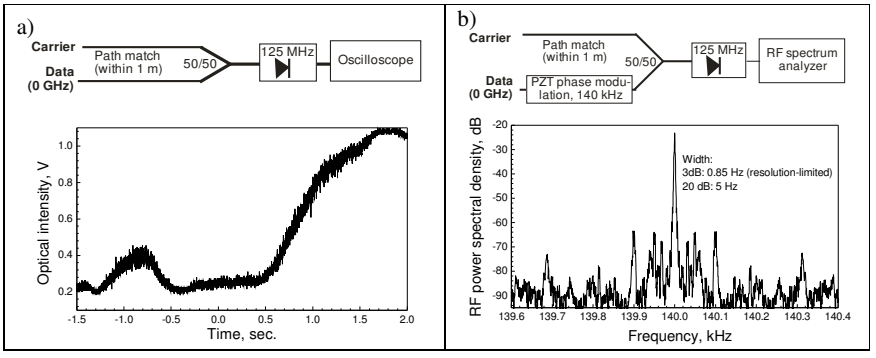

FIGURE B.3: Set-up (upper panels) and results (lower panels) of the static measurement - homodyne in temporal domain (a) and heterodyne in the RF frequency domain (b).

Following the static characterization, the system was tested using BPSK modulated data at various data rates (up to 56 Gbit/s) both straight from the transmitter and also in the presence of high residual dispersion (after propagation through 50 km of SMF-28 fiber).This time, the characterization was done by performing coherent homodyne detection at to 20 Gbit/s (limited in speed by the real time sampling oscilloscope). The recovered carrier served as the local oscillator for the coherent receiver. The constellation

diagrams were processed to compensate for dispersion, but not for any frequency difference between local oscillator and signal. The results are shown in Fig. B.4a and Fig. B.4b. Here, it could be seen that binary data was fully recovered with no intermediate frequency present. For comparison, the constellation obtained with a narrow-linewidth (kHz- range) free running local tuned carefully to obtain low intermediate frequency is also shown in Fig. B.4c, with the frequency offset between signal and local oscillator rotating the symbols (randomly).

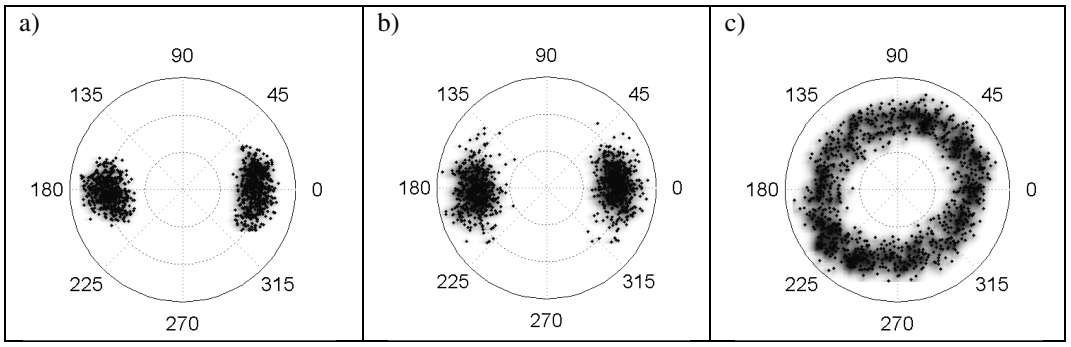

FIGURE B.4: Homodyne constellations at 20 Gbit/s stream with no added dispersion (a) and with 50 km propagation in SMF-28 followed by DSP dispersion compensation (b). For comparison, the constellation obtained with a free running local oscillator is also shown (c).

In conclusion, the novel scheme here presented for carrier recovery from PSK signals proved capable of recovering the carrier with precision better than 1 Hz. The processing bandwidth is virtually unlimited as it is based on the ultrafast FWM process. The scheme can be straightforwardly modified for carrier recovery to higher order MPSK formats by generating higher order FWM idlers in the HNLF (by increasing launch powers), and the comparing not the first signal and probe idlers as was the case for BPSK, but the (M-1)$^{\text{th}}$ idlers, and dividing the beat frequency by M.

List of publications

Journal Papers

1. **J.Kakande**, R.Slavík, F.Parmigiani, C.Lundström, M.Sjödin, P.Andrekson, R. Weerasuriya, S.Sygletos, A.D.Ellis, L.Grüner-Nielsen, D.Jakobsen, S.Herstrøm, R.Phelan, J.O'Gorman, A. Bogris, D. Syvridis, S.Dasgupta, P.Petropoulos and D.J.Richardson, "All-optical phase and amplitude regenerator for next-generation telecommunications systems", *Nature Photonics*, vol. **4**, pp. 690-695, (2010).

2. **J.Kakande**, R.Slavík, F. Parmigiani, A.Bogris, D.Syvridis, L.Grüner-Nielsen, R.Phelan, P.Petropoulos and D.J.Richardson, "Multi-Level Quantization of Optical Phase in a Novel Coherent Parametric Mixer Architecture", *Nature Photonics*, vol. **5**, 12, pp. 748-752, (2011).

3. **J.Kakande**, F.Parmigiani, M.Ibsen, P.Petropoulos and D.J.Richardson, "Wide bandwidth experimental study of nondegenerate phase-sensitive amplifiers in single- and dual-pump configurations", *IEEE Photonics Technology Letters*, vol. **22**, pp. 1781-1783, (2010).

4. **J.Kakande**, C.Lundström, P.A.Andrekson, Z.Tong, M.Karlsson, P.Petropoulos, F.Parmigiani and D.J.Richardson, "Detailed characterisation of a fiber-optic parametric amplifier in phase-sensitive and phase-insensitive operation", *Optics Express*, vol. **18**, pp. 4130-4137, (2009).

5. K.J.Lee, F.Parmigiani, S.Liu, **J.Kakande**, P.Petropoulos, K.Gallo and D.J. Richardson, "Phase sensitive amplification based on quadratic cascading in a periodically poled lithium niobate waveguide", *Optics Express*, vol. **17**, pp. 20393-20400, (2009).

6. R.Slavík, A.Bogris, F.Parmigiani, **J.Kakande**, M.Westlund, M.Sköld, L.Grüner-Nielsen, R.Phelan, D.Syvridis, P.Petropoulos and D.J.Richardson, "Coherent All-Optical Phase and Amplitude Regenerator of Binary Phase-Encoded Signals", **doi**:10.1109/JSTQE.2011.2136329, (2011).

7. R.Slavík, **J.Kakande** and D.J.Richardson, "Feed-forward True Carrier Extraction of High Baud Rate Phase Shift Keyed Signals Using Photonic Modulation Stripping and Low-Bandwidth Electronics", *Optics Express*, (Submitted).

8. M.A.Ettabib, L.Jones, **J.Kakande**, R.Slavík, F.Parmigiani, X.Feng, F.Poletti, G.M.Ponzo, J.Shi, M.N.Petrovich, W.H.Loh, P/Petropoulos, and D.J..Richardson, "Phase Sensitive Amplification in a Highly Nonlinear Lead-Silicate Fibre", *Optics Express*, (Submitted).

Conference Submissions

1. **J.Kakande**, A.Bogris, R.Slavík, F.Pamigiani, D.Syvridis, P.Petropoulos and D.J. Richardson, "First demonstration of all-optical QPSK signal regeneration in a novel multi-format phase sensitive amplifier", *Proceedings of the 36th European Conference on Optical Communications (ECOC)*, Postdeadline 3.3, (2010).

2. R.Slavík, **J.Kakande**, F.Parmigiani, L.Grüner-Nielsen, R.Phelan, J.Vojtech, P. Petropoulos and D.J.Richardson, "Field-trial of an all-optical PSK regenerator in a 40Gbit/s 38 channel DWDM transmission experiment", *Proceedings of the Optical Fiber Communication Conference (OFC/NFOEC) 2011*, Postdeadline PDPA7, (2011).

3. F.Parmigiani, R.Slavík, **J.Kakande**, C.Lundström, M.Sjödin, P.Andrekson, R. Weerasuriya, S.Sygletos, A.D.Ellis, L.Grüner-Nielsen, D.Jakobsen, S.Herstrøm, R.Phelan, J.O'Gorman, A.Bogris, D.Syvridis, S.Dasgupta, P.Petropoulos and D.J. Richardson, "All-optical phase regeneration of 40Gbit/s DPSK signals in a black-box phase sensitive amplifier", *Proceedings of the Optical Fiber Communication Conference (OFC/NFOEC) 2010*, Postdeadline PDPC3, (2010).

4. **J.Kakande**, R.Slavík, F.Parmigiani, P.Petropoulos and D.J.Richardson, "All-Optical Processing of Multi-level Phase Shift Keyed Signals", *Optical Fiber Communication Conference (OFC/NFOEC) 2012*, Invited, (2012).

5. **J. Kakande**, R.Slavík, P.Petropoulos and D.J.Richardson, "Phase Sensitive Parametric Mixers for Coherent All-Optical Signal Processing", *IEEE Summer Topical Meeting*, **doi**:0.1109/PHOSST.2011.6000088, Invited, (2011).

6. **J.Kakande**, F.Parmigiani, R.Slavík, L.Grüner-Nielsen, D.Jakobsen, S.Herstrøm, P.Petropoulos and D.J.Richardson, "Saturation effects in degenerate phase sensitive fiber optic parametric amplifiers", *Proceedings of the 36th European Conference on Optical Communications (ECOC)*, paper Th.10.C.2, (2010).

7. **J.Kakande**, A.Bogris, R.Slavík, F.Parmigiani, D.Syvridis, M.Westlund, M.Sköld, P.Petropoulos and D.J.Richardson, "QPSK phase and amplitude regeneration at

56 Gbaud in a novel input-idler-free non-degenerate phase sensitive amplifier", *Proceedings of the 2011 Optical Fiber Communication Conference (OFC/NFOEC)*, paper OMT4, (2011).

8. **J.Kakande**, P.Petropoulos and D.J.Richardson, "Fiber Optical Parametric Amplification of Optical Combs for Enhanced Performance and Functionality, *Proceedings of the 37th European Conference on Optical Communications (ECOC)*, paper Th.11.LeCervin.5, (2011).

9. R.Slavík, F.Parmigiani, **J.Kakande**, M.Westlund, M.Sköld, L.Grüner-Nielsen, R.Phelan, P.Petropoulos and D.J.Richardson, "Robust design of all-optical PSK regenerator based on phase sensitive amplification",*Proceedings of the Optical Fiber Communication Conference (OFC/NFOEC) 2011*, paper OMT2, (2011).

10. S.Liu, K.-J.Lee, **J.Kakande**, F.Parmigiani, R.Slavík, P.Petropoulos and D.J. Richardson, "Phase-sensitive wavelength conversion based on cascaded quadratic processes in periodically poled lithium niobate waveguides", *Proceedings of the Optical Fiber Communication Conference (OFC/NFOEC) 2011*, paper OThU5, (2011).

11. R.Slavík, **J.Kakande**, F.Parmigiani, P.Petropoulos and D.J.Richardson, "All-optical regeneration based on phase sensitive amplification", emphProceedings of the Conference on Lasers and Electro-Optics (CLEO) and Quantum Electronics and Laser Science Conference (QELS) 2011, paper CWD2, Invited, (2011).

12. F. Parmigiani, **J. Kakande**, R.Slavík, P. Petropoulos and D.J. Richardson, "Potential and practical implementations of phase sensitive amplifiers for all-optical signal regeneration", *The European Conference on Lasers and Electro-Optics (CLEO/ Europe) 2011*, paper CI1_3, Invited, (2011).

13. R.Slavík, **J.Kakande** and D.J.Richardson, "Feed-forward true carrier extraction of high baud rate PSK signals using slow electronics", *37th European Conference on Optical Communications (ECOC)*, poster We.10.P1.59, (2011).

14. P.Petropoulos, **J.Kakande**, R.Slavík, F.Parmigiani, A.Bogris, D.Syvridis and D.J. Richardson, "Phase regeneration of optical signals", *Information Photonics 2011*, Ottawa Canada 18-20 May, Invited, (2011).

15. D.J.Richardson, R.Slavík, **J.Kakande**, F.Parmigiani, A.Bogris, D.Syvridis and P.Petropoulos, "Phase-encoded signal regeneration exploiting phase sensitive amplification", *Proceedings of the 37th European Conference on Optical Communications (ECOC)*,paper Mo.1.A.3, Invited, (2011).

16. M.A.Ettabib, L.Jones, **J.Kakande**, R.Slavík, F.Parmigiani, X.Feng, F.Poletti, G.M.Ponzo, J.A.Shi, M.N.Petrovich, P.Petropoulos, W.H.Loh and D.J.Richardson, "Phase sensitive amplification in a highly nonlinear lead-silicate fibre", *Proceedings of the 37th European Conference on Optical Communications (ECOC)*, paper Th.11.LeCervin.3, (2011).

17. F.Parmigiani, R.Slavík, **J.Kakande**, L.Grüner-Nielsen, D.Jakobsen, S.Herstrøm, R.Weerasuriya, S.Sygletos, A.D.Ellis, P.Petropoulos and D.J.Richardson. "All-optical phase and amplitude regeneration properties of a 40 Gbit/s DPSK black-box phase sensitive amplifier", *Proceedings of the 36th European Conference on Optical Communications (ECOC)*, paper Mo.2.A.1, (2010).

18. R.Slavík, **J.Kakande**, F.Parmigiani, L.Grüner-Nielsen, D.Jakobsen, S.Herstrøm, P.Petropoulos and D.J.Richardson, "All-optical phase-regenerative multicasting of 40 Gbit/s DPSK signal in a degenerate phase sensitive amplifier", *Proceedings of the 36th European Conference on Optical Communications (ECOC)*, paper Mo.1.A.2, (2010).

19. F.Parmigiani, R.Slavík, **J.Kakande**, L.Grüner-Nielsen, D.Jakobsen, S.Herstrøm, R.Weerasuriya, S.Sygletos, A.D.Ellis, P.Petropoulos and D.J.Richardson, All-optical signal processing in highly nonlinear fibres, *Proceedings of the 15th OptoeElectronics and Communications Conference (OECC)*, pp. 486 - 487, Invited, (2010).

20. **J.Kakande**, F.Parmigiani, M.Ibsen, P.Petropoulos and D.J.Richardson, "Experimental investigation of wide bandwidth single and dual pump non-degenerate phase sensitive amplifiers",*Proceedings of the Optical Fiber Communication Conference (OFC/NFOEC) 2010*, paper OWT3, (2010).

21. **J.Kakande**, R.Slavík, F.Parmigiani, P.Petropoulos and D.J.Richardson, "Synthesis of phase-locked counter-phase modulated pumps for SBS-suppressed fibre parametric amplifiers", *Proceedings of the Conference on Lasers and Electro-Optics (CLEO) and Quantum Electronics and Laser Science Conference (QELS)*, paper CFN4, (2010).

22. F.Parmigiani, R.Slavík, A.Camerlingo, L.Grüner-Nielsen, D.Jakobsen, S.Herstrøm, R.Phelan, J.O'Gorman, S.Dasgupta, **J.Kakande**, S.Sygletos, A.D.Ellis, P.Petropoulos and D.J.Richardson, "Generation of high repetition rate (¿100 GHz) ultrastable pulse trains from a coherent optical beat-signal through non-linear compression using a high SBS-threshold fiber", *Nonlinear Photonics 2010*, paper NThA5, (2010).

23. F.Parmigiani, K.J.Lee, S.Liu, **J.Kakande**, P.Petropoulos, K.Gallo, D.J.Richardson, "Phase sensitive amplification based on cascaded SHG/DFG process in a periodically poled lithium niobate waveguide", *Institute of Physics Meeting London*, 21 Sep (2009).

24. C.Lundström, **J.Kakande**, P.A.Andrekson, P.Petropoulos, F.Parmigiani and D.J. Richardson, "Experimental comparison of gain and saturation characteristics of a parametric amplifier in phase-sensitive and phase-insensitive mode", *Proceedings of the 35th European Conference on Optical Communications (ECOC)*, (2009).

Bibliography

[1] P. A. Humblet and M. Azizoglu, "On the bit error rate of lightwave systems with optical amplifiers," *Journal of Lightwave Technology*, vol. 9, no. 11, pp. 1576–1582, 1991.

[2] M. Salsi, H. Mardoyan, P. Tran, C. Koebele, E. Dutisseuil, G. Charlet, and S. Bigo, "155x100gbps coherent pdm-qpsk transmission over 7,200km," *Proceedings of the35th European Conference on Optical Communication (ECOC)*, pp. 1–2, 2009.

[3] M. Salsi, C. Koebele, P. Tran, H. Mardoyan, E. Dutisseuil, J. Renaudier, M. Bigot-Astruc, L. Provost, S. Richard, P. Sillard, S. Bigo, and G. Charlet, "Transmission of 96x100gbps with 23 percent super-fec overhead over 11,680km, using optical spectral engineering," *Proceedings of the 2011 Optical Fiber Communication Conference (OFC/NFOEC)*, pp. 1–3, 2011.

[4] S. B. Poole, D. N. Payne, R. J. Mears, M. E. Fermann, and R. I. Laming, "Fabrication and characterization of low-loss optical fibers containing rare-earth ions," *Journal of Lightwave Technology*, vol. 4, no. 7, pp. 870–876, 1986.

[5] R. I. Laming, M. N. Zervas, and D. N. Payne, "Erbium-doped fiber amplifier with 54 db gain and 3.1 db noise figures," *IEEE Photonics Technology Letters*, vol. 4, no. 12, pp. 1345–1347, 1992.

[6] S. L. Hansen, K. Dybdal, and C. C. Larsen, "Gain limit in erbium-doped fiber amplifiers due to internal rayleigh backscattering," *IEEE Photonics Technology Letters*, vol. 4, no. 6, pp. 559–561, 1992.

[7] F. A. Flood, "L-band erbium-doped fiber amplifiers," *Optical Fiber Communication Conference 2000*, vol. 2, pp. 102–104, 2000.

[8] S. Aozasa, H. Masuda, H. Ono, T. Sakamoto, T. Kanamori, Y. Ohishi, and M. Shimizu, "1480-1510 nm-band tm doped fiber amplifier (tdfa) with a high power conversion efficiency of 42 percent," *Proceedings of the 2001 Optical Fiber Communication Conference and Exhibit, (OFC)*, vol. 4, PD1–3, 2001.

[9] M. N. Islam, "Raman amplifiers for telecommunications," *IEEE Journal of Selected Topics in Quantum Electronics*, vol. 8, no. 3, pp. 548–559, 2002.

[10] A. Mori, H. Masuda, K. Shikano, and M. Shimizu, "Ultra-wide-band tellurite-based fiber raman amplifier," *Journal of Lightwave Technology*, vol. 21, no. 5, pp. 1300–1306, 2003.

[11] T. Thomas, A. A. Peter, and O. Bengt-Erik, "Ultra high gain fiber optical parametric amplifier," *Proceedings of the 2006 Optical Fiber Communication Conference (OFC/NFOEC)*, OFH6, 2006.

[12] K. K. Y. Wong, M. E. Marhic, and L. G. Kazovsky, "Phase-conjugate pump dithering for high-quality idler generation in a fiber optical parametric amplifier," *IEEE Photonics Technology Letters*, vol. 15, no. 1, pp. 33–35, 2003.

[13] M. E. Marhic, *Fiber Optical Parametric Amplifiers, Oscillators and Related Devices*. 2007.

[14] J. P. Gordon and L. F. Mollenauer, "Phase noise in photonic communications systems using linear amplifiers," *Optics Letters*, vol. 15, no. 23, pp. 1351–1353, 1990.

[15] R. Loudon, "Theory of noise accumulation in linear optical-amplifier chains," *IEEE Journal of Quantum Electronics*, vol. 21, no. 7, pp. 766–773, 1985.

[16] Y. Mu and C. M. Savage, "Parametric amplifiers in phase-noise-limited optical communications," *Journal of the Optical Society of America B*, vol. 9, no. 1, pp. 65–70, 1992.

[17] J. A. Levenson, I. Abram, T. Rivera, and P. Grangier, "Reduction of quantum noise in optical parametric amplification," *Journal of the Optical Society of America B*, vol. 10, no. 11, pp. 2233–2238, 1993.

[18] W. Imajuku, A. Takada, and Y. Yamabayashi, "Inline coherent optical amplifier with noise figure lower than 3 db quantum limit," *Electronics Letters*, vol. 36, no. 1, pp. 63–64, 2000.

[19] A. Bogris, D. Syvridis, P. Kylemark, and P. A. Andrekson, "Noise characteristics of dual-pump fiber-optic parametric amplifiers," *Journal of Lightwave Technology*, vol. 23, no. 9, pp. 2788–2795, 2005.

[20] G. Kalogerakis, M. E. Marhic, K. K. Y. Wong, and L. G. Kazovsky, "Transmission of optical communication signals by distributed parametric amplification," *Journal of Lightwave Technology*, vol. 23, no. 10, pp. 2945–2953, 2005.

[21] M. Vasilyev, "Distributed phase-sensitive amplification," *Optics Express*, vol. 13, no. 19, pp. 7563 –7571, 2005.

[22] K. Inoue, "Optical level equalisation based on gain saturation in fibre optical parametric amplifier," *Electronics Letters*, vol. 36, no. 12, pp. 1016–1017, 2000.

[23] M. Matsumoto, "Regeneration of rz-dpsk signals by fiber-based all-optical regenators," *IEEE Photonics Technology Letters*, vol. 17, no. 5, pp. 1055–1057, 2005.

[24] —, "Performance improvement of phase-shift-keying signal transmission by means of optical limiters using four-wave mixing in fibers," *Journal of Lightwave Technology*, vol. 23, no. 9, pp. 2696–2701, 2005.

[25] C. S. Bres, A. O. J. Wiberg, J. M. Chavez-Boggio, and S. Radic, "Optical demultiplexing with extinction ratio enhancement based on higher order parametric interaction," *Proceedings of the 35th European Conference on Optical Communication (ECOC)*, pp. 1–2, 2009.

[26] A. Bogris and D. Syvridis, "Rz-dpsk signal regeneration based on dual-pump phase-sensitive amplification in fibers," *IEEE Photonics Technology Letters*, vol. 18, no. 17-20, pp. 2144–2146, 2006.

[27] K. Croussore and G. F. Li, "Phase regeneration of nrz-dpsk signals based on symmetric-pump phase-sensitive amplification," *IEEE Photonics Technology Letters*, vol. 19, no. 9-12, pp. 864–866, 2007.

[28] A. Lattes, H. Haus, F. Leonberger, and E. Ippen, "An ultrafast all-optical gate," *IEEE Journal of Quantum Electronics*, vol. 19, no. 11, pp. 1718–1723, 1983.

[29] T. Morioka, M. Saruwatari, and K. Nakagawa, "All-optical kerr switching techniques and applications," *IEEE Global Telecommunications Conference and Exhibition. 'Communications: Connecting the Future' (GLOBECOM '90)*, vol. 2, pp. 1311–1317, 1990.

[30] R. S. Tucker and K. Hinton, "Energy consumption and energy density in optical and electronic signal processing," *IEEE Photonics Journal*, vol. PP, no. 99, pp. 1–1, 2011.

[31] R. S. Tucker, "Green optical communications part ii: energy limitations in networks," *IEEE Journal of Selected Topics in Quantum Electronics*, vol. 17, no. 2, pp. 261–274, 2011.

[32] I. Dedic, "56gs/s adc : enabling 100gbe," *Proceedings of the 2010 Conference on Optical Fiber Communication (OFC)*, pp. 1–3, 2010.

[33] G. Agrawal, *Nonlinear Fiber Optics*. Academic Press, 2001.

[34] L. G. Cohen, W. L. Mammel, and S. J. Jang, "Low-loss quadruple-clad single mode lightguides with dispersion below 2 ps/nm/km over the 1.28 um to 1.65 um wavelength range," *Electronics Letters*, vol. 18, no. 24, pp. 1023–1024, 1982.

[35] M. Hirano, T. Nakanishi, T. Okuno, and M. Onishi, "Broadband wavelength conversion over 193-nm by hnl-dsf improving higher-order dispersion performance," *Proceedings of the 31st European Conference on Optical Communication (ECOC)*, vol. 6, pp. 43–44, 2005.

[36] O. Karlsson, J. Brentel, and P. A. Andrekson, "Long-term measurement of pmd and polarization drift in installed fibers," *Journal of Lightwave Technology*, vol. 18, no. 7, pp. 941–951, 2000.

[37] I. P. Kaminow, T. Li, and A. E. Willner, *Optical Fiber Telecommunications: Systems and Networks*. Academic Press, 2008.

[38] J. Noda, K. Okamoto, and Y. Sasaki, "Polarization-maintaining fibers and their applications," *Journal of Lightwave Technology*, vol. 4, no. 8, pp. 1071–1089, 1986.

[39] R. Boyd, *Nonlinear Optics, Second Edition*. Academic Press, 2003.

[40] R. Billington, "Effective area of optical fibres–definition and measurement technique," *National Physical Laboratory, Teddington, Middlesex, UK*, 2003.

[41] F. Parmigiani, P. Petropoulos, M. Ibsen, M. A. F. Roelens, and D. J. Richardson, "A novel xpm based pulse retiming system incorporating a fibre grating based parabolic pulse shaper," *Proceedings of the 31st European Conference on Optical Communication (ECOC)*, vol. 2, pp. 313–314, 2005.

[42] R. A. Baumgartner and R. L. Byer, "Optical parametric amplification," *IEEE Journal of Quantum Electronics*, vol. QE-15, no. 6, pp. 432–444, 1979.

[43] R. Stolen and J. Bjorkholm, "Parametric amplification and frequency conversion in optical fibers," *IEEE Journal of Quantum Electronics*, vol. 18, no. 7, pp. 1062–1072, 1982.

[44] J. A. Armstrong, N. Bloembergen, J. Ducuing, and P. S. Pershan, "Interactions between light waves in a nonlinear dielectric," *Physical Review*, vol. 127, no. 6, pp. 1918–, 1962.

[45] R. Olshansky, "Propagation in glass optical waveguides," *Reviews of Modern Physics*, vol. 51, no. 2, p. 341, 1979.

[46] E. Myslivets, C. Lundstrom, J. M. Aparicio, S. Moro, A. O. J. Wiberg, C. S. Bres, N. Alic, P. A. Andrekson, and S. Radic, "Spatial equalization of zero-dispersion wavelength profiles in nonlinear fibers," *IEEE Photonics Technology Letters*, vol. 21, no. 24, pp. 1807–1809, 2009.

[47] W. Steier and H. Stover, "Locking of laser oscillators by light injection," *IEEE Journal of Quantum Electronics*, vol. 2, no. 4, pp. 111–112, 1966.

[48] T. B. Simpson, J. M. Liu, and A. Gavrielides, "Small-signal analysis of modulation characteristics in a semiconductor laser subject to strong optical injection," *IEEE Journal of Quantum Electronics*, vol. 32, no. 8, pp. 1456–1468, 1996.

[49] E. K. Lau, X. Zhao, H.-K. Sung, D. Parekh, C. Chang-Hasnain, and M. C. Wu, "Strong optical injection-locked semiconductor lasers demonstrating > 100-ghz resonance frequencies and 80-ghz intrinsic bandwidths," *Optics Express*, vol. 16, no. 9, pp. 6609–6618, 2008.

[50] H. A. Haus and C. H. Townes, "Correspondence: comments on" noise in photoelectric mixing"," *Proceedings of the IRE*, vol. 50, no. 6, pp. 1544 –1546, 1962, ISSN: 0096-8390.

[51] C. M. Caves, "Quantum limits on noise in linear amplifiers," *Physical Review D*, vol. 26, no. 8, p. 1817, 1982.

[52] R. Slusher and B. Yurke, "Squeezed light for coherent communications," *Journal of Lightwave Technology*, vol. 8, no. 3, pp. 466 –477, 1990.

[53] M. E. Marhic, C. H. Hsia, and J. M. Jeong, "Optical amplification in a nonlinear fibre interferometer," *Electronics Letters*, vol. 27, no. 3, pp. 210–211, 1991.

[54] W. Imajuku, A. Takada, and Y. Yamabayashi, "Low-noise amplification under the 3 db noise figure in high-gain phase-sensitive fibre amplifier," *Electronics Letters*, vol. 35, no. 22, pp. 1954 –1955, 1999.

[55] R. Tang, P. Devgan, V. S. Grigoryan, and P. Kumar, "Inline frequency-nondegenerate phase-sensitive fibre parametric amplifier for fibre-optic communication," *Electronics Letters*, vol. 41, no. 19, pp. 1072–1074, 2005.

[56] R. Tang, J. Lasri, P. S. Devgan, V. Grigoryan, P. Kumar, and M. Vasilyev, "Gain characteristics of a frequency nondegenerate phase-sensitive fiber-optic parametric amplifier with phase self-stabilized input," *Optics Express*, vol. 13, no. 26, pp. 10 483–10 493, 2005.

[57] A. Takada and W. Imajuku, "In-line optical phase-sensitive amplifier employing pump laser injection-locked to input signal light," *Electronics Letters*, vol. 34, no. 3, pp. 274 –276, 1998.

[58] W. Imajuku and A. Takada, "In-line optical phase-sensitive amplifier with pump light source controlled by optical phase-lock loop," *Journal of Lightwave Technology*, vol. 17, no. 4, pp. 637 –646, 1999.

[59] Z. Tong, C. J. McKinstrie, C. Lundstrm, M. Karlsson, and P. A. Andrekson, "Noise performance of optical fiber transmission links that use non-degenerate cascaded phase-sensitive amplifiers," *Optics Express*, vol. 18, no. 15, pp. 15 426–15 439, 2010.

[60] C. E. Shannon, "A mathematical theory of communication," *Bell Systems Technology Journal*, vol. 27, 379423 and 623656, 1948.

[61] W. Imajuku and A. Takada, "Gain characteristics of coherent optical amplifiers using a mach-zehnder interferometer with kerr media," *IEEE Journal of Quantum Electronics*, vol. 35, no. 11, pp. 1657 –1665, 1999.

[62] M. Shirasaki and H. A. Haus, "Squeezing of pulses in a nonlinear interferometer," *Journal of the Optical Society of America B*, vol. 7, no. 1, pp. 30 –34, 1990.

[63] M. E. Marhic, Y. Park, F. S. Yang, and L. G. Kazovsky, "Widely tunable spectrum translation and wavelength exchange by four-wave mixing in optical fibers," *Optics Letters*, vol. 21, no. 23, pp. 1906–1908, 1996.

[64] Y. J. Chen and A. W. Snyder, "Four-photon parametric mixing in optical fibers: effect of pump depletion," *Optics Letters*, vol. 14, no. 1, pp. 87–89, 1989.

[65] O. K. Lim, V. Grigoryan, M. Shin, and P. Kumar, "Ultra-low-noise inline fiber-optic phase-sensitive amplifier for analog optical signals," *Proceedings of the 2008 Conference on Optical Fiber Communication(OFC)*, pp. 1332–1334, 2008.

[66] T. Zhi, C. Lundstrom, A. Bogris, M. Karlsson, P. Andrekson, and D. Syvridis, "Measurement of sub-1db noise figure in a non-degenerate cascaded phase-sensitive fibre parametric amplifier," *Proceedings of the 35th European Conference on Optical Communication (ECOC)*, pp. 1–2, 2009.

[67] Z. Tong, C. Lundstrom, P. A. Andrekson, C. J. McKinstrie, M. Karlsson, D. J. Blessing, E. Tipsuwannakul, B. J. Puttnam, H. Toda, and L. Gruner Nielsen, "Towards ultrasensitive optical links enabled by low-noise phase-sensitive amplifiers," *Nature Photonics*, vol. 5, no. 7, pp. 430–436, 2011.

[68] M. Karlsson, "Four-wave mixing in fibers with randomly varying zero-dispersion wavelength," *Journal of the Optical Society of America B*, vol. 15, no. 8, pp. 2269–2275, 1998.

[69] A. A. Vedadi, N. Grossard, J. Hauden, E. Lantz, H. Maillotte, and T. Sylvestre, "Demonstration of an integrated linbo3 synchronized double phase modulator and its application to dual-pump fiber optical parametric amplifiers and wavelength converters," *Journal of Lightwave Technology*, vol. 26, no. 7, pp. 777–781, 2008.

[70] P. Kylemark, J. Ren, M. Karlsson, S. Radic, C. J. McKinstrie, and P. A. Andrekson, "Noise in dual-pumped fiber-optical parametric amplifiers: theory and experiments," *Journal of Lightwave Technology*, vol. 25, no. 9, pp. 2837–2846, 2007.

[71] P. Kylemark, J. Ren, S. Radic, C. J. McKinstrie, M. Karlsson, and P. A. Andrekson, "Noise in orthogonally pumped fiber-optical parametric amplifiers," *IEEE Photonics Technology Letters*, vol. 19, no. 2-4, pp. 88–90, 2007.

[72] K. K. Y. Wong, M. E. Marhic, G. Kalogerakis, and L. G. Kazovsky, "Fiber optical parametric amplifier and wavelength converter with record 360 nm gain bandwidth and 50 db signal gain," *Proceedings of the 2003 Conference on Lasers and Electro-Optics (CLEO)*, p. 2, 2003.

[73] P. Myslinski, D. Nguyen, and J. Chrostowski, "Effects of concentration on the performance of erbium-doped fiber amplifiers," *Journal of Lightwave Technology*, vol. 15, no. 1, pp. 112–120, 1997.

[74] S. Oda, H. Sunnerud, and P. A. Andrekson, "High efficiency and high output power fiber-optic parametric amplifier," *Optics Letters*, vol. 32, no. 13, pp. 1776–1778, 2007.

[75] L. Gruner-Nielsen, S. Herstrom, S. Dasgupta, D. Richardson, D. Jakobsen, C. Lundstrom, P. A. Andrekson, M. E. V. Pedersen, and B. Palsdottir, "Silica-based highly nonlinear fibers with a high sbs threshold," *2011 IEEE Winter Topicals (WTM)*, pp. 171–172, 2011.

[76] T. Udem, R. Holzwarth, and T. W. Hansch, "Optical frequency metrology," *Nature*, vol. 416, no. 6877, pp. 233–237, 2002.

[77] G. Grosche, O. Terra, K. Predehl, R. Holzwarth, B. Lipphardt, F. Vogt, U. Sterr, and H. Schnatz, "Optical frequency transfer via 146 km fiber link with 10 to -19 relative accuracy," *Optics Letters*, vol. 34, no. 15, pp. 2270–2272, 2009.

[78] M. Kourogi, K. Nakagawa, and M. Ohtsu, "Wide-span optical frequency comb generator for accurate optical frequency difference measurement," *IEEE Journal of Quantum Electronics*, vol. 29, no. 10, pp. 2693–2701, 1993.

[79] K. Croussore, I. Kim, C. Kim, Y. Han, and G. F. Li, "Phase-and-amplitude regeneration of differential phase-shift keyed signals using a phase-sensitive amplifier," *Optics Express*, vol. 14, no. 6, pp. 2085–2094, 2006.

[80] N. Sugimoto, T. Nagashima, T. Hasegawa, S. Ohara, K. Taira, and K. Kikuchi, "Bismuth-based optical fiber with nonlinear coefficient of 1360 /w/km," *Proceedings of the 2004 Conference on Optical Fiber Communication (OFC)*,

[81] A. Camerlingo, X. Feng, F. Poletti, G. M. Ponzo, F. Parmigiani, P. Horak, M. N. Petrovich, P. Petropoulos, W. H. Loh, and D. J. Richardson, "Near-zero dispersion, highly nonlinear lead-silicate w-type fiber for applications at 1.55 micron," *Optics Express*, vol. 18, no. 15, pp. 15747 –15 756, 2010.

[82] R. Slavik, Y. Liao, E. Austin, P. Petropoulos, and D. J. Richardson, "Full characterization and comparison of phase properties of narrow linewidth lasers operating in the c-band," *Proceedings of SPIE 21st International Conference on Optical Fiber Sensors, May 15-19, 2011 Ottawa*, vol. 7753, 2011.

[83] A. Bononi, N. Rossi, and P. Serena, "Transmission limitations due to fiber nonlinearity," *Proceedings of the 2011 Optical Fiber Communication Conference and Exposition (OFC/NFOEC), and the National Fiber Optic Engineers Conference*, pp. 1–3, 2011.

[84] M. Matsumoto, "A fiber-based all-optical 3r regenerator for dpsk signals," *IEEE Photonics Technology Letters*, vol. 19, no. 5, pp. 273–275, 2007.

[85] R. Weerasuriya, S. Sygletos, S. K. Ibrahim, R. Phelan, J. O'Carroll, B. Kelly, J. O'Gorman, and A. D. Ellis, "Generation of frequency symmetric signals from a bpsk input for phase sensitive amplification," *Proceedings of the 2010 Optical Fiber Communication (OFC)*, pp. 1–3, 2010.

[86] G.-W. Lu and T. Miyazaki, "Optical phase erasure based on fwm in hnlf enabling format conversion from 320-gb/s rzdqpsk to 160-gb/s rz-dpsk," *Optics Express*, vol. 17, no. 16, pp. 13 346–13 353, 2009.

[87] J. Wang, J. Sun, X. Zhang, D. Huang, and M. M. Fejer, "Optical phase erasure and its application to format conversion through cascaded second-order processes in periodically poled lithium niobate," *Optics Letters*, vol. 33, no. 16, pp. 1804–1806, 2008.

[88] S. Kobayashi and T. Kimura, "Optical fm signal amplification by injection locked and resonant type semiconductor laser amplifiers," *IEEE Journal of Quantum Electronics*, vol. 18, no. 4, pp. 575–581, 1982.

[89] M. G. Taylor, "Coherent detection method using dsp for demodulation of signal and subsequent equalization of propagation impairments," *IEEE Photonics Technology Letters*, vol. 16, no. 2, pp. 674–676, 2004.

[90] R. Slavik, A. Bogris, F. Parmigiani, J. Kakande, M. Westlund, M. Skold, L. Gruner-Nielsen, R. Phelan, D. Syvridis, P. Petropoulos, and D. J. Richardson, "Coherent all-optical phase and amplitude regenerator of binary phase-encoded signals," *IEEE Journal of Selected Topics in Quantum Electronics*, vol. tba, no. 99, pp. 1–11, 2011.

[91] H. J. Caulfield and S. Dolev, "Why future supercomputing requires optics," *Nature Photonics*, vol. 4, no. 5, pp. 261–263, 2010.

[92] D. Miller, "Device requirements for optical interconnects to silicon chips," *Proceedings of the IEEE*, vol. 97, no. 7, pp. 1166–1185, 2009.

[93] D. A. B. Miller, "Are optical transistors the logical next step?," *Nature Photonics*, vol. 4, no. 1, pp. 3–5, 2010.

[94] M. J. Offside, J. E. Carroll, M. E. Bray, and A. Hadjifotiou, "Optical wavelength converters," *Electronics & Communication Engineering Journal*, vol. 7, no. 2, pp. 59–71, 1995.

[95] C. Koos, P. Vorreau, T. Vallaitis, P. Dumon, W. Bogaerts, R. Baets, B. Esembeson, BiaggioI, T. Michinobu, F. Diederich, W. Freude, and J. Leuthold, "All-optical high-speed signal processing with silicon-organic hybrid slot waveguides," *Nature Photonics*, vol. 3, no. 4, pp. 216–219, 2009.

[96] M. Hochberg, T. Baehr-Jones, G. Wang, M. Shearn, K. Harvard, J. Luo, B. Chen, Z. Shi, R. Lawson, P. Sullivan, A. K. Y. Jen, L. Dalton, and A. Scherer, "Terahertz all-optical modulation in a silicon-polymer hybrid system," *Nature Materials*, vol. 5, no. 9, pp. 703–709, 2006.

[97] M. Skold, M. Westlund, H. Sunnerud, and P. A. Andrekson, "All-optical waveform sampling in high-speed optical communication systems using advanced modulation formats," *Journal of Lightwave Technology*, vol. 27, no. 16, pp. 3662–3671, 2009.

[98] J. Azana, "Ultrafast analog all-optical signal processors based on fiber-grating devices," *Photonics Journal, IEEE*, vol. 2, no. 3, pp. 359–386, 2010.

[99] D. Hillerkuss, T. Schellinger, R. Schmogrow, M. Winter, T. Vallaitis, R. Bonk, A. Marculescu, J. Li, M. Dreschmann, J. Meyer, S. Ben Ezra, N. Narkiss, B. Nebendahl, F. Parmigiani, P. Petropoulos, B. Resan, K. Weingarten, T. Ellermeyer, J. Lutz, M. Moller, M. Huebner, J. Becker, C. Koos, W. Freude, and J. Leuthold, "Single source optical ofdm transmitter and optical fft receiver demonstrated at line rates of 5.4 and 10.8 tbit/s," *Proceedings of the 2010 Conference on Optical Fiber Communication (OFC)*, pp. 1–3, 2010.

[100] G. C. Valley, "Photonic analog-to-digital converters," *Optics Express*, vol. 15, no. 5, pp. 1955–1982, 2007.

[101] J. Capmany and D. Novak, "Microwave photonics combines two worlds," *Nature Photonics*, vol. 1, no. 6, pp. 319–330, 2007.

[102] P. V. Mamyshev, "All-optical data regeneration based on self-phase modulation effect," *Proceedings of the 24th European Conference on Optical Communication (ECOC)*, vol. 1, pp. 475–476, 1998.

[103] N. J. Doran and D. Wood, "Nonlinear-optical loop mirror," *Optics Letters*, vol. 13, no. 1, pp. 56–58, 1988.

[104] Z. Zheng, L. An, Z. Li, X. Zhao, and X. Liu, "All-optical regeneration of dqpsk/qpsk signals based on phase-sensitive amplification," *Optics Communications*, vol. 281, no. 10, pp. 2755–2759, 2008.

[105] M. Matsumoto, "All-optical dqpsk signal regeneration using 2r amplitude regenerators," *Optics Express*, vol. 18, no. 1, pp. 10–24, 2010.

[106] N. N. Kimchau, K. Tomofumi, M. G. John, P. Henrik, and J. B. Daniel, "All-optical 2r regeneration of bpsk and qpsk data using a 90 degree optical hybrid and integrated soa-mzi wavelength converter pairs," *Proceedings of the 2011 Optical Fiber Communication Conference (OFC/NFOEC)*, OMT3, 2011.

[107] R. H. Walden, "Analog-to-digital converter survey and analysis," *IEEE Journal on Selected Areas in Communications*, vol. 17, no. 4, pp. 539–550, 1999.

[108] C. Yu, S. Zhang, P. Y. Kam, and J. Chen, "Bit-error rate performance of coherent optical m-ary psk/qam using decision-aided maximum likelihood phase estimation," *Optics Express*, vol. 18, no. 12, pp. 12 088–12 103, 2010.

[109] A. Fragkos, A. Bogris, D. Syvridis, and R. Phelan, "Amplitude noise limiting amplifier for phase encoded signals using injection locking in semiconductor lasers," *Journal of Lightwave Technology*, 2011. DOI: 10.1109/JLT.2011.2178816.

[110] P. Frascella, S. Sygletos, S. K. Ibrahim, L. Gruner-Nielsen, R. Phelan, J. O'Gorman, and A. D. Ellis, "Two channel phase regeneration based on a black-box phase sensitive amplifier," *Proceedings of the 37th European Conference and Exhibition on Optical Communication (ECOC), paper Th.11.LeCervin.2*, 2011.

[111] P. L. Voss, K. G. Kprl, and P. Kumar, "Raman-noise-induced quantum limits for chi(3) nondegenerate phase-sensitive amplification and quadrature squeezing," *Journal of the Optical Society of America B*, vol. 23, no. 4, pp. 598–610, 2006.

[112] J. Hansryd and P. A. Andrekson, "Broad-band continuous-wave-pumped fiber optical parametric amplifier with 49-db gain and wavelength-conversion efficiency," *IEEE Photonics Technology Letters*, vol. 13, no. 3, pp. 194–196, 2001.

[113] H. Min-Chen, M. E. Marhic, K. Y. K. Wong, and L. G. Kazovsky, "Narrow-linewidth idler generation in fiber four-wave mixing and parametric amplification by dithering two pumps in opposition of phase," *Journal of Lightwave Technology*, vol. 20, no. 3, pp. 469–476, 2002.

[114] K. J. Lee, F. Parmigiani, S. Liu, J. Kakande, P. Petropoulos, K. Gallo, and D. Richardson, "Phase sensitive amplification based on quadratic cascading in a periodically poled lithium niobate waveguide," *Optics Express*, vol. 17, no. 22, pp. 20 393–20 400, 2009.

[115] A. Chiuchiarelli, M. J. Fice, E. Ciaramella, and A. J. Seeds, "Effective homodyne optical phase locking to psk signal by means of 8b10b line coding," *Optics Express*, vol. 19, no. 3, pp. 1707–1712, 2011.

[116] I. Kim, K. Croussore, X. Li, G. Li, T. Hasegawa, and N. Sugimoto, "All-optical carrier phase and polarization recovery using a phase-sensitive oscillator," *Proceedings of the 2007 Optical Fiber Communication and the National Fiber Optic Engineers Conference (OFC/NFOEC)*, pp. 1–3, 2007.